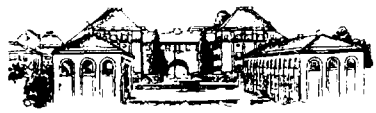

KUNGL TEKNISKA HÖGSKOLAN
Royal Institute of Technology
Nuclear Power Safety Division

ISSN 1403-1701 Kärnkraftsäkerhet 3
ISBN 91-7170-277-6
TRITA EKS.Avhandling
ISRN KTH/NPS/MVI2-9805-SE

PHENOMENOLOGICAL AND MECHANISTIC MODELING OF MELT-STRUCTURE-WATER INTERACTIONS IN A LIGHT WATER REACTOR (LWR) SEVERE ACCIDENT

Doctoral Thesis

by

Bui Viet Anh

Stockholm
1998

Department of Energy Technology
Division of Nuclear Power Safety
The Royal Institute of Technology
Stockholm, Sweden

Institutionen för Energiteknik
Avd. för Kärnkraftsäkerhet
Kungliga Tekniska Högskolan
Stockholm

KUNGL TEKNISKA HÖGSKOLAN

ISSN 1403-1701 Kärnkraftsäkerhet 3
ISBN 91-7170-277-6
TRITA EKS.Avhandling
ISRN KTH/NPS/MVI2-9805-SE

PHENOMENOLOGICAL AND MECHANISTIC MODELING OF MELT-STRUCTURE-WATER INTERACTIONS IN A LIGHT WATER REACTOR (LWR) SEVERE ACCIDENT

Doctoral Thesis

by

Bui Viet Anh

June 03, 1998

SPONSORS:
European Union • 4th Framework Program • MVI Project • MFCI Project • SKI, US NRC, HSK, Swedish and Finnish Power Companies • MSWI Project

---

Division of Nuclear Power Safety

Royal Institute of Technology (KTH)

Stockholm, Sweden

KUNGL TEKNISKA HÖGSKOLAN
Royal Institute of Technology
Ecole Royale Polytechnique
Kgl. Technische Hochschule

Avdelningen för Kärnkraftsäkerhet
Nuclear Power Safety Division

Postadress:	S-100 44 STOCKHOLM
	Drottning Kristinas väg. 33A
Telephone:	08-790 9251 (National)
	+46 8-790 9251 (International)
Fax:	08-790 9197 (National)
	+46 8-790 9197 (International)
URL:	http://www.egi.kth.se/nps/
Email:	anh@ne.kth.se

Nuclear Power Safety Division
Royal Institute of Technology
100 44 STOCKHOLM
June 1998

Abstract

Severe accidents in light water reactors have been the focal point of much research, performed in the last two decades, aimed at understanding the inherent physical phenomena and to evaluate proposed accident management schemes for mitigating the consequences of such accidents. Severe accident progression and consequences, as the reactor core overheats and melts, are intimately related to the interactions of the melt with coolant (water) and structures.

The objective of this work is to address the modeling of the thermal hydrodynamic phenomena and interactions, occurring during the progression of reactor severe accidents. The main theme of the present work is to integrate phenomenological modeling with mechanistic modeling. Integrated phenomenological models are developed to describe the accident scenarios, which consist of many processes, while mechanistic modeling, including direct numerical simulation, is carried out to describe separate effects and selected physical phenomena of particular importance.

Modeling of the in-vessel melt-structure interactions is the topic of the first chapter. In its first part, models are developed for the core debris heat up and the formation of a melt pool in the lower head of reactor vessel and the resultant thermal loads on the vessel. The heat transport and interactions, occurring in this scenario, are represented through energy-conservation formulation. In order to describe the phase change associated with core debris and vessel wall melting, a temperature-based enthalpy method is employed and the initial energy-conservation equation is modified. Natural convection heat transfer inside the decay-heated melt pool is accounted for in this work by an effective diffusivity-convectivity model. Its application has also been extended to the case of metallic layers, heated from below and cooled from top and sides. These models, implemented in a computer code named MVITA, have been applied to predict the vessel thermal loads during core debris heat up and melting in the reactor lower head. It was found that the formation of melt pool is quite coherent and large melt pool volumes result coherently. If the reactor vessel is not cooled from outside, the vessel melt-through is inevitable. With vessel external cooling, the melt pool can be retained inside the vessel for moderate power densities (or reactor power level), even though partial wall melting may occur. Modeling of the crust formation has been included in the MVITA code. We believe that it is the first time that the melt pool, crust layers, metallic layer

and the vessel have been described in an integrated two-dimensional fashion and the results obtained showed that the vessel thermal loads are reduced due to the 2D heat diffusion in the vessel.

The second part of the first chapter deals with the issue of *local vessel failure* and its modeling. Specifically, the process of melt discharge from the local failure of the vessel and the dynamics of the failure enlargement caused by the melt discharge process are considered. A general model, integrating major physical aspects of melt discharge and failure site enlargement, is developed. Analysis, based on this integrated model, was performed to study the effects of various parameter uncertainties. It was shown that significant narrowing of the uncertainty range of the process important parameters, such as the final size of the failure in the vessel and the mean discharge rate of the core melt to the containment, could be achieved when employing the new understanding of hole ablation phenomenology.

In the second chapter, modeling efforts are directed towards investigating the phenomenology of the mixing of a corium melt jet, discharging from the reactor vessel, with water, present in the BWR containment lower drywell. Particular attention is focused on the break-up of the melt jet in water, the behavior of the fragments, as well as on the dynamics of the mixing zone and its feedback to the break-up process. Numerical methods, which allow solution of the mathematical models of the multiphase system with minimal numerical diffusion, are developed and used to investigate relevant interfacial phenomena, such as Kelvin-Helmholtz instabilities and jet/drop fragmentation in a flow field. The development of surface instabilities and fragmentation of melt jet or drops were found to be affected strongly by the property variations in the melt-coolant system caused, e.g., by the melt solidification and water vaporization. It was found that break-up of a high-density melt drop in the water flow field is dominated by the shear break-up mode, except when the melt drop has high viscosity. The break-up of a heavy melt at the leading edge due to Rayleigh-Taylor instabilities was found to be governed by the jet-water density ratio and jet velocity. An integrated model of melt-water interactions is also developed in this work, which takes into account major physical phenomena and inter-relations. Results of the analysis using this model indicate the sensitivity of the general behavior of the melt, drop, and water fields on a number of key factors, e.g., the heat transfer regimes (film boiling and radiation), final fragment size, dynamics of water vaporization and steam condensation, etc.

The third chapter of the dissertation is devoted to the problem of ex-vessel debris bed coolability, i.e., behavior of a core debris bed, located on the containment floor, and the ablation of containment concrete basemat. The relevant

physical processes are described by a simple model, which takes into account the dynamics of crust growth and the physical-chemical aspects of molten corium-concrete interactions. Stability of the crust layer, separating the melt pool portion of the debris bed and the molten concrete, as well as the heat transfer through this layer (which is similar to that of film boiling) were found to be important factors for concrete ablation. Coolability of an ex-vessel core debris bed is determined by the bed *geometrical configuration and structure*, which define the area available for cooling from outside. If such cooling is insufficient, concrete melt-through is feasible.

Keywords: *light water reactor, severe accidents, melt-structure-coolant interaction, melt pool formation, hole ablation, jet fragmentation, drop breakup, premixing, debris coolability, natural convection, heat transfer, instabilities, multiphase flow, phase change.*

Preface

This thesis is based on the results of research activities, carried out by the author during the period from 1994 to 1998 at the Nuclear Power Safety Division, Royal Institute of Technology (KTH). The results of these research activities have been summarized and described in the following publications:

1. **V.A. Bui**, "Chapter 9: Debris Coolability", *SKI Report 95:76 by T. Okkonen, T.N. Dinh, V.A. Bui, and B.R. Sehgal*, "Quantification of the Ex-Vessel Severe Accident Risks for the Swedish Boiling Water Reactors", July 1995.

2. **V.A. Bui** and T.N. Dinh, "An Approximation of Turbulent Prandtl Number in Thermally Developing Flows", *Proceedings of the Second CFD Colloquium on "Process Simulation"*, Helsinki University of Technology, Espoo, Finland, pp.149-163, 1995.

3. T.N. Dinh, **V.A. Bui**, R.R. Nourgaliev, T. Okkonen, and B.R. Sehgal, "Modeling of Heat and Mass Transfer Processes During Core Melt Discharge From A Reactor Pressure Vessel", *Int. J. Nuclear Engineering and Design*, Vol. 163, pp.191-206, 1996.

4. **V.A. Bui** and T.N. Dinh, "Modeling of Heat Transfer in Heat-Generating Liquid Pools by an Effective Diffusivity-Convectivity Approach", *Proceedings of the 2nd European Thermal-Sciences Conference*, Rome, Italy, 29-31 May 1996, pp.1365-1372.

5. **V.A. Bui**, T.N. Dinh and B.R. Sehgal, "Numerical Modeling of Heating and Melting Processes in Internally-Heated Debris Beds in a Reactor Vessel Lower Plenum", *Proceedings of the Fourth International Conference "Heat Transfer-96"*, 8-10 July 1996, Udine, Italy.

6. **V.A. Bui**, T.N. Dinh, and B.R. Sehgal, "In-Vessel Core Melt Pool Formation during Severe Accidents", *Proceedings of the National Heat Transfer Conference*, Houston, Texas, August 3-6, 1996, HTC-Vol.9, pp.86-94.

7. T.N. Dinh, **V.A. Bui**, R.R. Nourgaliev, and B.R. Sehgal, "Crust Dynamics under PWR In-Vessel Melt Retention Conditions", *Proceedings of the 1996 National Heat Transfer Conference*, Houston, Texas, August 3-6, 1996, HTC-Vol.9, pp.368-375.

8. B.R. Sehgal, T.N. Dinh, J.A. Green, **V.A. Bui**, R.R. Nourgaliev, T.J. Okkonen, A.T. Dinh, "Experiments and Analyses of Melt-Structure-Water Interactions during Severe Accidents", *Research Report submitted to Swedish Nuclear Power Inspectorate (SKI) and US Nuclear Regulatory Commission (NRC)*, April 1997, 250p.

9. **V.A. Bui**, T.N. Dinh and B.R. Sehgal, "Deformation and Fragmentation of a Melt Drop in the Flow Field: Results of a Numerical Study", *Proceedings of Intern. Seminar on "Vapor Explosion and Explosive and Eruptions, AMIGO-IMI"*, Sendai-City, Japan, May 22-24, 1997.

10. T.N. Dinh, **V.A. Bui**, R.R. Nourgaliev, J.A. Green, and B.R. Sehgal, "Experimental and Analytical Study of Molten Jet-Coolant Interactions: The Synthesis", *OECD/CSNI Specislist Meeting on "Fuel Coolant Interactions (FCI)"*, JEARI-Tokai, Japan, May 19-21, 1997.

11. **V.A. Bui**, T.N. Dinh, and B.R. Sehgal, "Numerical Simulation of Surface Instability Phenomena Associated with Fuel-Coolant Interaction", *Proceedings of the Eighth International Topical Meeting on "Nuclear Reactor Thermal Hydraulics (NuReTH-8)"*, Kyoto, Japan, September 1997.

12. T.N. Dinh, **V.A. Bui**, R.R. Nourgaliev, and B.R. Sehgal, "Modeling of Heat Transfer Processes in Reactor Vessel Lower Plenum during the Late Phase of In-Vessel Core Melt Progression", *Proceedings of the Eight International Topical Meeting on Nuclear Reactor Thermal Hydraulics (NuReTH-8)*, Kyoto, Japan, September 1997.

13. **V.A. Bui**, T.N. Dinh, and B.R. Sehgal, "Numerical Investigation of Surface Phenomena Using The Front-Capturing Level Set Method", *Proceedings of the Int. Symposium on "Liquid-Liquid Two-Phase Flow and Transport Phenomena"*, Antalya, Turkey, 1997.

14. B.R. Sehgal, **V.A. Bui**, T.N. Dinh, and R.R. Nourgaliev, "Heat Transfer Processes in Reactor Vessel Lower Plenum during the Late Phase of In-Vessel Core Melt Progression", *J. Advances in Nuclear Science and Technology*, Plenum Publ. Corp, 1998 (to appear).

15. B.R. Sehgal, **V.A. Bui**, R.R. Nourgaliev, A.T. Dinh, A.A. Gubaidulline and T.N. Dinh, "Simulation of Intense Multiphase Interactions by CFD and DNS Methods: Exploring Capabilities and Limitations", *1998 Annual Meeting of Institute for Multifluid Science and Technology*, Santa Barbara, February 26-28, 1998.

16. B.R. Sehgal, T.N. Dinh, **V.A. Bui**, and R.R. Nourgaliev, "Investigation of Risk-Dominating Phenomena in Swedish LWRs", *Report for APRI-3/RAF Project*, March 1998, 180p. (to be published as SKI Report).

17. **V.A. Bui**, R.R. Nourgaliev, Z.L. Yang, T.N. Dinh, and B.R. Sehgal, "Advances in MVITA Modeling of Thermal Processes in the Reactor Pressure Vessel Lower Plenum with a Core Melt Pool", *CD-ROM Proceedings of International Conference on Nuclear Engineering, ICONE-6*, San Diego, CA, USA, May, 1998.

18. **V.A. Bui** and B.R. Sehgal, "Solidification and its Effect on Fragmentation of Melt Drop in Coolant", *3rd International Conference on Multiphase Flows*, Lyon, France, June 8-12, 1998.

19. A.A. Gubaidullin, Jr., **V.A. Bui**, and B.R. Sehgal, "Simulation of Bubble and Vapor Film Behavior in a Steam Explosion", *3rd International Conference on Multiphase Flows*, Lyon, France, June 8-12, 1998.

Contents

Abstract iii

Preface vii

Nomenclature xvii

Acknowledgements **xxi**

Executive Summary **xxiii**

1 Introduction **1**

2 Modeling of Melt-Structure Interactions **11**

2.1 Introduction 11

2.2 Modeling of the Thermal Transients Associated With the Debris Heatup/Melting and the Assessment of In-Vessel Melt Retention 12

2.2.1 Phenomenological picture and problem formulation 12

2.2.2 Model of heat transfer with anisotropic heat conduction . 14

2.2.3 Fixed-grid temperature-based enthalpy model for phase change 14

2.2.4 Effective conductivity-convectivity heat transfer model and its validation 15

2.2.5 Extending the predictive capability of ECCM for the heat transfer inside a molten metallic layer 17

2.2.6 Application of the models and integrated MVITA code for reactor predictions 19

2.2.7 Summary of the findings 22

2.3 Ablation of A Local Vessel Failure Site and Its Assessment . . . 24

2.3.1 Phenomenological picture and problem formulation 24

2.3.2 Modeling of turbulent heat transfer from the in-hole flow 26

2.3.3 Two-dimensional hole ablation model 27

2.3.4 Probabilistic analysis of the hole ablation and melt discharge processes 28

2.4 Concluding remarks 30

3 Modeling of Fuel Melt-Coolant Interactions 33

3.1 Simulation of the interfacial phenomena associated with hydrodynamic melt-water interactions 35

3.1.1 Background 35

3.1.2 Description of the modeling approach and solution algorithm 37

3.1.3 Summary of the simulation results 40

3.1.4 Summary of the modeling method and results 45

3.2 Integrated assessment of the ex-vessel melt-water interactions . . 47

3.2.1 Background and problem formulation 47

3.2.2 Quantification of the ex-vessel melt-coolant premixing . . 49

3.2.3 Mechanistic modeling of melt-coolant premixing 64

3.2.4 Summary of the results 70

3.3 Concluding remarks 71

4 Modeling of Melt-Concrete Interactions and Debris Coolability 73

4.1 Background and Problem formulation 74

4.2 The modeling approach 75

4.2.1 General features 75

4.2.2 Heat balance of the debris melt pool 78

4.2.3 The mass balance of the debris melt pool 79

4.2.4 Heat balance of the crust layers 79

4.2.5 Heat and mass balances of the concrete slag layer 80

4.2.6 Concrete decomposition and melting 80

4.2.7 Closure correlations 81

4.3 Summary of prediction results 84

4.3.1 Validation against the SWISS experimental data 84

4.3.2 The effects of the metal oxidation - Prediction of the SURC-4 experimental data 86

4.3.3 Prediction for the experiments using prototypic melt - the SURC-2 experimental data 88

4.3.4 The effects of the pool boundary condition change - Prediction of ACE-series experimental data 89

4.4 Concluding remarks 90

5 Conclusions **93**

Bibliography 96

A Paper 1: Heat Transfer Processes in Reactor Vessel Lower Plenum during a Late Phase of In-Vessel Core Melt Progression **105**

B Paper 2: In-Vessel Core Melt Pool Formation during Severe Accidents **143**

C Paper 3: An Approximation of Turbulent Prandtl Number in Thermally Developing Flows **159**

D Paper 4: Modeling of Heat and Mass Transfer Processes During Core Melt Discharge From A Reactor Pressure Vessel **177**

E Paper 5: Numerical Simulation of Surface Instability Phenomena Associated with Fuel-Coolant Interaction **203**

F Paper 6: Deformation and Fragmentation of a Melt Drop in the Flow Field: Results of a Numerical Study **221**

G Paper 7: Solidification and its Effect on Fragmentation of Melt Drop in Coolant **235**

Nomenclature

Arabic

A	Area, m^2
C	Mass concentration, kg/m^3
C_D	Friction coefficient
c_p	Specific heat capacity, J/kg·K
D	Diameter, m
d	Distance, m
Fr	Froude number, $Fr = U^2/(gD)$
G	Mass flow rate, kg/s
g	Gravitational acceleration, m/s^2
H	Height, m
h	Enthalpy, J/kg; Heat transfer coefficient, $W/(m^2.K)$
k	Thermal conductivity, W/(m.K)
L, l	Length, m
m	Mass, kg
Nu	Nusselt number, $Nu = hD/\lambda$
P, p	Pressure, Pa
Pe	Peclet number,
Pr	Prandtl number, $Pr = \nu/\alpha$
Q_v	Internal heat generation, W/m^3
Q, q	Heat flux, W/m^2
R, r	Radius, m
Rox	Oxidation rate, kg/s
Ra	Rayleigh number, $Ra = g\beta\Delta TH^3/\alpha\nu$
Re	Reynolds number, $Re = UD/\nu$
t	Time, s
T	Temperature, K
U, u V, v	Velocity, m/s
V	Volume, m^3
W	Work, J
x, y	Coordinates

Greek

α	Thermal diffusivity, m^2/s; Volume fraction, $1/m^3$

δ	Dirac delta function; thickness
κ	Surface curvature, 1/m
λ	Thermal conductivity, W/(m K)
μ	Dynamic viscosity, Pa·s
ν	Kinematic viscosity, m^2/s
ϕ	Level function
ρ	Density, kg/m^3
σ	Surface tension, N/m; Stephan-Boltzmann constant
τ	Time scale, s

Subscripts/Superscripts

a	ambient fluid
ab	ablation
bott	bottom
br	break-up
c	coolant, condensation
calc	calculation
cond	heat conduction
conc	concrete
cont	containment
cr	crust
D	Decomposition
d	melt drop/particle
db	debris bed
dc	discharge
dec	decay heating
fb	film boiling
ex	explosion
fus	fusion
h	homogeneous, hole
int	interfacial
j	jet
liq	liquid, liquidus
m	melt
mfb	min. film boiling
mp	melting point
mz	mixing zone
rad	radiation
s	surface, slug
sat	saturation
sd	sedimentation

sl	slug
sol	solid, solidus
sub	subcool
sup	superheat
t	turbulent
v	vessel, vapor, vaporization
w	wall, water
o	initial
$'$	saturated liquid
$''$	saturated vapor
∞	free-stream conditions

Abreviations

BWR	Boiling Water Reactor
CFD	Computational Fluid Dynamics
CIP	Cubic-Interpolated Pseudo-particle method
$ECCM$	Effective Conductivity-Convectivity Model
EPR	European Pressurized Reactor
LWR	Light Water Reactor
MAC	Marker And Cell method
$MCCI$	Molten Corium - Concrete Interactions
$(M)FCI$	(Molten) Fuel-Coolant Interactions
$MVITA$	Melt-Vessel InTeraction Analysis
NPP	Nuclear Power Plant
NPS	Nuclear Power Safety Division
PSA	Probabilistic Safety Assessment
PWR	Pressurized Water Reactor
RIT	Royal Institute of Technology (KTH)
RPV	Reactor Pressure Vessel
SKI	Svensk Kärnkraft Inspektorate (Swedish Nuclear Power Inspection)
TMI	Three-Miles-Island Reactor
VOF	Volume Of Fluid method
$VVER$	Russian version of PWR

Acknowledgements

First of all, I would like to thank my superviser, Prof. Bal Raj Sehgal, for providing excellent guidance and practical support during the whole time of my graduate research at NPS/RIT. I am also especially grateful to my advisor, Dr. Truc Nam Dinh, who has always been ready to help, answer questions and discuss ideas - often by suggesting new ones. Much of the work performed in this thesis could not have been done without the stimulation provided by Dr. Nam Dinh. Further, I would like to thank all my friends and colleagues at the division of Nuclear Power Safety, who, like myself, spend most of their time on the computer monitors, or at the experimental facilities, but are still willing to discuss various severe accident problems during their valuable timebreaks for coffee or lunch. Valuable comments and criticism from my former colleagues, Dr. Joseph Green (Joe) and Timo Okkonen, are also gratefully acknowledged. Special thanks to Louise Forshell for her assistance in preparing for the defense. Finally, I would like to thank my wife Loan for all love, understanding and endless support during these 4 years and, especially, the last three months. My family in Vietnam provides me great encouragement and I appreciate their patience for all the time I am faraway from home.

The work performed in this thesis was financially supported, in the frame of the following projects:

1. *"Experiments on Melt-Structure-Water Interactions during Severe Accidents"* funded by Swedish Nuclear Power Inspectorate (SKI), Swedish Power Companies Vattenfall, Sydkraft, Forsmark, Finnish Power Company TVO under the auspice of the APRI project;
2. *"Experiments on Melt-Structure-Water Interactions during Severe Accidents"* funded by Finnish Power Companies IVO and TVO and the Finnish National Laboratory VTT;
3. *"Experiments on Melt-Structure-Water Interactions during Severe Acci-*

dents" funded by Swiss Nuclear Power Safety Inspectorate (HSK);

4. *"Experiments on Melt-Structure-Water Interactions during Severe Accidents"* funded by the Nordic joint Nuclear Safety Project NKS;

5. *"Analysis of Natural Convection in Volumetrically-Heated Melt Pools"* jointly funded by Swedish Nuclear Power Inspectorate (SKI) and US Nuclear Regulatory Commission (US NRC);

6. *"Melt-Vessel Interactions MVI"* Project funded by European Union (Fourth Framework Programme);

7. *"Molten Fuel-Coolant Interactions MFCI"* Project funded by European Union (Fourth Framework Programme).

I would like to thank all the sponsors for the financial support provided and, particularly, to their representatives Dr. W. Frid, Mr. R. Espefal, Mr. V. Gustavsson, Mr. H. Dubik, Dr. S. Basu, Dr. H. Tuomisto, Dr. S. Chakraborty, Dr. U. Schmocker, and Dr. A. Zurita, who provided encouragement and several reviews of the work performed in this thesis.

Summary of Individual Contributions and Technical Accomplishments

	Technical Accomplishments and Contributions	*Chapters Appendices*
	I. Modeling of Melt-Structure Interactions	
1	The Effective Convectivity-Conductivity Method (ECCM) was formulated, which is able to provide correct descriptions of the energy split as well as the heat flux distribution on the side wall for a highly-turbulent decay heated core melt pool. Extensive validation of the method against experimental data was provided. The modeling method was also extented and validated for the case of natural convection heat transfer in a metallic layer, heated from the bottom and cooled from the top and side.	Chapter 2, App.A, App.B
2	The MVITA code, based on the energy conservation equation with anisotropic heat conduction and phase change and employing the ECCM, was developed. The essential aspects of the thermal interactions, e.g. anisotropic heat conduction, debris melting, natural convection heat transfer in the melt pool, convection heat transfer in the sep-	Chapter 2, App.A, App.B

	Technical Accomplishments and Contributions	*Chapters Appendices*
I. Modeling of Melt-Structure Interactions (cont.)		
2	arated metallic layer, vessel melting, etc., are included in the modeling. The code was employed to assess the possibility of melt retention inside a PWR vessel with external cooling as well as the timing of melt-through for a BWR RPV without external cooling. The reactor analyses using this model indicated the feasibility of the melt retention accident management scheme, based on the vessel external cooling. The analyses also helped to clarify the negative effect of a thin metallic layer and the positive effect of the multi-dimensional heat diffusion in the vessel wall on the margin available for in-vessel melt retention, especially for high-power reactors. It is the first time that the melt pool, crust layers, metallic layer and the vessel have been described in an integrated two-dimensional fashion.	Chapter 2, App.A, App.B
3	Heat transfer of the melt flow inside a hole was investigated. A formulation of the turbulent Prandtl number, Pr_t, in the thermal entrance region was developed, which is coupled with a low-Reynolds $k-\epsilon$ turbulence model to account for the thermal laminarization of the flow in that region. This formulation was validated against experimental data and has been employed to study the heat transfer of the in-hole melt flow.	Chapter 2, App.C
4	A two-dimensional model of the wall melting process while taking into account the protective effect of core melt crust has been developed. This model and numerical procedure are implemented in the HAMISA.2D/WALL code to describe the hole ablation process and the code has been employed to analyze the experimental data obtained from the NPS/RIT hole ablation experiments.	Chapter 2, App.D

	Technical Accomplishments and Contributions	*Chapters Appendices*
I. Modeling of Melt-Structure Interactions (cont.)		
5	A probabilistic assessment of melt discharge process was performed for selected 'bounding' scenarios of severe accident in the Swedish BWRs, based on the simple models of hole ablation and melt discharge processes. The assessment employed the new understanding obtained from the NPS/RIT hole ablation experiments to narrow the uncertainty ranges of the melt discharge parameters.	Chapter 2
II. Modeling of Melt-Coolant Interactions		
6	A numerical method, based on an advanced Navier-Stokes solver, coupled with the Level Set front-capturing algorithm, has been developed to investigate the interfacial phenomena, associated with hydrodynamic melt-water interactions. The method was realized in a computer code and was emloyed to study the interfacial phenomena associated with the hydrodynamic interactions between high-density melt with water. Particularly, the Kelvin-Helmholtz instability and the progression and fragmentation of melt jets and melt droplets in water flows were investigated by this method and code. A reasonably accurate picture of the interfacial behavior was observed. Insights into the physics of melt-water hydrodynamic interactions were gained and the effects of melt and coolant property variations were studied.	Chapter 3 , App.E App.F, App.G

	Technical Accomplishments and Contributions	*Chapters Appendices*
	II. Modeling of Melt-Coolant Interactions (cont.)	
7	Probabilistic analysis of melt-water premixing was performed. The analysis was based on the hydrodynamic balance assumption to define the melt mass in the mixing zone and on simplified models of jet fragmentation, droplet transport, and coolant thermal hydraulics, with emphasis placed on the detailed description of heat conduction and phase change inside the melt particles, and on the multiple thermal grouping of melt particles present in the mixing zone. Variation of the heat-radiation absorption by water for high melt temperature was taken into account. Analysis performed for the conditions typical for a severe accident in Swedish BWRs helps to estimate the uncertainty ranges of important premixing parameters, such as masses of melt particles and molten particles present in the mixing zone, average melt particle temperature, average void fraction of the mixing zone, etc.	Chapter 3
8	A mechanistic model based on the simplified multifluid models of melt jet, droplets, water and vapor, was developed to simulate the transient melt-coolant premixing. The model was successfully validated against the FARO L-24 experimental data and has been employed to perform the sensitivity studies on the effects of melt particle size and water subcooling on the premixing.	Chapter 3

	Technical Accomplishments and Contributions	*Chapters Appendices*
	III. Modeling of Melt-Concrete Interactions and Debris Coolability	
9	A 'lumped-parameter' model of melt-concrete interactions was developed to study the behavior and coolability of a core debris bed, which interacts with concrete at the bottom with water on the other sides. The most essential physical processes, i.e., the heat transfer from the melt pool to water and concrete, the formation of crust at the boundaries of the melt pool, the heat conduction inside the concrete, the change of the pool properties, i.e. density, viscosity, liquidus and solidus temperatures, etc., due to the mixing of concrete slag with pool materials and the change of pool temperature, were modeled. The model and code were extensively tested against the available experimental data.	Chapter 4

Chapter 1

Introduction

Beginning with the TMI-2 accident and later after the Chernobyl catastrophe, accidents beyond design basis, or severe accidents, become the focus of reactor safety. In the last 16 years, many analytical and experimental studies have been performed to shed light on the physical nature of the thermal and hydrodynamic phenomena, associated with severe accident progression. A more recent focus is on establishing the severe accident management schemes, which may mitigate the consequences of a severe accident if it occurs. The greatest concern of all of the research efforts directed towards severe accidents is the prevention and mitigation of release of radioactivity to the environment.

The progression of the core melt in LWR severe accidents is characterized by the interactions of the melt with in- and ex-vessel structures and with coolant (water) (see Fig.1.1). While the melt-structure (melt-vessel, melt-concrete) interactions usually occur at length, during which gradual degradation of the structure under attack occurs, the melt-coolant interactions are violent and of very short duration, during which rapid pressurization may occur inside the reactor vessel/containment resulting in dynamic loading of the vessel and containment structures. Water, as the coolant, is present in the vessel lower head and in the BWR containment dry well in most PWR and BWR scenarios.

Much research has been carried out in the past, and currently, to improve the understanding of the crucial physical phenomena associated with the melt-structure-water interactions during severe accidents. Experimental studies, performed in the framework of national and international collaboration, have been providing a large data base about various aspects of these interactions. The melt-vessel interactions and the in-vessel melt retention issues, for instance, led

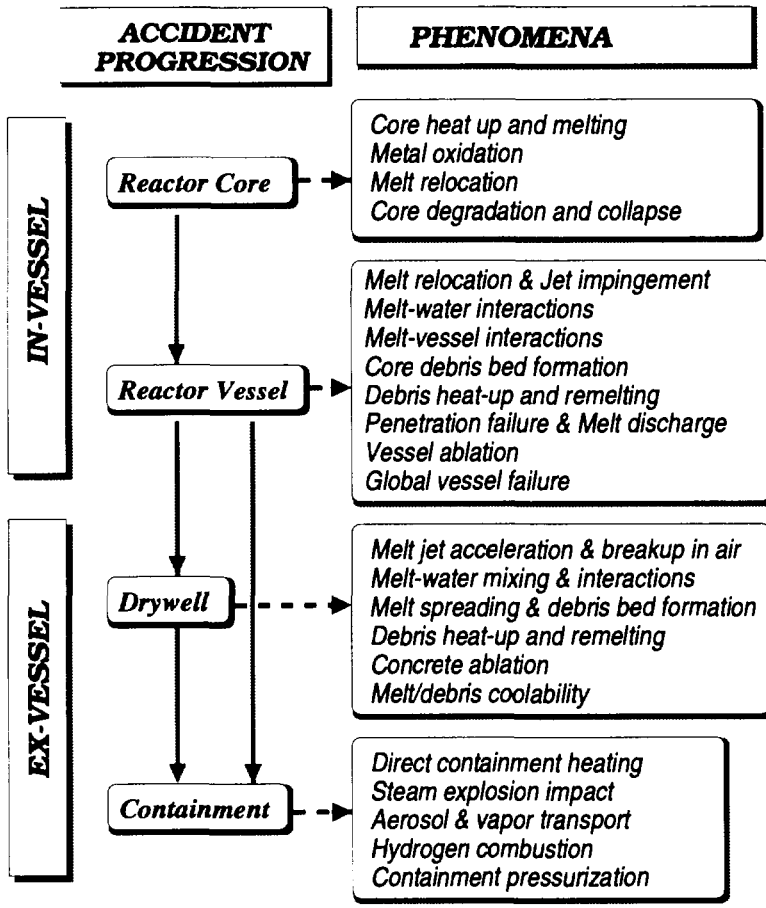

Figure 1.1: *Severe accident progression and associated physical processes/interactions for a BWR.*

to the initiation of many experimental programs around the world to study the *melt pool natural convection heat transfer* (e.g., COPO [49], ACOPO [82], UCLA [82], BALI [14], and RASPLAV [76] research programs, etc.), *structural behavior under high temperatures*, and other related phenomena. Local vessel failure and its development (ablation) have been intensively studied in the experimental program, carried out at the Nuclear Power Safety Division, Royal Institute of Technology (NPS/RIT)[71]. In more than a decade, many experimental programs have also been initiated to study molten fuel-coolant interactions (MFCI), which could be the cause of early containment failure. The experiments FARO, addressing melt jet fragmentation and premixing issue, and KROTOS, addressing steam-explosion issue, have been conducted for a number of years [38][53][54]. Melt spreading and debris coolability issues, which define

the long-term survival of the containment under melt attack, have also been the objective of many experimental studies, such as ACE[69], MACE[70], SURC[26], COMET[1], etc.

Recently, analytical models and numerical simulation are playing an important role in the development of the knowledge base about the relevant physical processes and phenomena. Basically, there are two reasons for it. First, severe accident physical phenomena involve extremely high temperatures, high pressures, high heat generation rates, etc., which can not be easily reproduced in the laboratory conditions. Second, together with the great improvement in our understanding of the micro-physics associated with severe accident phenomena and the quick advances of computational methods and the computer power, the modern numerical simulation methods can be used efficiently to obtain insights about a particular physical phenomenon. At the same time, these methods can provide an integrated description of a big process with many phenomena together with their interactions and feedbacks. In severe accident studies, mechanistic modeling has been employed to investigate, for instance, the melt pool convection heat transfer [30], the effects of convection heat transfer inside a metallic layer [31], melt jet instabilities and break-up in water [18], etc. Besides mechanistic modeling, integrated models and codes have been developed and applied to study complete processes, e.g., vessel local-failure ablation (HAMISA code) [28], melt-water premixing (PM-ALPHA code) [81], core debris-vessel interactions (MVITA[72] and LOWHED[84] codes), etc. Additionally, integrated analyses have been also used to investigate the probabilities of global/local vessel failure, frequency of a steam explosion under melt-water interactions, or timing of containment basemat melt-through.

The current work summarizes results of modeling efforts, directed to describe the various processes of melt-structure-water interactions, occurring during the severe accident progression in LWRs. Particular focus is placed on the melt progression period beginning with a quenched debris bed, located on the lower head of a LWR vessel, and ending with a core debris bed, attacking the concrete floor of the containment. From the spectrum of possible physical processes and interactions occurring during this period (see Fig.1.1), the following processes have been selected for study in this dissertation:

1. Melt pool formation in a quenched debris bed and the thermal loads exerted on the vessel

Since the RPV is a major line of defense for preventing release of radioactivity, maintaining the integrity and survival of the RPV under thermal attack of the decay-heated core debris bed is of great importance. During the severe accident scenario, if an early vessel failure due to jet impingement or in-vessel steam explosion did not occur, the reactor vessel might be subjected to a long-term thermal attack from the debris bed. If the amount of water in the vessel lower head is sufficiently large and the rate of melt relocation is not so large, a quenched debris bed may form in the lower head. If no more water is supplied to the vessel, the core debris bed will eventually dry out and remelt to form a melt pool. In contrast to the case of a solid debris bed, where the heat flux from the bed surfaces to the vessel wall is almost uniform, the natural convection flows inside the internally heated liquid melt pool impose a non-uniform distribution of heat flux on the vessel hemispherical wall. The peak heat flux occurs near the upper pool corner and the vessel wall at that location becomes most vulnerable to a melt-through or a creep rupture. This scenario could result in global vessel failure.

The correct prediction of the effects of natural convection heat transfer inside a prototypic melt pool is, therefore, very important for the assessment of the vessel failure mode and as a corollary for the assessment of in-vessel retention through cooling of the external vessel wall. So far, the empirical work, directed towards melt pool convection investigation has been mostly restricted to small scale experiments with use of prototypic melt materials (RASPLAV[76], SCARABEE BF1[42]) or to larger scale experiments with use of melt simulants (COPO, UCLA, ACOPO, BALI, etc.). The experimental results from the simulant material experiments have been extrapolated to the prototypic melt pool configurations, although some questions have been raised. So far, analyses of natural convection heat transfer, based on 'first-principle' flow and turbulence modeling, suffers from the inaccuracy of the standard turbulence models for the stable and unstable stratified flow conditions (the Rayleigh number can be as high as 10^{17}) and the inefficiency of the current numerical solver. In the present work, an innovative and efficient model of the melt pool convection heat transfer based on measured heat transfer correlations has been developed and validated in Chapter 2.

The magnitude of thermal attack from the debris bed on the vessel wall is affected by the thickness of the crust layer, located between the melt pool and the vessel wall. The thickness of the protective crust layer is largely determined

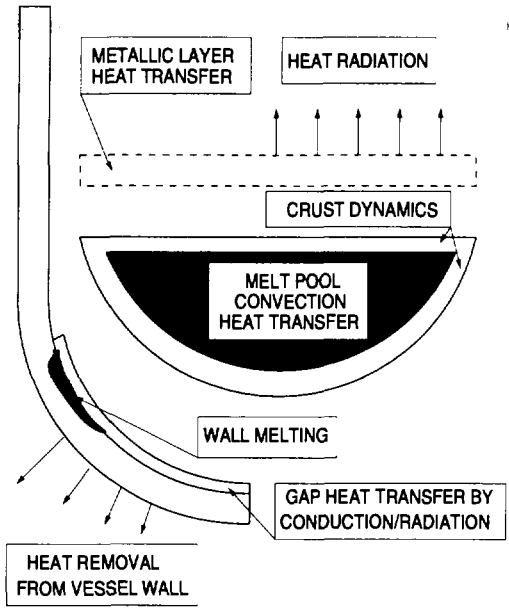

Figure 1.2: *In-vessel Melt-Structure Interactions under Debris Heatup and Melting.*

by the temperature of the vessel wall, which, in turn, is governed by the efficiency of the heat removal from the vessel outer surface. Moreover, local vessel wall melting beneath the crust may also affect the stability of this layer. A crust layer may also exist on the top of the core melt pool, which maintains a constant-temperature boundary condition for the melt pool. The top crust layer may crack when it becomes too thin and unstable. For such conditions, the top boundary condition of the melt pool may also change, which can affect both the convection inside and the heat removal from the pool. A mechanistic assessment of the effects and behavior of such a crust layer is also presented in Chapter 2.

During debris melting and pool formation in the lower head of reactor vessel, segregation of melt components may occur because of density differences. The metallic components (mainly Ze and Fe), which are lighter than the oxidic ones, may float on the top and form a metallic layer above the oxidic melt pool. Under such conditions, the path of heat removal from the top of the debris bed may change due to the effects of greater heat conduction and natural convection heat transfer in the metallic layer. The presence of such a metallic layer raises some concern for the vessel integrity, since a large fraction of the heat removed from the top of the oxidic melt pool could be focused to the side of the metallic layer and threaten the vessel wall at that location [82]. Physically, the heat transfer inside such a layer is governed by a mixture of the

Rayleigh-Benárd and the side boundary layer development convections, which has been studied on separate-effect basis both analytically and experimentally. An integrated multidimensional assessment of the effects of the metal layer for prototypic conditions has been performed in Chapter 2.

Recently, the accident management concept of melt retention inside the vessel has been accepted for the Finnish Loviisa (VVER-440) and is under review for the AP-600 reactor by providing for the RPV submergence is submerged into water in the event a severe accident is threatened. In this case, heat removed by water nucleate boiling on outer surface of the RPV may be sufficient to prevent the vessel melt-through and even preclude vessel wall creep-rupture [79][82]. This scenario has been analyzed in the present work with the use of the MVITA modeling approach, presented in Chapter 2.

2. Local vessel failure and its dynamics - hole ablation issue

Local vessel failure of LWR vessels is of primary interest, since these vessels have an array of penetration tubes in the lower head, housing the control rods and instrumentation lines for BWRs and instrumentation lines for PWRs. Under thermal attack from the in-vessel core debris bed, these penetration tubes may fail for several reasons, e.g., (a) creep of vessel wall around the tubes, (b) tube weld failure and subsequent tube ejection under system pressure, and (c) melt entry into the penetration channels [66]. The liquefied melt, accumulated on the vessel lower head, may flow through the holes and discharge into the containment. If the hole diameter is small, and the melt's superheat is low, an in-hole crust may develop and grow to form a blockages. Larger diameter holes may ablate and grow larger in size if sufficient melt discharge occurs.

The timing of the local vessel failure is of interest for severe accident assessment and management. On the one hand, it is desirable to retain the melt inside the reactor vessel as long as possible, however, on the other hand, it is also desirable to not have a large amount of core melt discharging from the vessel at the time of vessel failure. In addition, accumulation of a large quantity of core melt inside the vessel lower head could pose a threat of global vessel failure.

A review of experiments conducted in the past, mainly at Sandia National Laboratory (SNL), can be found in the paper by Pilch [63]. Experiments and model development have been conducted at NPS/RIT in order to gain an improved understanding of the complex melt-vessel interaction processes which occur during vessel failure and melt discharge [29].

Uncertainty in hole ablation predictions arise from a number of sources. The hole ablation dynamics is driven by the melt flow thermal hydraulics and the dynamics of the in-hole crust. Since the hole length is comparable to its diameter, the hydrodynamics and heat transfer in the hole may differ from that of a developed flow. The instability of the in-hole crust, separating the hot melt stream and the molten wall, also complicates the boundary conditions for heat transfer under ablation. Some aspects of the in-hole thermal hydraulics as well as hole ablation process are addressed in the present work (see Chapter 2, part 2.3).

The characteristics of melt discharge, i.e., the melt jet diameter and the mass flow rate, affect the later phases of the accident progression, especially when it involves ex-vessel melt-water interactions. A high speed, large diameter melt jet may not completely fragment in the lower dry well pool of a Swedish BWR and a melt pool may attack the concrete basemat. A smaller diameter melt jet may break up, fragment and premix sufficiently with the subcooled water to develop a containment-threatening steam explosion. In this work (Chapter 2, part 2.3) probabilistic distributions of melt discharge characteristics are defined employing as basis the deterministic models for hole ablation developed at NPS/RIT.

3. Ex-vessel melt-water interactions - premixing phase

Investigation of the ex-vessel melt jet behavior has been conducted in the past, but primarily for ejection under high pressure and without water under RPV [36]. The deliberate flooding with water of the lower dry well in the containment space below RPV is provided in the severe accident management strategy adopted for the ABB BWRs. This strategy has raised concern about the possibility of a steam explosion with impulse loadings large enough to fail the containment early. Alternatively the melt-water interactions may be benign, i.e., they may fragment the melt jet and create a permanently coolable particulate debris bed of temperature much below the concrete decomposition temperature.

In the last decade, several experimental programs were performed to investigate the melt-water interaction issue. Specifically, the MAGICO [3], BILLEAU [12], and QUEOS [57] tests were conducted, using jet-like configurations of hot spheres, in order to obtain data for validation of the pre-mixing models and codes [81][55][39][11]. The interactions of melt with coolant have been experimentally investigated in FARO (Ispra, Italy)[53][54] and PREMIX (FzK, Karlshure, Germany)[41][11] tests at high temperatures, using both prototypic and

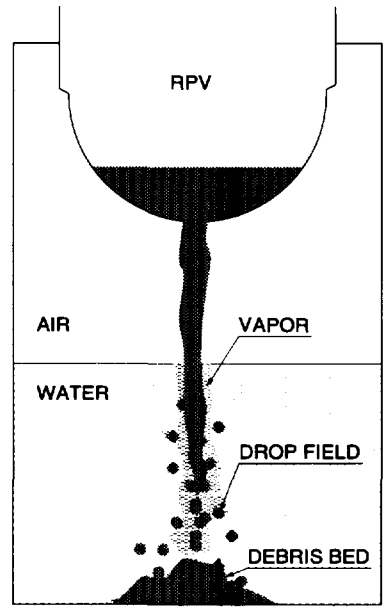

Figure 1.3: Conceptual illustration of the ex-vessel melt discharge and corium-water interactions

thermite melts, and in JEFRI tests (IKE, Stuttgart, Germany)[20] at low temperatures, using Wood's metal as jet simulant fluid and freon R113 as coolant. It is worth noting that in high-temperature tests the melt mass was limited, so that a quasi-steady state of melt-water interactions, which is relevant to the prototypic severe accident case, might not have been achieved.

Difficulties in the analysis of melt-water premixing arise due to various phenomenological uncertainties associated with the complex nature of and feedbacks between melt-water hydrodynamic and thermal interactions. In general, hydrodynamic corium-water interactions are characterized by the *fragmentation behavior* of the melt in water and thermal interactions are characterized by *melt quenching/solidification* and *water vaporization*. Thermal interactions between corium and water could indirectly feedback to the fragmentation behavior of the corium due to the change in the characteristics of the coolant (void content) and of the corium properties (due to solidification). Recently, direct influence of thermal interactions on fragmentation under shock propagation conditions has also been reported [25].

In this work (Chapter 3), some aspects of the hydrodynamic melt-water interactions, i.e. break-up and fragmentation of melt jets and droplets in water, are investigated by means of a 'first-principle' direct numerical simulation,

which employs an advanced numerical method with explicit interfacial tracking. Further on, quantification of the ex-vessel melt-water premixing is performed by means of a probabilistic assessment and mechanistic modeling. In the probabilistic assessment, important scenario and phenomenological uncertainties are addressed and as a result probabilistic distributions of important premixing characteristics are obtained. Finally, an integrated mechanistic model of melt-water premixing is developed and validated against experimental data.

4. Ex-vessel debris bed coolability

Ex-vessel debris bed could form as a result of melt deposition on the containment floor after discharge from the reactor vessel. If the containment floor is dry, the melt could reach it without significant change in temperature. The liquid melt, therefore, could spread on the floor and form a homogeneous melt layer. The coolability of such a layer is largely defined by the layer thickness and its heat removal area, which, in turn, are determined by the characteristics of the melt spreading. When the containment is filled with water (as a result of the severe accident management procedure, adopted by the ABB BWRs, for instance), the melt can partly or fully fragment before reaching the containment floor; the melt temperature could decrease significantly during the melt-water interactions; and, as a result, a quenched particulate debris bed may form. The porosity of the debris bed formed is defined by the size distribution of the debris fragments. Coolability of such a particulate debris bed depends on the competing processes of decay heat generation and cooling. Cooling of the debris bed by water is quite efficient and, for a porous debris bed, water ingress into the porous structure of the debris bed may intensify debris cooling. If cooling is insufficient, the debris bed can heat up and remelt, which leads to the formation of a core melt pool on the containment floor. Under the thermal attack from the debris bed, the concrete temperature may exceed the decomposition temperature and concrete ablation results. The generation of large amount of gases from concrete ablation may cause containment over-pressurization to failure.

Most uncertainties associated with the assessment of ex-vessel debris coolability are related to the unknown form, composition, and porosity of the initial debris bed, which are defined from the previous stages of accident progression (ex-vessel melt discharge, possible melt-water interactions, melt spreading). The long-term coolability of an ex-vessel debris bed is also determined by the cooling condition around the bed. Spreading can also be considered as a measure to provide large areas for heat removal from a melt layer (EPR severe accident management strategy). Moreover, more active way to achieve debris coolability

may also be provided by top or bottom flooding and quenching of the debris bed by water. The possibility of debris cooling by top flooding has been studied in the MACE experiments [69][56], where it was found that cooling with a water overlayer may not be sufficient for a thick debris layer, since a tough crust formed on the upper surface of the debris bed may restrict the access of the water from overlayer to the melt. Results of COMET-H experiments [1] showed that bottom injection is an efficient mechanism providing long-term debris coolability.

The issue of debris bed coolability is addressed in Chapter 4 where the processes of debris heatup, melting and concrete ablation are included in the modeling.

The severe accident issues considered in this dissertation form a logical sequence of melt progression and melt-structure-water interaction investigation. A combination of 'first-principle' phenomenological and integrated modeling approaches have been developed to study different physical processes, involved in this sequence. The 'first-principle' modeling approach is utilized, when ever possible, to study particular physical phenomena (such as jet/drop deformation and fragmentation), while integrated, but still highly mechanistic, modeling is developed to assess processes comprising of many inter-related phenomena (such as in-vessel melt retention, melt-water premixing, etc.). It is worth noting that there are other relevant problems, which are out of the scope of this dissertation. From which, one can count, for instance, the issues of penetration failure, melt spreading, steam explosion, etc. The process of melt relocation prior to the formation of an in-vessel quenched debris bed and containment phenomena (hydrogen propagation and combustion) have also not been studied in this dissertation.

Chapter 2

Modeling of Melt-Structure Interactions

2.1 Introduction

On melt relocation from the reactor core to the lower head, the processes of thermal and hydrodynamic interactions of the high-temperature core melt with the in-vessel structures and vessel itself begin, which may potentially compromise the vessel integrity. During the course of such interactions, the reactor vessel lower head may fail because of several mechanisms, which have been identified [66] as

- *Jet Impingement.* Relocation of the melt from the reactor core in the form of a coherent jet, impinging directly onto the vessel wall causes local ablation and failure of the vessel lower head.

- *Penetration Tube Heatup and Failure.* Various penetration tubes in the vessel lower head may fail as a result of melt entry into the penetration channels, or tube-vessel weld failure, and subsequent tube ejection under gravity or system pressure.

- *Lower Head Global Failure.* Heatup of the wall of the vessel lower head under sustained heating from the accumulated debris bed may lead to vessel melt-through or creep deformation, which may lead to a global rupture of the lower head.

Prediction of the integrity of the RPV lower head during core melt-vessel interaction has been the subject of much experimental and analytical research, performed for both PWR and BWR reactors. A review of previous studies, related to the assessment of RPV thermal loadings and vessel failure, can be found, for example, in the work by Rempe et. al. [66]. Separate-effect modeling and assessment directed to obtain detailed information about specific processes and phenomena involved, e.g. debris heat up and melting, melt pool convection heat transfer, jet impingement heat transfer, etc. have been performed in the last decades. In addition, integrated assessment has also been pursued to investigate *plausible modes* of reactor vessel lower head failure and to define the major factors and accident scenarios, which can affect or lead to these failures.

In this work, two important issues associated with vessel lower head failure under melt-vessel interactions are investigated. The first issue concerns the failure of RPV under *sustained thermal attack* from an *initially quenched in-vessel core debris bed.* Models are developed for the debris melting and the melt natural convection heat transfer. Based on the developed models, the probability of the vessel survival and in-vessel melt retention is analyzed. The second issue is related to some important aspects of the physics of *local vessel failure*, e.g. dynamics of the failure size enlargement and the character of the melt discharge from the RPV. A phenomenological model has been developed for the hole ablation process.

2.2 Modeling of the Thermal Transients Associated With the Debris Heatup/Melting and the Assessment of In-Vessel Melt Retention

2.2.1 Phenomenological picture and problem formulation

The thermal transients developing inside an initially quenched debris bed, located on the lower head of a RPV, are due to the decay heat generation, which results in the heat-up and subsequent melting of the debris bed. During such transients, the characteristics of the heat transport and thermal loads on the reactor vessel may change greatly as a result of melt pool formation and changes in the crust thickness. Formation of a melt pool as a result of debris remelting and the domination of natural convection heat transfer over heat conduction in such a pool change the distribution of the heat flux imposed on the vessel wall. In addition, if a metallic melt layer is resident on top of the oxidic, heat

generating pool due to phase separation, the focusing of heat flux at the upper boundary of the melt pool towards the side wall of the vessel may reduce the margin for melt retention inside the vessel. The focusing effect is particularly large for a thin metallic layer and vessel wall failure at near $90o$ angle could occur either as a melt-through or with large creep deformation. A thermal steady state inside such a system can only be reached if the heat removal from the debris bed balances the decay heat generation.

So far, the issue of melt-vessel interactions has been addressed in different ways. Besides the large- and small-scale experimental studies, performed to investigate this issue, e.g., the melt pool natural convection heat transfer experiments (COPO, UCLA, ACOPO, etc.), melt pool stratification experiments (RASPLAV), experiments on focusing effect in metallic layer (BALI, MELAD), analytical work has also been carried out to assess both separate effects and intergal phenomenology of debris-vessel interactions and in-vessel melt retention. The analytical assessment can be based on simple 'lumped-parameter' models such in the MAAP, MELCOR, and APRIL codes, or on more complex 2D/3D mechanistic models of the debris bed and reactor vessel such in the case of RELAP-5/COUPLE, PASULA, LOWHED, and CORIUM-2D/3D codes. It is worth noting that, due to the difficulties associated with the direct numerical simulation of *highly-turbulent* pool convection, the representation of natural convection heat transfer in the molten debris may be omitted (PASULA) or provided by some *simplified* models (RELAP-5/COUPLE, CORIUM-2D/3D) in the 2D/3D codes. A review of existing modeling approaches and computer codes is provided in Table 2.1 (see also Appendix A). [17].

Table 2.1: Summary of MVI codes and modeling approaches

Approach	Code/Model	Remark
Lumped-Parameter	MAAP MELCOR APRIL BWRSAR MARCH/STCP	
Multi-dimensional	RELAP5/COUPLE PASULA LOWHED CORIUM-2/3D	2D/effective heat conduction 2D/conduction only 2D vessel/1D debris bed simplified convection heat transfer

The current study is motivated by the need for an integral analysis of the behavior of debris bed and reactor vessel during relatively long-term (several

hours) thermal transients and the timing of possible vessel failure before a thermal steady-state, if any, can be reached. A *mechanistic model* of thermal transients inside an initially quenched debris bed, located on the lower head of LWR reactor vessel was developed. The model is based on (i) a description of homogeneous anisotropic heat conduction inside the porous debris bed; (ii) a fixed grid phase-change model, employing the temperature-based enthalpy method; (iii) an effective conductivity-convectivity model (ECCM) of natural convection heat transfer in the molten part of the debris bed; (iv) a simple creep-rupture model for RPV. The effect of a separate metallic layer was also accounted for by extending the ECCM for the Rayleigh-Bénard type natural convection heat transfer inside the metallic layer. The general model was realized in a computer code (MVITA), which was extensively validated against available experimental data and has been applied to analyze the coolability and retention of the debris bed with cooling of the vessel outside wall, as well as the timing of RPV global failure, if any.

2.2.2 Model of heat transfer with anisotropic heat conduction

The current modeling approach is based on the solution of an energy conservation equation, derived for a two-dimensional general curvilinear domain in Cartesian and cylindrical axisymmetric coordinate systems. The equation was modified to account for *the anisotropic heat conduction* inside the debris bed with assumptions about the homogeneous orthotropic characteristics of the thermally anisotropic medium. This formulation of energy equation can be employed to describe the anisotropic heat conduction inside the debris bed caused by non-uniform material distribution. Moreover, as described later, natural convection heat transfer inside the melt pool can also be modeled using this anisotropic heat conduction model. The full description of the analysis method can be found in Appendix A.

2.2.3 Fixed-grid temperature-based enthalpy model for phase change

Phase change associated with remelting inside the debris bed is described by a fixed grid, temperature-base, enthalpy method [21]. Based on a formulation of enthalpy conservation, which is common for the solid, liquid, and interfacial (mushy) regions, the energy equation was modified to account for the phase change in the debris and the formation of a molten debris pool. The final form of the energy conservation equation is given in Appendix B. In general, accounting

for phase change results in a modification of the specific heat coefficient and an additional source term in the energy equation.

2.2.4 Effective conductivity-convectivity heat transfer model and its validation

In the decay-heated melt pool, natural convection heat transfer is the dominant mechanism governing the heat transport inside the pool and the magnitude of heat removal at the pool boundaries. The flow intensity is characterized by the Rayleigh number, which can be as high as 10^{17} for a prototypic reactor melt pool. In this dissertation, an innovative modeling approach is developed [16], based

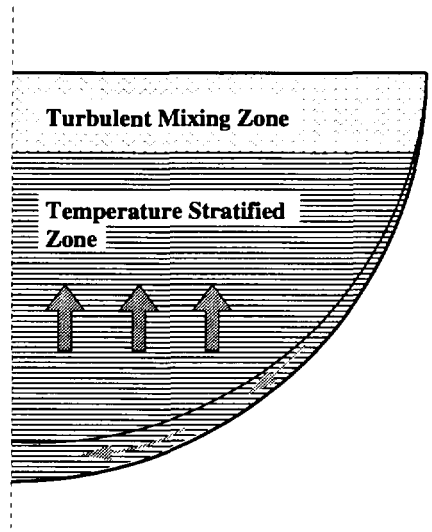

Figure 2.1: *Physical representation of natural convection inside an internally heated pool.*

on an *effective* representation of the convective and diffusive terms in the energy conservation equation, thus eliminating the need for solving the momentum equations. The heat transfer inside an internally heated, convective melt pool, cooled from all sides, is assumed to be driven by two major mechanisms (see Fig.2.1): (1) vertical movement of stratified fluid layers in the lower part of the pool and vertical turbulent mixing at its upper part; and (2) heat transfer to the side wall through a boundary layer, developing downwards along the cooled wall. The first mechanism is modeled by means of a newly developed *effective convectivity approach*, in which the heat transfer in the vertical direction is assumed to be driven by an effective velocity field, analytically derived from the

pool characteristics and the cooling conditions at the pool boundaries. Since a uniform velocity field is specified for the entire pool, mass and energy loss may occur as a result of in- and out flows at top and bottom boundaries. A treatment has been introduced to ensure energy and mass conservation inside the system, which is based on *redistribution of the heat and mass fluxes at the boundaries to the inner part of the pool.* In this modeling approach, when cooling takes place on the side of the pool, another mechanism is introduced and modeled using the *effective diffusivity approach*, which was first developed by Cheung et al.[78][23]. In this approach the heat conductivity in the horizontal direction inside the boundary layer or the pool is modified in accordance with the heat transfer coefficient at its boundary. Combination of above two modeling approaches allows to describe the heat transfer inside fluid layers or pools, cooled at all boundaries. More details about the method and the formulation of the effective velocity for a fluid layer and a pool can be found in [16] (and Appendix A). Together, the models described in previous sections comprise the MVITA code.

Table 2.2: Summary of the ECCM Validation [16].

Geometrical configuration	Experimental data
Top-cooled fluid layers	Kulacki et al. [48][47]
Top- & bottom cooled fluid layers	Kulacki et al. [46]
Side-cooled fluid layers	Steinberner & Reineke [75]
Isothermal boundary square cavities	Steinberner & Reineke [75]
Semicircular pools	Jahn & Reineke[40], COPO [50]
Hemispherical pools	UCLA[5], mini-ACOPO[82]

Validation of the MVITA models has been performed by analyzing a number of experiments employing internally-heated fluid layers and pools under different boundary conditions (see Table 2.2). In the calculations, the effective vertical velocity is estimated from the heat transferred at the top and bottom boundaries, while the effective heat conductivity is derived by employing Eckert-type formulation for heat transfer across a developing boundary layer [22] on the side boundaries. This procedure provided reasonably accurate description of the heat flux distribution on the side boundary and the temperature field inside the layer (or the pool) for both steady-state and transient cases. In addition, the calculated amounts of heat removal from all boundaries of the layer (pool) are in good agreement with the experimental data, which means the energy split was correctly predicted.

Validation was also performed against the COPO and UCLA experimental data, which were obtained for the pool natural convection heat transfer at very high Rayleigh numbers ($1.34 \cdot 10^{14}$-$1.61 \cdot 10^{15}$ in COPO and 10^{11}-10^{14} in UCLA experiments). The COPO experiments employed a two-dimensional "slice" of the Loviisa torospherical lower head (including a portion of the cylindrical vessel) at half scale. In UCLA experiments the pools had spherical form and contained Freon-113, which was volumetrically heated using microwave energy. For both cases, the ECCM modeling approach provided not only correct heat transfer coefficients on the cooling surfaces but also the correct heat flux distributions on the cooled side wall for the whole range of Rayleigh numbers (see Figs.2.2-2.3 [17]).

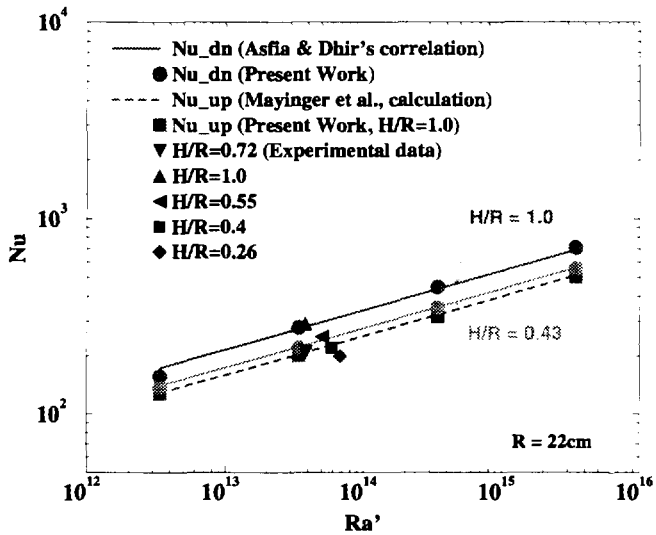

Figure 2.2: Comparison of the MVITA calculated Nusselt numbers with other analytical and experimental results.

2.2.5 Extending the predictive capability of ECCM for the heat transfer inside a molten metallic layer

In a postulated severe accident scenario with core melt-down, a metallic layer may form on top of the debris bed (or melt pool) as a result of the pool material separation (due to density difference) or due to direct deposition of molten in-vessel metallic structures on top of the oxidic debris bed. A metallic layer, due to its high heat conductivity, may focus some of the heat directed to the top

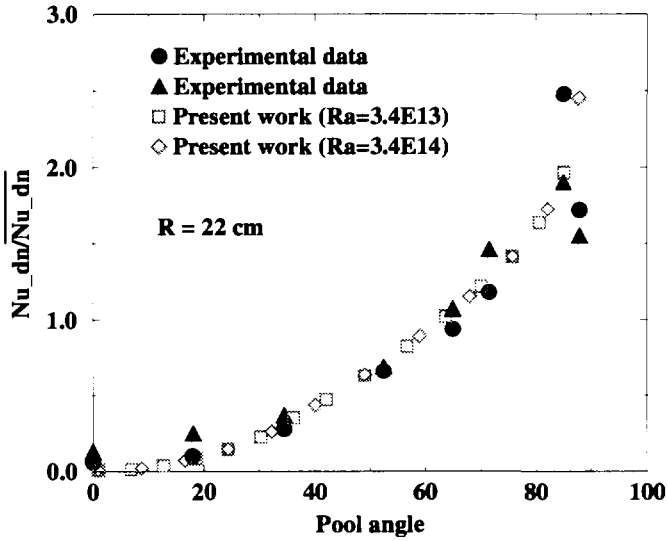

Figure 2.3: Ratio of local to average Nusselt numbers on the curved wall - comparison to the UCLA experimental data.

boundary of the debris bed (melt pool) to the vessel wall and, thereby, subjecting that location to inordinately high heat fluxes.

Inside a liquefied metallic layer cooled from top and heated from bottom, the heat transfer is governed by Rayleigh-Bénard convection. In the reactor case, besides the heat transfer by Rayleigh-Bénard convection, there is also heat transfer to the vessel wall, which is governed by the heat transfer through the boundary layer developing downwards along the cooling side wall. When both of these heat transfer mechanisms are active (termed as mixed convection), the relative significance of each heat transfer mechanism depends on the layer thickness/radius ratio and the boundary conditions applied to the top and side surfaces of the layer.

In order to include the metallic layer into the integrated assessment of the thermal transients in the late phase of in-vessel melt progression, the ECCM approach was extended to include both of the above-mentioned heat transfer mechanisms for the case without internal heat generation ($Q_v = 0$). The heat transported by the Rayleigh-Bénard convection is modeled by employing a pair of effective velocities, directed upwards and downwards from the layer center. The heat transport to the layer side wall is simulated by means of effective heat conductivity as before.

This model was validated separately for the cases of pure Rayleigh-Bénard convection and for mixed convection. The calculated temperature distributions and energy-splitting qualitatively agree with experimental data (MELAD, BALI) and direct numerical simulation (DNS) data [19] (see Fig.2.4).

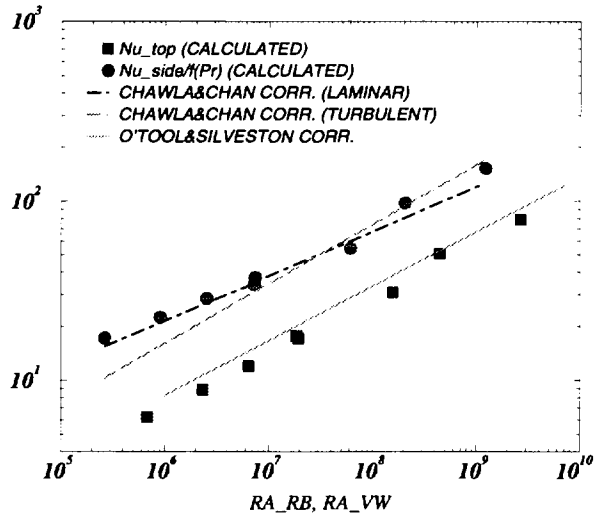

Figure 2.4: Heat transfer in cavity with Rayleigh-Benárd and mixed convection.

2.2.6 Application of the models and integrated MVITA code for reactor predictions

The models described above and the corresponding computer code (MVITA) have been employed extensively to assess the possibility of melt retention inside a PWR vessel with external cooling as well as the timing of melt-through for a BWR RPV without external cooling. The configuration chosen for the assessment is an initially quenched debris bed located on the lower head of a reactor vessel. No transient melt relocation and separation are considered.

Results of this assessment are presented in [17][31][72] (Appendices A-B). The calculated results showed that the duration of the thermal transient in the debris bed and vessel wall before the melt pool formation depends primarily on the initial temperature and the decay power density. It is interesting to note that, because of the large size of the debris bed, and its relatively low heat conductivity, the effect of the bed boundary conditions on the thermal transient prior to the formation of a melt pool is small; and, as a result, a large part of

the debris bed reaches the melting temperature at almost the same time and the initial melt pool already occupies a large volume fraction of the debris bed.

From the results of numerical assessment of melt retention inside an externally-cooled PWR with the MVITA code, external cooling was able to remove the heat incident from the melt pool on the vessel wall and prevent vessel melt-through. The vessel wall was also protected by a crust layer, separating the liquefied melt pool from the wall surface, and hence preventing a direct thermal attack to the vessel wall by melt convection. Due to the natural convection, the incident heat flux from the debris bed is highest near its upper corner. At this location, partial wall melting may occur (see Fig.2.5) and the crust at this place would 'float' between the core melt and the vessel melt fluids. Stability of this relatively thin crust layer may be under question, this is, however, out of the scope of this work. The heat flux from the outer surface of the vessel wall was shown to be well below the limit of boiling crisis (see Fig.2.6). For an externally cooled PWR vessel loaded with 11 m^3 of core debris, the calculations showed that a time of about 3-4 hours is needed by the system to dissipate 100% of the decay power produced inside the core debris bed and this time duration varies depending on the decay heat generation rate and the initial debris temperature.

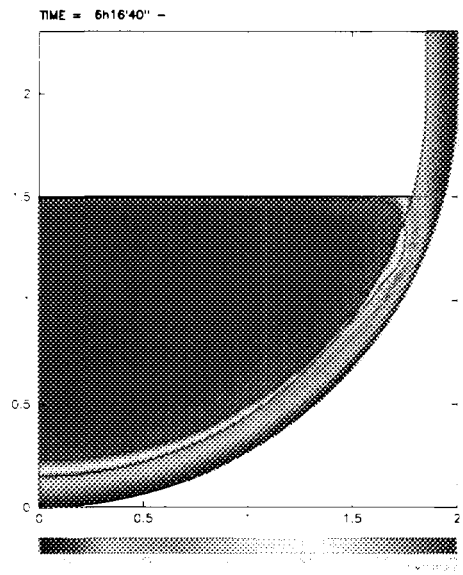

Figure 2.5: Thermal steady-state in PWR lower head with external cooling - MVITA simulation (q_v= 1.4 MW/m^3).

Simulations, carried out for the case of debris bed covered by a thick or a thin metallic layer, show strong effect of the thin layer on vessel thermal loads (see Fig.2.6). Significant wall melting at the layer side wall and consider-

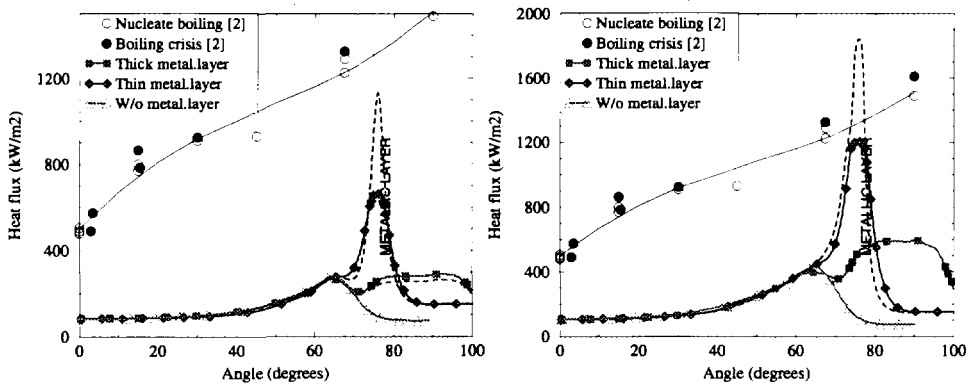

$q_v = 0.85\,MW/m^3$ $q_v = 1.4\,MW/m^3$

Figure 2.6: Thermal margins of in-vessel core melt retention by external vessel cooling, with thin and thick upper metallic layers above the oxidic debris.

able reduction of thermal margin available for melt retention are predicted for the debris bed with thin metallic layer (see Fig.2.7). In this sense, this work confirms the results of previous assessments performed by other authors [82]. Two-dimensional thermal diffusion inside the thick vessel wall significantly decreased the heat flux incident at outer surface of the vessel wall for the case of the thin metallic layer. Fig.2.6 shows that the heat flux on the vessel outside surface for the 2D calculation (solid line) is significantly lower than that for the 1D calculation (dashed line). It is also seen in the figure that there is very little margin left for in-vessel melt retention for decay power densities greater than 1.4 MW/m^3. It should be noted that the metallic layer is located on top of a very thin crust. If this crust is unstable and the metallic layer comes in contact with core melt, the change in the temperature of the boundary condition at the upper boundary of the melt pool could change the energy split in the pool, which, in turn, could change the distribution of the thermal loads on the vessel wall.

Without external cooling, the global vessel failure may occur as a result of vessel melt-through or creep rupture. Fig.2.8 displays the evolution of debris temperature and vessel melting in time. The results of the MVITA code calculations indicate that for the given debris configuration and initial debris temperature of 2000K, the vessel circumferential melt-through occurs at about 2 hour after the beginning of the calculation.

In this work, the melt-though of BWR vessel without external cooling was also calculated. The melt-through of the reactor vessel wall occurs, respectively,

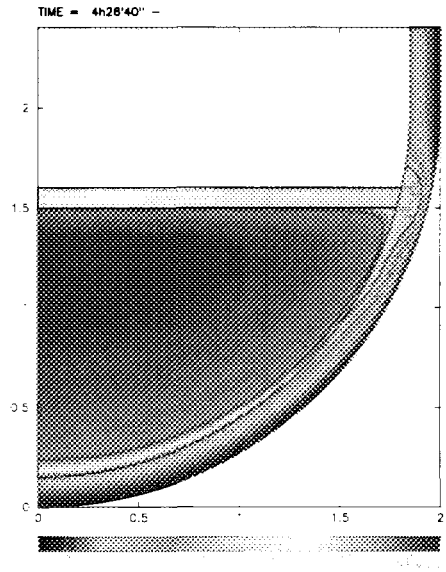

Figure 2.7: Effects of thin metallic layer (q_v= 1.4 MW/m^3).

at 3 hours 46 minutes and 1 hour 54 minutes for the values of $q_v = 1.0\,MW/m^3$ and $q_v = 2.0\,MW/m^3$ (Fig.2.9). However, estimation of the vessel failure due to structural and/or creep loading, based on the Larson-Miller criteria, gave a much shorter time for failure in comparison to that of vessel melt-through. The vessel melt-through is predicted to happen at the upper corner of the debris bed, which implies a global vessel failure. However, we believe that much before the melt-through shown in Fig.2.9, one or more of the vessel penetrations located near the vessel bottom will fail, since in the Swedish BWR, the instrumentation line welds are high above the vessel bottom and will be subjected to thermal attack from the melt pool.

2.2.7 Summary of the findings

The mechanistic models presented in this part are able to capture the phenomenology of the thermal transients occurring during debris heat-up and melting in the late phase of in-vessel melt progression. Hence, it could provide reasonable predictions for the prototypic cases of vessel failure due to melt-through (BWR) or melt retention by external cooling (PWR). It is the first time that the melt pool, crust layers, metal layer and the vessel have been described in an integrated fashion in two dimensions. The results of numerical simulations obtained show that the vessel thermal loads are reduced due to the two-dimensional heat

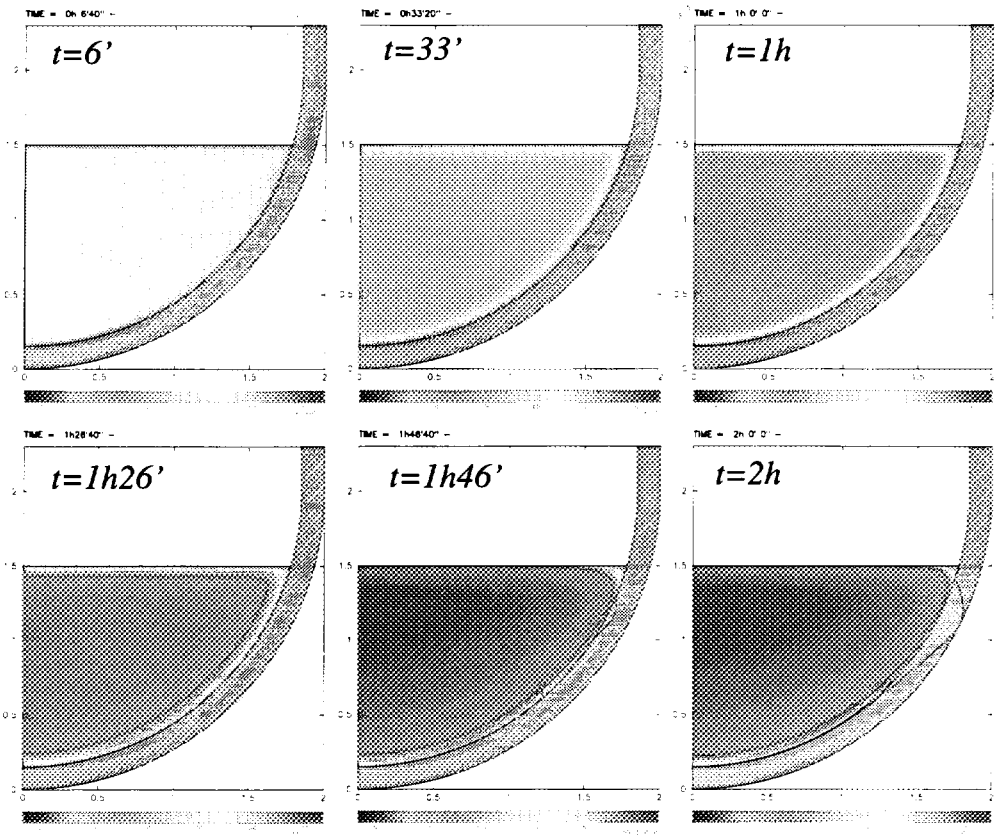

Figure 2.8: Vessel melt-through without external cooling. $q_v = 1.4$ MW/m^3.

diffusion in the vessel wall. The ECCM approach to model the natural convection heat transfer is the major 'invention' in this part, which is able to provide correct descriptions of the energy split as well as the heat flux distribution on the side wall for highly-turbulent decay heated core melt pool and metallic layer with mixed convection.

Since the structural strength character of the vessel steel may change greatly under the effects of high temperature and high heat flux, imposed from the decay heated debris bed, and the in-vessel pressurization, earlier vessel failure may occur as a result of creep rupture or structural failure. This factor necessitates the coupling of structural with thermal analyses in future work.

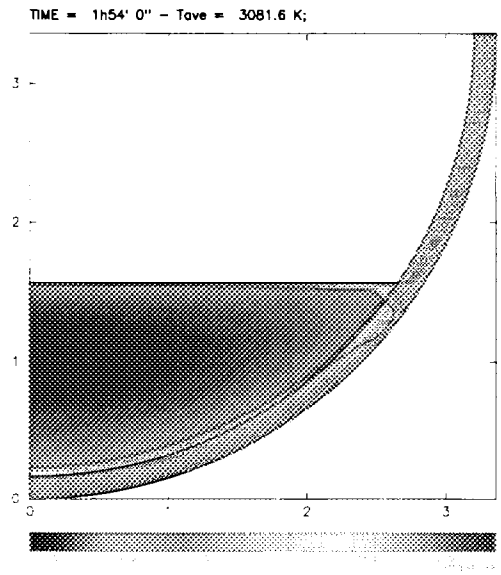

Figure 2.9: Temperature distribution and melt pool configuration at BWR vessel melt-through (debris decay heat flux $q_v = 2.0\,MW/m^3$).

2.3 Ablation of A Local Vessel Failure Site and Its Assessment

2.3.1 Phenomenological picture and problem formulation

Local failure may occur at a penetration, when the core melt attacks penetration tubes, housing the control rods or instrumentation systems (in both PWRs and BWRs). From the assessment by Rempe et al.[66], failure of penetration tubes (control rod or instrumentation tubes), or local vessel creep failure, are much more likely in comparison to the global vessel failure. Due to the high heat flux from the melt flow, which is at a temperature much higher than the vessel melting point, initial local failure will enlarge in size. The melt discharge rate and other characteristics (composition, superheat) are important for determining the consequences of the ex-vessel accident progression, i.e. ex-vessel fuel-coolant interactions (FCIs), direct containment heating, debris coolability, etc. Thus, an improved understanding of lower head ablation during melt discharge through a local failure site, is a necessary step towards defining the consequences of the ex-vessel melt-structure-coolant interaction processes.

The melt ejection out of the vessel would be governed by the driving forces

(vessel over-pressure, hydraulic head of the melt pool) as well as the melt flow and heat transfer-induced ablation of the lower head wall around the initial failure site. The lower head failure location may affect the discharge flow, although eventually, most heat-generating material could be ejected. Phenomenological considerations of vessel-local failure ablation are built around three key elements: (1) the thermal-hydraulic behavior of the core melt in the vessel lower head; (2) the fluid dynamics and heat transfer in the ablating hole; and (3) the thermal and physical (phase-change, mass-transfer) response of the lower head wall (see Fig.2.10). During the core melt discharge, convective heat flux (from melt flow) is the driving mechanism for (vessel) hole ablation. The heat transfer, in its turn, depends on the hydrodynamics of the in-hole melt flow. Since the hole may be quite short, the *thermal developing* region may occupy the most of the hole length. Besides heat transfer from the melt flow, other factors may also have strong impacts on ablation process. Based on a tentative identification, ranking and evaluation of related physical mechanisms, the most important phenomena are found to be [28] (i) crust behavior under high-Reynolds number flow conditions, (ii) convective heat transfer with phase change (freezing/melting) boundary conditions, and (iii) the multi-dimensional heat conduction and ablation front propagation in the vessel wall beneath the crust.

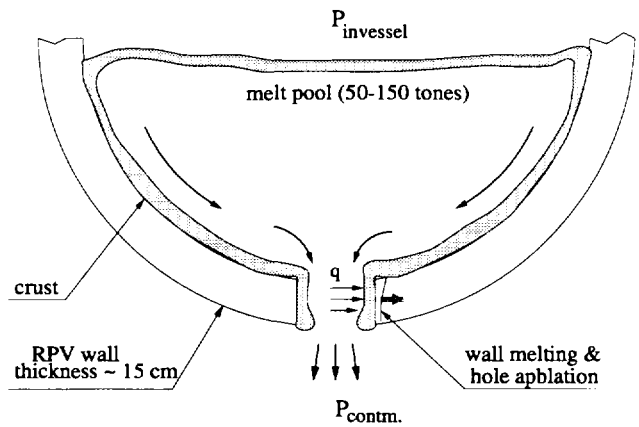

Figure 2.10: Vessel local-failure ablation scenario.

In this work, some phenomenological aspects of the vessel local-failure ablation are addressed. First, attention is given to the modeling of the in-hole heat transfer under thermal developing conditions. A correlation for turbulent number is introduced, which can be used to relate the thermal characteristics of the flow in the developing region with its turbulent properties. Further, a two-dimensional model of the wall ablation front was developed and implemented

in a code named HAMISA, which has been successfully applied to predict and analyze the hole-ablation experimental data. In order to assess the sensitivity of the key melt-discharge parameters, e.g. the mean discharge rate and the final failure(hole) size, on various factors, such as crust stability, heat transfer parameters, presence of in-vessel crust, etc., probabilistic analysis is performed, which is based on the simple models of relevant physical phenomena coupled with new understandings gained from the KTH experimental observations about the hole ablation phenomenology.

2.3.2 Modeling of turbulent heat transfer from the in-hole flow

The melt flow in the vessel failure hole is characterized by the thermal and hydrodynamic boundary layer development. Analysis of heat transfer in the thermal developing flow is important because of *high heat transfer coefficient in that region.* The flow regime in that region may be laminar or turbulent. The entrance effects on heat transfer in the laminar flows have been studied extensively in the past [74]. However the flows of important practical interests are mainly turbulent. Recently the two-equation $k-\epsilon$ model has been widely utilized in the modeling of turbulent flows. While the models of that kind can be successfully applied to describe the characteristics of thermally and hydrodynamically developed flows, their straight use for the thermal entrance region may fail to give a satisfactory result. The reason of that failure might be the absence of Reynolds analogy in that region, since the eddy diffusivity of heat, α_t, changes in the flow direction along with the development of a thermal boundary layer, while the eddy viscosity, ν_t, remains unchanged. So far, the most common approach to include the effects of turbulence into heat transfer simulation is to model the turbulent heat fluxes with the classical Boussinesq approximation. The unknown eddy diffusivity for heat α_t is expressed by the known (from solution of k and ϵ equations) eddy viscosity ν_t, so that $\alpha_t = \frac{\nu_t}{Pr_t}$. Unfortunately, this formulation with the assumption of the analogy between turbulent heat and momentum transfer, when the turbulent Prandtl number Pr_t is prescribed as a constant, may not be valid in the thermally developing region.

In this work (see Appendix D) a formulation of Pr_t in the thermal entrance region is developed, which is coupled with a low-Reynolds $k-\epsilon$ turbulence model and has been employed to investigate the heat transfer in this region [15]. The formulation is derived from the set of Reynolds-stress and turbulent heat flux equations while taking into consideration the non-equilibrium heat transfer in developing region and the thermal anisotropy near the wall. The full description of the formulation as well as some validation results can be found in Appendix D.

Practically, the corrections brought about by this formulation cause an increase of the turbulent Prandtl number in the thermal entrance region to account for the thermal laminarization of the flow in that region. Validation of this model against available experimental data by Babus'Haq et al.[6][7] is presented in [15](Appendix C).

2.3.3 Two-dimensional hole ablation model

In this section the effects of preheating and multi-dimensional heat conduction inside the vessel wall on hole ablation are investigated. The HAMISA.2D/WALL model has been developed to describe *two-dimensional heat conduction with phase change* below the ablated hole. A two-dimensional model of the process, coupled with an efficient numerical technique, has been developed. This model and numerical procedure are realized in a computer code named HAMISA.2D/WALL. The numerical method prescribes a dominant direction of boundary movement, which is assumed to be perpendicular to the initial hole surface. The heat conduction in the other direction is taken into account in a semi-implicit manner. The speed of the melt front of a given horizontal layer in cylindrical coordinate system (r, z) is defined through the difference between the heat flux imposed on the interface, q_{int}, and that taken away by heat conduction, q_{cond}, as follows (see also Fig.2.10)

$$V_{ab}(z,t) = \frac{\sqrt{r_o^2 + \frac{2(q_{int}-q_{cond})r_o\Delta t}{\rho_w L_{fus,w}}} - r_o}{\Delta t} \tag{2.1}$$

where r_o is the position of the melt front at time t_o, and Δt is time step, $\Delta t = t - t_o$. Calculated values of V_{ab} are then used to track the phase-change interface.

Analyses performed with the HAMISA.2D/WALL code were used to design the experiments, e.g., define the initial thermal state of the test plate, set requirements for melt pouring times, and design the test plates. Moreover, this model also provided accurate pre-test predictions for many hole ablation experiments (see Appendix D).

Table 2.3: Initial parameters for the 'bounding' scenarios [59].

Parameter/ Bounding scenario	Scenario 1	Scenario 2	Scenario 3	Scenario 4
ΔP (bar)	2-7	2-7	2-7	4.5
$D_{h,o}$ (cm)	5-15	50-400	5-15	6.5
$m_{m,1}$ (tonnes)	40-160	40-160	20-60	10
$\Delta T_{sup,1}$ (K)	10-190	10-190	10-390	150
Composition	oxidic	oxidic	metallic	metallic
$m_{m,2}$ (tonnes)	20-100	20-100	20-100	40
$\Delta T_{sup,2}$ (K)	10-390	10-390	10-190	100
Composition	metallic	metallic	oxidic	oxidic
$m_{m,3}$ (tonnes)	-	-	160-$m_{m,2}$	120
$\Delta T_{sup,3}$ (K)	-	-	10-190	100
Composition	-	-	oxidic	oxidic
p_{cont} (bar)	2	2	2	2
T_{pool} (K)	323	323	323	323
h_{pool} (m)	4,7,10	4,7,10	4,7,10	4,7,10
Masses $m_{m,1}$ and $m_{m,2}$ are directly correlated.				
Melt mass $m_{m,3}$ is released gradually.				
"Oxidic" composition refers to mainly oxidic melt.				
"Metallic" composition refers to fully metallic melt.				

2.3.4 Probabilistic analysis of the hole ablation and melt discharge processes

As mentioned before, the process of melt discharge is accompanied by hole ablation and enlargement, which feedbacks to the discharge rate and time. Since there are many scenario-related and phenomenological uncertainties associated with initial conditions for melt discharge and in-hole ablation process, it is, perhaps, appropriate to apply probabilistic analysis to investigate the process. The purpose of this analysis is to investigate the sensitivity of the important process parameters, such as the final failure size and the mean discharge rate, to the uncertainties of the scenario-related factors (initial conditions such as melt temperature and vessel pressurization) and phenomenological factors (heat transfer coefficients, crust existence, etc.). As in the previous work performed in the framework of APRI-2 [59], the initial and input conditions for the melt discharge and vessel ablation processes are given in the form of *bounding scenarios*, in which various important factors are sampled from probability distributions

(see Table 2.3).

The probabilistic analysis is based on the simple models of hole ablation and melt discharge processes. The melt discharge regimes can be classified as coherent release and gradual release [59]. The coherent melt release is mainly driven by the pressure difference (between the in-vessel and containment pressures) and the hydraulic head, while the gradual release is controlled by the thermal processes (melting) in the in-vessel debris bed. As in [59] the models for coherent and gradual melt releases are defined by

Coherent release

$$\frac{dm_m}{dt} = -\rho_m v_{dc} \cdot \frac{\pi D_{dc}^2}{4} \tag{2.2}$$

$$v_{dc} = C_D \sqrt{\frac{2\Delta p'}{\rho_m}} \tag{2.3}$$

$$\Delta p' = p_{vessel} - p_{cont} + \rho_m g H_m \tag{2.4}$$

For the coherent release of melt, the discharge coefficient may change as a function of the hole height. In this work, this coefficient is given by

$$C_D = \frac{1}{\sqrt{f_e + f_0}}, \tag{2.5}$$

where $f_e = 0.45$ and

$$f_0 = \begin{cases} 0.75 & \text{if } \frac{L_h}{D_{dc}} \geq 1 \\ 1.60 & \text{otherwise} \end{cases} \tag{2.6}$$

Equations 2.5 and 2.6 are based on data measured at RIT/NPS [71].

Gradual release

$$\frac{dm_m}{dt} = \frac{Q'_{dec}}{\Delta h_m} \tag{2.7}$$

$$Q'_{dec} = \frac{m_{m,oxid}}{m_{total}} Q_{dec} \tag{2.8}$$

$$\Delta h_m = c_{p,m,sol}(T_{mp,m} - T_{m,o}) + \Delta h_{fus} + c_{p,m,liq}(T_{m,dc} - T_{mp,m}) \tag{2.9}$$

Ablation of the lower head of the reactor vessel is defined by

$$\frac{dD_{dc}}{dt} = \frac{2h_{m-v}\Delta T_{m-v}}{\rho_v[c_{p,v}(T_{mp,v} - T_v^0) + h_{v,fus}]} \tag{2.10}$$

The most important factor here is the temperature difference between the melt and the vessel wall, which defines the heat flux to the wall. If no crust on the

wall is assumed, this temperature difference can be very large

$$\Delta T_{m-v} = T_m - T_{mp,w}, \quad T_{mp,w} \approx 1700K. \tag{2.11}$$

However, with the assumption about the existence of the melt crust on the vessel wall around the hole, the temperature difference reduces to

$$\Delta T_{m-v} = T_m - T_{mp,m}, \ with \ T_{mp,w} \approx 2800K. \tag{2.12}$$

If the probability of crust existence is assumed to be 0.5, a wide dispersion of the discharge parameters, e.g. final hole diameter and mean discharge rate, was obtained (see figures 2.11-2.13). The series of hole ablation experiments performed at KTH emphasizing a binary melt simulant, as well as the analytical results obtained using the HAMISA code, indicated that the crust always exists in the hole. Including this information into the probabilistic estimates greatly reduces the uncertainties in the discharge parameters as shown in figures 2.11-2.13.

With the in-hole heat transfer coefficient, h_{m-v}, given by a deterministic condition:

$$h_{m-v} = Nu_{m-v}\frac{k_m}{D_{dc}} = (0.0025 \div 0.0030) \cdot Pe, \tag{2.13}$$

uncertainty range of discharge parameters can be narrowed even further as shown in figures 2.12-2.14.

The effect of the crust formed at the lower part of the bottom head on the melt discharge rate was also investigated in this analysis by introducing an even-distributed crust thickness in the range [0..10cm]. The existence of this in-vessel crust did not affect the value of final failure diameter. However, the uncertainty in the crust thickness at the lower part of the bottom head could change the probability distribution of the melt discharge rate (see Fig.2.14).

2.4 Concluding remarks

The modeling and numerical analyses, performed in this work, help to resolve some important issues, associated with the in-vessel phase of melt progression and melt-structure interactions.

The thermal transients during late phase of melt-vessel interactions were *effectively* addressed by means of a mechanistic heat transfer model, which combines the essential aspects of the thermal interactions included, e.g. anisotropic

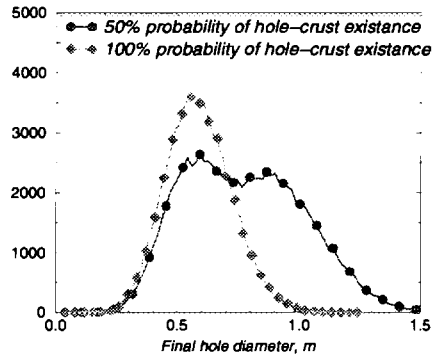

Figure 2.11: Final hole failure diameter [Scenario 1]

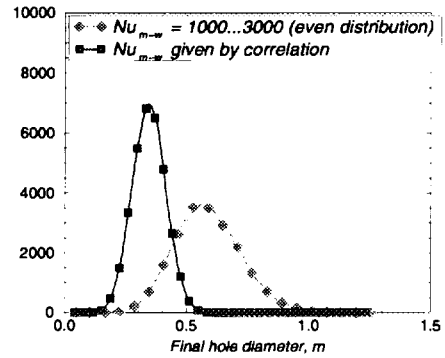

Figure 2.12: Final hole failure diameter [Scenario 1]

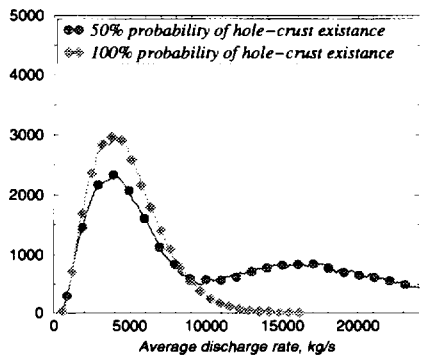

Figure 2.13: Average discharge rate [Scenario 1]

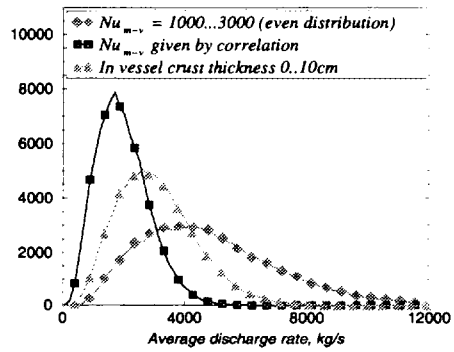

Figure 2.14: Average discharge rate [Scenario 1]

heat conduction, debris melting, natural convection heat transfer in the melt pool, convection heat transfer in the separated metallic layer, vessel melting, etc. The reactor analyses using this model indicated the feasibility of the melt retention accident management scheme, based on the vessel external cooling. It was also found that the presence of a thin metallic layer could significantly reduce the margin available for in-vessel melt retention, especially for high-power reactors. The analyses also emphasized the great importance of the crust layers, separating the hot melt pool from the wall on its side or the metallic layer on its top, thus providing a protection for the wall against direct melt contact. Stability and dynamics of such crust layers should be the focus of future work.

The melt-structure interactions involved during the ablation of a local vessel

failure (hole) are important issues, which were also addressed in this work. Some in-depth understandings about the heat transfer inside the hole and wall ablation were gained here with help of the separate-effect modeling and investigations. The effects of many other factors, which can only be prescribed with some uncertainty ranges, were studied by means of a probabilistic analysis. It was found that narrow distributions of important process parameters, such as mean discharge rate and final hole enlargement, could be obtained with employment of new understanding about the hole ablation phenomenology.

Chapter 3

Modeling of Fuel Melt-Coolant Interactions

Mixing of melt and water before an energetic interaction (steam explosion) may occur is usually termed as *premixing*. The general picture of melt-coolant interactions under ex-vessel premixing is schematically presented in Fig.3.1. As can be seen from the figure, difficulties related to the premixing assessment are due to the complex nature of and feedbacks between melt-coolant hydrodynamic and themal interactions. In general, hydrodynamic corium-water interactions are characterized by the *break-up and fragmentation behavior* of the melt in water, and thermal interactions are characterized by *melt quenching/solidification* and *water vaporization*. Thermal interactions between corium and water feedback to the break-up and fragmentation behavior of the corium through the changing characteristics (voiding) of the coolant and the corium (due to solidification). Recently, direct influence of thermal interactions on fragmentation under shock propagation conditions has also been reported [25].

In the premixing phase, the fragmentation behavior of the core melt is governed by various instability mechanisms, developed as a result of (liquid-liquid) contact and relative moverment between corium and coolant. Fragmentation of thin melt jets, for instance, is governed by the capillary instability, brought about by surface tension effects at low velocities. Fragmentation of larger jets is driven by two major mechanisms, termed as *Rayleigh-Taylor* and *Kelvin-Helmholtz* instabilities. At the head of the jet, Rayleigh-Taylor instability is likely to occur, when the jet penetration is resisted by the stagnation pressure exerted by the ambient fluid, which has to be displaced. As the flow velocity into the head is likely to be greater than the velocity of moving down head,

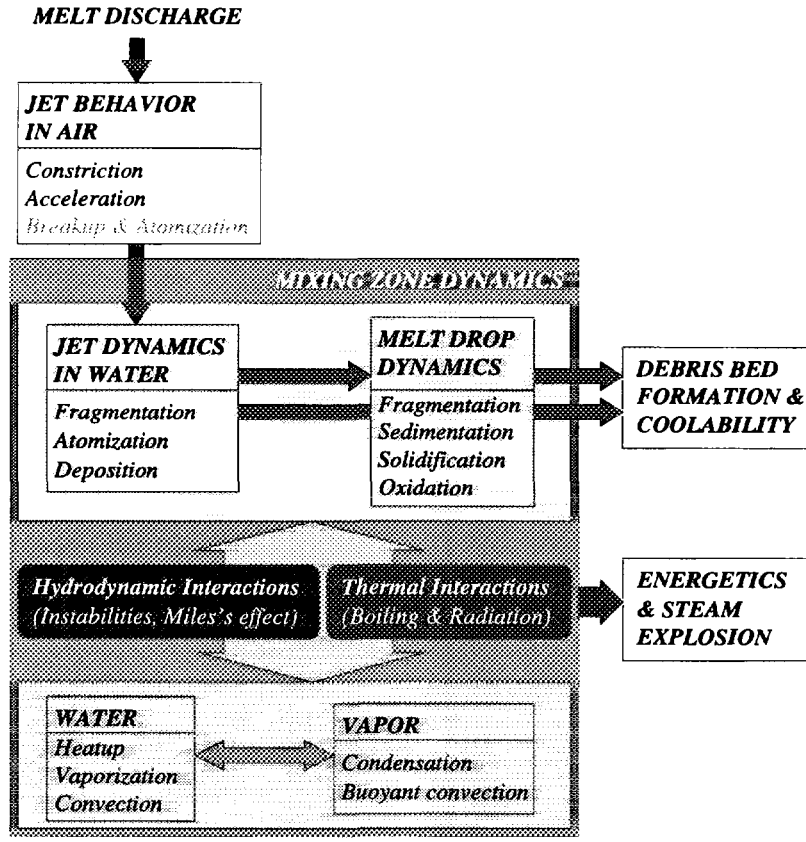

Figure 3.1: Physical phenomena and interactions under ex-vessel melt progression.

the flow of jet material must spread sideways, even swept back by the up-flow of the ambient liquid. Further, the development of unstable perturbations at the leading edge would lead to break-up of the head structure. Away from the jet head, Kelvin-Helmholtz instabilities (instabilities that occur when there is strong shear in the velocity profiles: here between the fluid in the jet and the ambient liquid outside) may occur on the body of the jet. Such type of instability leads to oscillations of the jet surface, which may cause stripping of jet material from the jet (jet erosion) or break-up of jet body into melt droplets (jet atomization). Jet fragmentation will lead to a particulate field. Corium drops or particles might further fragment in the flow field due to the same instability mechanisms, which govern jet fragmentation.

Thermal interactions between the very high temperature core melt jet, or droplets, and water are governed by the heat transfer from the melt to water by film boiling and/or heat radiation. With the energy exchange the melt droplets

would cool down and solidify, while the water would heat up and vaporize. The change of melt properties during its solidification, as well as the formation of a two-phase (water-steam) zone around the melt particulate field would provide significant feedbacks to further melt fragmentation and mixing.

In this chapter, some aspects of the non-explosive ex-vessel melt-coolant interactions are addressed. First, numerical analysis is performed to investigate the instabilities and fragmentation of a melt jet, or a melt drop, in a flow field under isothermal conditions. This analysis is based on 'first-principle' modeling with use of advanced numerical tools, which help to minimize numerical diffusion associated with property discontinuities across the interfaces. Then, a full scope assessment of the ex-vessel melt-water interactions, which combines the effects of the major physical phenomena and processes, e.g. jet fragmentation, particle formation and dynamics, heat transfer by boiling and radiation, water vaporization and steam condensation, is pursued. The purpose of this assessment is to identify the factors, which may have significant effects on the dynamics of the process (melt-coolant interactions) as a whole.

3.1 Simulation of the interfacial phenomena associated with hydrodynamic melt-water interactions

3.1.1 Background

The phenomenology of melt-water interactions is very complex and consists of a wide spectrum of thermal and hydrodynamic processes, which interact with each other. Among these processes, fragmentation of the melt in water is perhaps the most important, since it defines the further thermal and hydrodynamic interactions between melt and water. Even though there are some indications that thermal fragmentation may take place when hot melt mixes with water, the current analysis of melt fragmentation is based mostly on the hydrodynamic breakup mechanisms.

Hydrodynamics of the melt-water interactions is characterized by the development of instability waves on the interfaces, which may lead to interface deformation and destruction. As noted before, there are two mechanisms, responsible for the development of these instability waves, which are termed as Rayleigh-Taylor and Kelvin-Helmholtz instabilities. Under the sustained melt pouring and mixing scenario the Kelvin-Helmholtz instabilities seem to be the most important mechanism, governing the interfacial interactions.

Isothermal instability and fragmentation of a melt jet in water field can be assessed with use of linear, non-linear, or asymptotic analyses, which help to identify the fastest growing instability modes as well as the corresponding growth rates for some simple cases of interfacial geometry (planar or cylindrical) [20]. In these analyses, a great deal of simplifications and assumptions are introduced, which, in general, reduce the generality of the analysis and the applicability of the analytical results to practical cases.

Currently, CFD methods have been also applied to simulate interfacial phenomena and the behavior of multiphase systems. The continuum modeling approach is most well known and has been widely applied to investigate the system with multiphase inclusions. In severe accident analysis, there are several computer codes developed to simulate melt-water mixing, which employ this modeling approach (CHYMES [35], PM-ALPHA [2], IVA [44] [45], MC-3D [10] and IFCI [27] codes). Generally, this approach is based on multivelocity, multifluid continuum and interpenetrative motion of its components. The multiphase system is, therefore, described by the Eulerian formulation of conservation equations, derived for each system component (fluid). Interactions between components are presented by the time- and space-averaged, interface-exchange, closure correlations, which are generally obtained from the separate-effect experiments. The major drawback of this modeling approach is the non-generality and inaccuracy of closure correlations. While this approach may naturally be applied for dispersed multiphase problems, its application to the highly heterogeneous problems is very questionable.

In order to model the multiphase system with distinct separation of phases, there exist other CFD methods, which are based on a single continuous description applied for every phases. In general, they can be classified as the 'Lagrangian' and the 'Eulerian' approaches. In the 'Lagrangian' approach, only the equation of interface motion is solved. This generally reduces the computational demand considerably and eliminates numerical diffusion altogether. However, this approach is best suited for initially well-defined interfaces, which may not develop into a complex topology. In the Eulerian modeling approach, a multiphase system is described by a single field and the phase component distributions are represented by variation of the field properties across the computational domain. To solve the system of conservation equations, a high-order numerical scheme may be needed in order to reduce numerical diffusion and oscillations, arising around the phase discontinuities.

Hybrid 'Eulerian-Lagrangian' methods combine the advantages of the both modeling approaches. On one hand, they can track both the motion of the interfaces and the behavior of the outside media. On the other hand, the interface

can be kept sharp with very small numerical diffusion. Some hybrid 'Eulerian-Lagrangian' methods are based on the 'volume-tracking' (MAC, VOF), while the others are based on 'front-tracking'. The 'front-tracking' methods do not require the reconstruction of the interface after each time step and, therefore, enjoy considerable popularity. Recently, a front-tracking algorithm named Level Set, which was first formulated by Osher and Sethian [61], has been more and more widely applied for multiphase flow modeling.

3.1.2 Description of the modeling approach and solution algorithm

The melt-water hydrodynamic interactions were analyzed in this work with use of 'first-principle' modeling, based on the solution of the flow (Navier-Stokes) equations, coupled with a high-order numerical scheme CIP, and the level set front-tracking algorithm. The effects of the interfaces on the flow motion (surface tension) are accounted for in this approach. These are described in the following paragraphs.

Dynamics of the two-phase flow system with interfaces are described by the Navier-Stokes equations, written in the fixed Eulerian coordinate system:

$$\mathbf{u}_t + (\mathbf{u}\cdot\nabla)\mathbf{u} = \mathbf{F} + \frac{1}{\rho}\left[-\nabla p + \nabla\cdot(\mu D) + \sigma\kappa\delta(d)\mathbf{n}\right], \tag{3.1}$$

$$\nabla\cdot\mathbf{u} = 0; \tag{3.2}$$

where $\mathbf{u} = (u, v, w)$ is the fluid velocity, $\rho = \rho(\mathbf{x}, t)$ is the fluid density, $\mu = \mu(\mathbf{x}, t)$ is the fluid viscosity, D is the viscous stress tensor, and $\mathbf{F}$ is the body force. The last term in Eq. 3.1 is the surface tension term, which is concentrated on the interface. We denote σ as the surface tension, κ as the curvature of the front, d as the normal distance to the front, δ as the Dirac delta function, and $\mathbf{n}$ as the unit outward normal vector at the front. Note that, in the previous formulations, only one system of the Navier-Stokes equations is derived to describe the two-phase medium. Therefore, the local properties in these equations should be modified to present the spatial distribution of phases.

The high-order Navier-Stokes solver - CIP algorithm

In order to solve the system of Navier-Stokes equations a finite-difference, high-order numerical scheme is employed, which mitigates numerical diffusion. In most finite-difference methods the accuracy is increased by increasing the

number of discretization points used in the approximation of derivatives. This leads to an extension of the stencil which is often undesirable (loss of the tridiagonal nature of the matrices, difficulties near a boundary, etc.). In this work, another method, named the Cubic-Interpolated Pseudoparticle (CIP) Method, is employed to solve the Navier-Stokes equations with high accuracy. This method was developed by Yabe et al.[87] and has been successfully employed to solve the system of Navier-Stokes equations for both compressible and incompressible fluid flows [88]. In general, the CIP method solves general convective-diffusion differential equations by dividing them into non-advection and advection phases. These are symbolically written as

$$\frac{\partial \mathbf{f}}{\partial t} = \mathbf{g} \tag{3.3}$$

$$\frac{d\mathbf{f}}{dt} = 0 \tag{3.4}$$

where $\mathbf{f}$ is the computed variables and $\mathbf{g}$ is the right-hand side of the Navier-Stokes equations, which includes the diffusion and source terms. The non-advection phase can be solved by finite difference or finite volume methods. Then, a cubic-interpolated profile of the intermediate solution is shifted in space according to Eqn.3.4. In determining this profile, $\mathbf{f}$ and its spatial derivatives are used as independent variables. In each time step, not only the values but also their spatial derivatives are updated. As a result, significantly large computational memory is needed in CIP method, compared to the other methods.

The level set front-capturing algorithm

For the case of melt-water mixing, since the local properties ρ and μ change sharply at the interface, conventional finite difference schemes will incur excessive numerical diffusion when solving the equations, and thus transforming the property distribution in time. Instead, we shall use the level set technique to capture the moving interface. The main idea of the level set methodology is to embed the propagating interface as the zero level set of a higher dimensional function ϕ. The level function ϕ is initialized as a signed distance function, i.e.

$$\phi(\mathbf{x}, t = 0) = \pm d, \tag{3.5}$$

where d is the distance from $\mathbf{x}$ to interface, and the plus (minus) sign is chosen if the point $\mathbf{x}$ is outside (inside) the region bounded by the initial interface.

If the interface propagates normal to itself with speed V, then motion of the interface can be described by a Hamilton-Jacobi type equation [61]

$$\phi_t - V|\nabla\phi| + (\mathbf{u} \cdot \nabla)\phi = 0. \tag{3.6}$$

This equation will move the zero level of ϕ on the Eulerian grid exactly as the actual interface moves. Since ϕ is a smooth function, unlike ρ or μ, the above equation is easily solved numerically.

Property smoothing using the level function

Special care must be taken when solving the Navier-Stokes equations at the interface ($\phi = 0$), where the physical properties change sharply, and when computing the delta function which appears in the momentum and energy equation. In order to smooth the changes at the interface and to eliminate the numerical oscillations, the properties are computed using a regularization Heaviside function, H, as follows:

$$\rho_\epsilon(\mathbf{x}) = \rho_1 + (\rho_2 - \rho_1)H_\epsilon(\phi(\mathbf{x})), \tag{3.7}$$

$$\mu_\epsilon(\mathbf{x}) = \mu_1 + (\mu_2 - \mu_1)H_\epsilon(\phi(\mathbf{x})), \tag{3.8}$$

where H is defined as

$$H_\epsilon(d) \equiv \begin{cases} 0 & \text{if } d < \epsilon, \\ (d+\epsilon)/(2\epsilon) + sin(\pi d/\epsilon)/(2\pi) & \text{if } |d| \leq \epsilon, \\ 1 & \text{if } d > \epsilon; \end{cases} \tag{3.9}$$

and ϵ is the regularization parameter.

Correspondingly, we define the regularized delta function δ_ϵ as [77]

$$\delta_\epsilon(d) \equiv \begin{cases} \frac{1}{2}(1 + cos(\frac{\pi d}{\epsilon}))/\epsilon & \text{if } |d| < \epsilon, \\ 0 & \text{otherwise.} \end{cases} \tag{3.10}$$

The resulting surface tension force, defined in the Navier-Stokes equation 3.1, is, therefore, represented by the following smoothing formulation

$$\sigma\kappa\delta(d)\mathbf{n} = \sigma\delta(\phi)\nabla\phi\nabla\cdot\left(\frac{\nabla\phi}{|\nabla\phi|}\right) \tag{3.11}$$

Using the level function, intrinsic geometric properties of the interface can be determined as follows:

Normal vector:

$$\mathbf{n} = \frac{\nabla\phi}{|\nabla\phi|} \tag{3.12}$$

Interfacial curvature:

$$\kappa = \nabla\cdot\frac{\nabla\phi}{|\nabla\phi|} \tag{3.13}$$

3.1.3 Summary of the simulation results

The modeling approach presented above was employed to investigate three important issues of the melt-water interactions. First, behavior of the Kelvin-Helmholtz instability waves, which appear on the jet body as a result of its relative motion in water, are studied. The factors, which may affect the instability, are identified and investigated numerically. Second, deformation and fragmentation of a melt jet in water under isothermal conditions are simulated. The simulation results are then compared to the case of a pseudo-jet, consisting of spherical balls. The comparison helps to clarify the effects of surface phenomena on jet progression and fragmentation. Finally, the deformation and breakup of a single melt drop in flow field is considered. The effects of the drop solidification and water vaporization are represented by changing the corresponding field properties.

Development of the Kelvin-Helmholtz instability waves

The development of surface instability waves caused by shear on the surface between two fluids (melt - water) in relative motion is numerically investigated. The fluids chosen are Cerrobend and water. These simulant materials have been employed in the experimental program of jet fragmentation performed at NPS/RIT. These two fluids are moving relative to each other. The velocity difference is 3m/s.

The evolution of the interfacial waves of different wavelengths was investigated. The initial wave amplitudes were chosen depended on the wavelengths. For the long and medium waves (wavelengths λ equal to 5cm and 2.5cm, respectively), the initial wave amplitude is 5mm. For waves of length, the initial wave amplitude of 2.5mm was chosen. Fig.3.2 depicts the SIPHRA simulation results for a long-wave case.

The simulation results show that in most cases the initial disturbances roll and form wave leading edges. The results also indicate that further evolution of the leading edge is affected not only by the shear, but also by the vortex field formed.

Long waves were found to be more unstable than short waves for the chosen conditions. The computational results indicate that the development of only the very short wave instability is more-or-less irrotational. Surface tension and viscosity both were found to have a damping effect on the instability development, especially for the short waves. Development of the instabilities for the

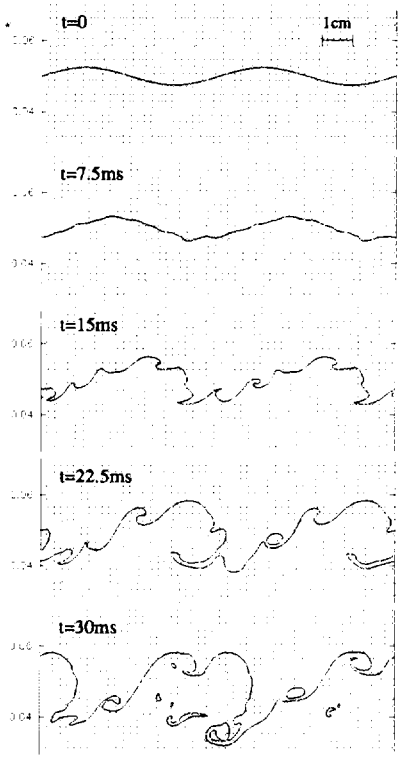

Figure 3.2: Long-wave Kelvin-Helmholtz instability, $\lambda = 5$ cm.

long waves is governed by the rotational flow and, therefore, is less affected by the surface tension and viscosity variations.

The propagation speed of the waves, C_r, was estimated from the simulation results and is found to be $(1.23 \div 1.25)$ m/s. This data is then compared with an analytical solution of the Kelvin-Helmholtz instability in irrotational perturbed flows; Eqn.(3.14).

$$C_r = \frac{\rho_m \cdot coth(k \cdot h_m) u_m + \rho_a \cdot coth(k \cdot h_a) u_a}{\rho_m \cdot coth(k \cdot h_m) + \rho_a \cdot coth(k \cdot h_a)}. \tag{3.14}$$

where h is the height of the layer and k is the wave number determined from the wavelength. For the given conditions, the equation (3.14) provides $C_r \simeq$ 1.2 m/s. As can be seen from the comparison, good agreement between the SIPHRA results and Eqn.(3.14) is observed.

Jet instability and breakup

Penetration of melt jets into water pools and instability behavior of the jets are simulated by the SIPHRA code. Isothermal hydrodynamic interactions are assumed. Two fluids with different densities, i.e. ρ_m =2710 kg/m^3 or ρ_m = 7810 kg/m^3, are employed as melt materials. Viscosity of melt phase is chosen as $\mu_m = 1.6 \cdot 10^{-3}$ Pa.s, which is that of Wood's metal. The inlet jet velocities are set to the values, similar to those employed in the tests FPD98 and FPA97 of the BILLEAU experimental program [12] (see Figs.3.3-3.4).

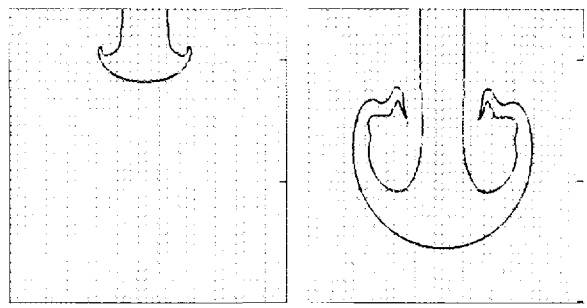

Figure 3.3: The SIPHRA simulation results for FPD-98 conditions, t = 0.2 s and 0.4 s. (melt properties: ρ_m = 2710kg/m^3, $\mu_m = 1.6 \cdot 10^{-3}$Pa.s, σ = 0.4 N/m).

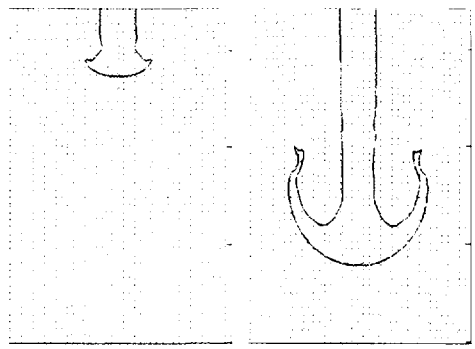

Figure 3.4: The SIPHRA simulation results for FPA-97 conditions, t = 0.2 s and 0.4 s. (melt properties: ρ_m = 7810 kg/m^3, $\mu_m = 1.6 \cdot 10^{-3}$ Pa.s, σ = 0.4 N/m).

The results of the simulation indicated that the deformation of the jet leading edge and the jet progression rate could be well defined using this modeling approach. The calculated deformation and the progression speed of the jet leading edge are in good agreement with the experimental data (see Appendix

E). No difference was found between the results obtained for the cases with and without surface tension, which indicates that the surface tension has little effect on the development of the Rayleigh-Taylor instability and the jet progression rate. It is also worth noting that in the BILLEAU experiments the jets were made of spherical balls. Good agreement between our results and experimental data seem to indicate that fragmentation of a heavy jet in water seems to be driven primarily by the dynamic effects, not by the interfacial interactions.

Deformation and fragmentation of a high-density drop in flow field

Deformation and fragmentation of high-density molten metal drops (ρ_d = 9200 kg/m^3, σ = 0.4 N/m) in water (ρ_a = 1000 kg/m^3) were investigated for different drop-ambient relative velocities (varying from 1m/s up to 15m/s). The initial drop size was chosen to be 9mm.

The results of the simulation are presented in Appendices F-G (see also Fig.3.5). In most cases, bowl-shaped drops appear at the very beginning of the drop deformation process. The results of the present study imply that shear breakup is the dominant breakup regime in liquid-liquid systems. In particular, the drop breakup is associated with stripping of smaller drops from the periphery of the core drop. It is interesting to note that the calculated results indicate that, for high Weber number conditions, the drop may feature significant deformation before breaking up.

The calculated results are analyzed in terms of the breakup time, τ_{br}, and the drop displacement length, L_{disp}. Table 3.1 shows that the calculated total breakup time and the displacement length compare reasonably well to those derived by Pilch and Erdman.

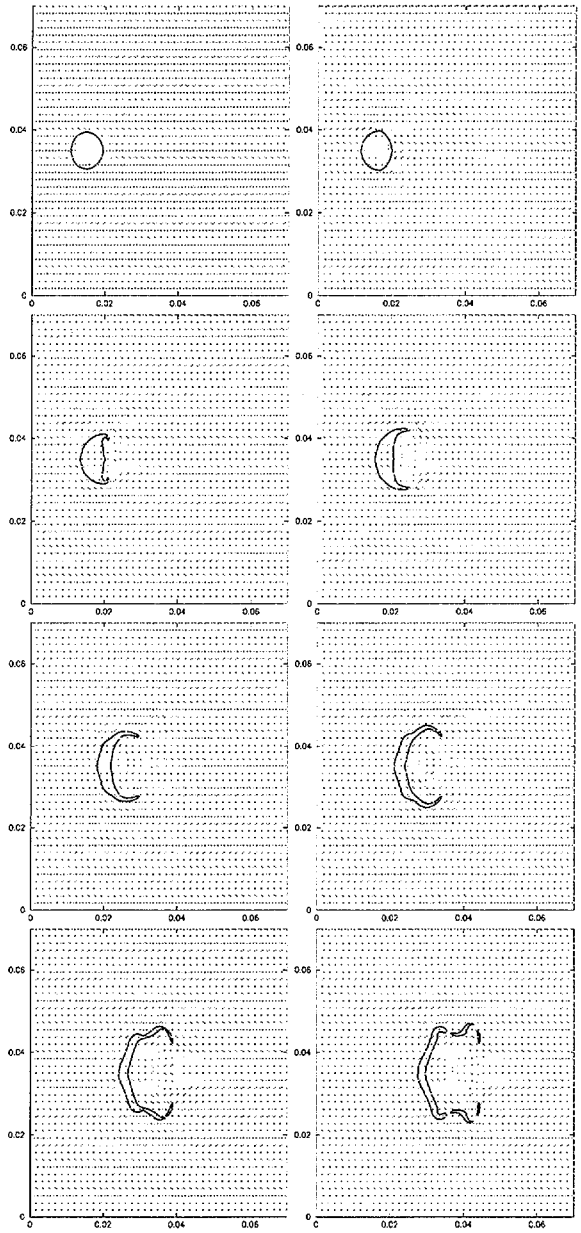

Figure 3.5: Drop breakup in liquid-liquid system. $We = 5062$. $Oh = 2.8{\cdot}10^{-3}$. Time interval between the pictures is 0.375 ms.

Table 3.1: Calculated results *vs* semi-empirical method of Pilch and Erdman (1987) (P&E).

Parameter/ Cases	1	2	3
We	22.5	455	5062
τ_{br}, ms (P&E)	121	21.5	10.
τ_{br}, ms (calc.)	120	18	5.75
L_{disp}, mm (P&E)	65	51	66
L_{disp}, mm (calc.)	70	50	50
D_{max},mm (P&E)	15*	3.6	0.18

* - corrected (see Fig.14 in Pilch and Erdman (1987) [62]).

It must be noted, however, that the computational grid utilized does not allow capturing instability-induced length scales, which are comparable to the grid size. As a result, small fragments or drops in neighboring regions tend to form a larger fragment, thus limiting the resolution of the calculated drop size.

The effects of viscosity and density variation because of drop solidification or water vaporization were also investigated here. While the change of the ambient-fluid viscosity was found to have a minor effect on the drop behavior, the increase in drop viscosity (e.g., due to drop solidification) may greatly change the mode of the drop deformation and breakup. It was found that drop-fluid viscosity begins affect the deformation and breakup of the drop when Oh ($Oh = \mu_d/(\rho_d \cdot D_d \cdot \sigma)^{1/2}$) becomes larger than 0.1. For very high viscosity ($Oh = 3$), amplitude of the deformation is significantly reduced (see Figs.3.6-3.7 and Appendix G). It was also seen that a change in the melt density has a strong effect on the melt drop deformation and breakup. The lower the melt density, the less deformation and fragmentation the drop experiences for the same We and Re numbers.

3.1.4 Summary of the modeling method and results

Summarizing the work in this part, an advanced numerical method has been developed to investigate the interfacial phenomena, associated with hydrodynamic melt-water interactions. All essential aspects of the interfacial phenomena were found to be satisfactorily captured by the modeling approach adopted. Moreover, the effects of surrounding flow field and their property variation were included in the simulation and analysis.

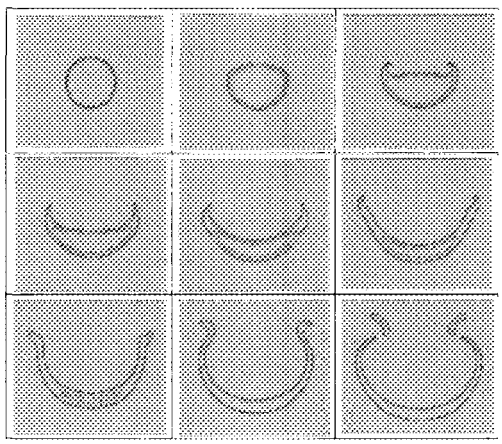

Figure 3.6: *Drop behavior without solidification. Time interval between the pictures is 2 ms.*

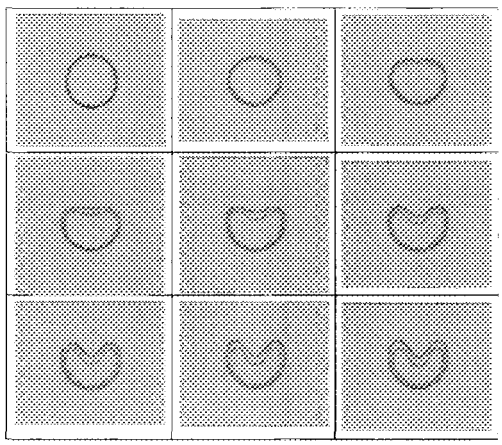

Figure 3.7: *Drop behavior with solidification.*

Fragmentation of the melt jet and drops in water is an important part of MFCI, addressed here. The numerical simulation, based on an advanced flow solver, coupled with a front-capturing algorithm, helps to identify the most common break-up mode and to clarify the effects of most important factors, governing the jet and drop fragmentation. It is known that cooling and freezing of the interface melt layer may occur in prototypical FCI situations, rendering significant changes in the melt fluid properties. The sensitivity analysis performed in this work revealed the dominant effect of density ratio on both jet and drop fragmentation. Significant viscosity increase due to surface solidification was found to hinder the breakup of melt drop. Even though a liquid-liquid isothermal contact mode was analyzed in this section, the calculated complex wave structure on the interfaces tends to indicate that phase inter-penetration may initiate mechanisms of violent interactions in non-isothermal cases. For example, penetration of water into the body of a high-temperature jet/drop would induce rapid vaporization and cause the jet/drop to break up.

3.2 Integrated assessment of the ex-vessel melt-water interactions

3.2.1 Background and problem formulation

The major body of research on molten-fuel-coolant interactions (MFCI) and steam explosion research was reviewed earlier in the report performed for APRI-2 project [60]. Since 1995 remarkable progress in the description of the premixing and expansion phases of the steam explosion has been achieve. Several large-scale experimental programs and analyses efforts are underway to determine physical mechanisms associated with FCIs and to provide models and methods, which could be used to predict the consequences of FCIs in reactor accident situations; see e.g. recent reviews in [2][85], [11], [55]. However, we believe that the initial phase of the FCI process has not been as well understood yet. This includes jet break up, droplet formation and subsequent fragmentation.

A number of computer codes have been developed to integrally assess the thermal hydrodynamics of melt-water interactions. Among them, the codes CHYMES [35], PM-ALPHA [2], IVA [44] [45], MC-3D [10] and IFCI [27], use a single field to represent the fuel (both jet and drops). In some other codes (COMETA [4], TEXAS [24], TRIO MC [9]), the model of jet fragmentation has been added to complete the physical picture of melt-water premixing. It is worth noting that in the latter codes, while the water, steam, and drop fields

are modeled more or less mechanistically with use of multifluid concept, the jet field is usually represented by a point or 1D model.

Table 3.2: FCI code comparison by main features [37]

Code	Features				
	Type of Code	Type of Subcooled Boiling Model	Dynamic Fragmentation Model	Metal Oxidation Model	Type of Hydrodynamic Model
IFCI	Integral	Surface	Yes	Yes	2D
IVA	Integral	Bulk	Yes	No	2D
PM-ALPHA	Mixing	Bulk	No	No	3D
ESPROSE.m	Propagation	N/A	N/A	No	3D
CHYMES	Mixing	Bulk	Yes	No	2D
THIRMAL	Jet mixing	Mixing zone	Yes	Yes	1D
MC-3D	Integral	Bulk	Yes	Yes	3D
TEXAS(IV)	1-D mixing	Surface	Yes	Yes	1D

It is worth noting that large uncertainties are associated with the physics of the melt fragmentation and melt-coolant thermal interaction phenomena. The modern FCI codes usually rely on various empirical models and closure correlations, obtained in the conditions much different from those of the prototypic integral-mixing conditions. Therefore, a lot of 'fine-tuning' of the phenomenological models or correlations may be required for predictions of the experiments, such as FARO, PREMIX, etc. In order to estimate the effects of various phenomenological uncertainties, a probabilistic assessment may be appropriate.

The integral assessment of melt-coolant premixing presented in this section consists of two parts. In the first part, a probabilistic analysis is performed to assess the effects of scenario and phenomenological uncertainties on the final distribution of the important premixing parameters, such as the amount of molten melt available in the mixing zone, the average melt temperature, the configuration of the mixing zone, etc. In the second part, a simple mechanistic model of premixing process is developed, which is based on the multi-field description of the mixing zone components (melt jet, melt particles, water, coolant). The model is validated against experimental data.

Note that even in the probabilistic assessment, mechanistic models are employed to reduce the phenomenological uncertainties inherent in the thermal hy-

drodynamics of premixing process. The change of surface temperature of melt drops, for instance, is determined in a mechanistic manner, since it can strongly affect the heat transfer between melt drops and coolant, which is governed by heat radiation under high melt temperature.

In the mechanistic modeling the following factors are considered as essential and will be accounted for:

- Fragmentation of a melt jet in water;
- Sedimentation of the melt particles;
- Solidification of melt particles in water;
- Convective and radiative heat transfer from melt and debris to the surrounding medium (steam-water mixture);
- Thermal hydraulics (boiling, condensation, buoyant convection) of water-steam medium;

Based on the physical considerations, some simplifications of the models for water and for vapor motion have been introduced, which may significantly simplify the solution procedure and reduce the computational time needed.

3.2.2 Quantification of the ex-vessel melt-coolant premixing

In this part, probabilistic assessment is performed to investigate the process of melt-coolant premixing. The assessment is based partly on the mechanistic models of the themal hydrodynamic interactions, occurring in the mixing zone, and partly on the Monte-Carlo treatment of other uncertainties related to the melt discharge scenario and the mixing phenomenology.

Fig.3.8 displays the simplified picture of the melt-coolant mixing process including major thermal hydrodynamic interactions and feedbacks. The figure does not show the effects of input parameters, such as the mode and dynamics of core melt coming to water pool, melt composition, initial pool depth and temperature. These factors are included in the assessment as uncertainty parameters.

In the current assessment, several thermal and hydrodynamic processes and interactions are described by means of the mechanistic modeling, which include,

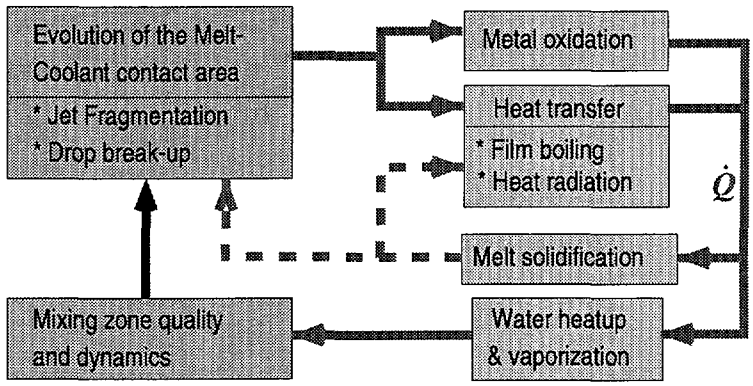

Figure 3.8: Simplified picture of melt-coolant premixing.

for instance, processes of metal oxidation, melt particle heat transfer and solidification, etc. In these mechanistic models, there appear several phenomenological uncertainties, which can also be presented as uncertainty parameters and taken into account by means of the Monte-Carlo treatment. Some other thermal hydrodynamic processes, such as jet breakup or melt-coolant heat transfer are treated in a parametric manner.

The list of scenario and phenomenological uncertainties treated for in this work are presented in Table 3.3. Note that phenomenological uncertainties can be independent (as for the cases of particle size or film boiling heat transfer coefficient) or parts of the mechanistic models (as for friction factors, jet and particle emissivities, etc.). The independent uncertainties can be substituted by mechanistic models, if necessary.

As can be seen from the table, the key uncertainties in the present assessment are:

1. Initial configuration of the water pool, formed as a result of the accident management activities. The pool configuration will vary depending on the water available, the geometrical characteristics of the drywell, and the history of accident management activity.

2. Melt discharge manner. The discharge rate and diameter, the melt temperature and composition at discharge, the number of discharging jets, etc. depend on the vessel failure scenario. In this work, only local vessel failure is considered and the reactor vessel depressurization is assumed to precede the vessel failure.

3. Melt particle size, which results from jet and drop sequential fragmenta-

Table 3.3: Scenario and phenomenological uncertainties associated with melt-coolant premixing

Type	Uncertainty	Symbol
Scenario	- Water pool depth	H_w
	- Water pool temperature	T_w
	- Distance of melt passage in the air	H_{air}
	- Initial ex-vessel pressure	$P_{ex-vessel}$
	- Melt discharge rate	G_{dc}
	- Discharge diameter	D_{dc}
	- Melt temperature at discharge	$T_{m,dc}$
	- Number of discharging melt jets	$N_{j,dc}$
	- Composition of the melt at discharge	$OxFrac$, $ZrFrac$
Phenome-nology	- Probability of melt atomization in the air	$\mathcal{P}_{atom}$
	- Friction factor of core melt jet in coolant	$C_{D,j}$
	- Jet radiation emissivity	ε_j
	- Melt particle average diameter	D_d
	- Melt particle friction factor	$C_{D,d}$
	- Initial lateral particle velocity	$V^0_{d,\perp}$
	- Drop radiation emissivity	ε_d
	- Film boiling heat transfer coefficient	h_{fb}

tion. This parameter varies greatly depending on the characteristics of the heat transfer between melt and coolant, which, in turn, are function of melt temperature and water subcooling.

Major assumption

The current assessment of melt-coolant premixing is based on the assumption that the ex-vessel melt discharge may last much longer than the initial transient period of melt entry in water. As a result, a steady state of melt pouring and mixing zone dynamics may be established after a short while. Under such conditions, a constant melt mass could be available in the mixing zone, and the rates of heat transfer and vaporization would remain constants. Steady state conditions could be established in the mixing zone due to the various feedbacks affecting the mixing zone. The larger the rate of melt mass entering the mixing zone, the larger the heat transfer from it, which causes larger steam generation, greater void fraction, and lower coolant density. These conditions will increase the rate of particle sedimentation and, therefore, balance the larger rate of

melt entry into the mixing zone. In this analysis, the effect of containment pressurization on water and vapor properties is neglected.

In the following subsections, mechanistic models used in this work are presented in some detail.

Jet-in-air description

Before coming to water, the core melt may accelerate in the air under the gravity. If the heat transfer from the core melt to the air is neglected, the melt would reach the water pool without decrease in temperature. The velocity of the melt at the inlet of the water pool and the corresponding constriction of the jet, if not atomizing in the air, are easily defined by the following equation

$$u_{j,inlet} = \sqrt{u_{dc}^2 + 2gH_{air}} \tag{3.15}$$

$$D_{j,inlet} = D_{dc}\sqrt{\frac{u_{dc}}{u_{j,inlet}}} \tag{3.16}$$

Fragmentation of the core melt in coolant

When progressing in the water pool, the core melt jets would be destabilized and break up due to the various hydrodynamic or thermal instabilities, developed on the jet body and its leading edge. The melt jets might first fragment into relatively large melt particles, which can further break up in the mixing zone to smaller particles. Such a sequence of melt particle size evolution will not be considered in this work. Instead, the melt jet(s) is(are) assumed to break up immediately into the final-size particles and the final size of the melt particles is provided with an uncertainty range. For the case of melt atomization in the air, the melt is assumed to enter the water pool in form of a 'particle rain' and the melt drops are assumed to retain the specific size on their passage through the mixing zone.

The breakup length of melt jet in water is given by the Saito's correlation, which was obtained experimentally [68],

$$L_{j,br} = 2.1\, D_{j,inlet} \left(\frac{\rho_j}{\rho_w}\right)^{1/2} Fr^{1/2}. \tag{3.17}$$

Note that in the Saito's experiments, jet break-up was found to to be driven by surface stripping due to Kelvin-Helmholtz instabilities along the vertical column, with coarse fragmentation at the leading edge by capillarity, due to thinning of the jet core. Even though the Saito's correlation accommodates available

non-isothermal experimental data quite well, there is still certain uncertainty in applying this correlation to the reactor case. The reason is that jet-vapor interaction dominates for a high temperature jet instead of jet-liquid interaction.

In order to define the source of particle field formation, fragmentation is assumed to occur linearly along the jet breakup length. If the breakup length is larger than the pool depth, part of the melt is assumed to deposit directly at the bottom in the form of a melt cake, without participation in the premixing. The jet temperature is also assumed to not change significantly along the jet length and the temperature of the drops, stripped from the jet body, is, therefore, equal to the jet temperature at its entrance to the water pool. In defining the Froud number, Fr, the jet velocity is assumed as its value at the inlet to the water pool.

Thermal hydraulics of the particle field

The particle field is the most important heat source in the mixing zone due to its long stay in the zone and its large heat transfer area. The distance of the particle lateral movement would also determine the radius of the mixing zone.

Under steady state the vertical motion of the melt particles is defined from the balance of the gravity and the friction forces

$$(\rho_d - \rho_a)g = \frac{1}{8}C_{D,d}\frac{6\rho_a}{D_d}(u_d - u_a)|u_d - u_a| \tag{3.18}$$

The average time of melt particle staying in the mixing zone (sedimentation time) and the mass concentration of melt particles participating in the thermal hydrodynamic interaction in the zone are, therefore, defined by

$$\tau_{sd} = \frac{H_w}{u_d} \tag{3.19}$$

$$C_d = \frac{\dot{m}_{frag}}{u_d \pi R_{mz}} \tag{3.20}$$

where $\dot{m}_{frag}$ is the particle formation rate and R_{mz} is the radius of the mixing zone.

The radius of the mixing zone is determined from the lateral movement of the melt particle, which is governed by

$$\rho_d\left(\frac{dv_d}{dt}\right) = -\frac{1}{8}C_{D,d}\frac{6\rho_a}{D_d}v_d|v_d|. \tag{3.21}$$

In this formulation it is assumed that there is no motion of ambient fluid in the lateral direction.

Equation 3.21 can be transformed in to the equation of lateral migration length using the dependence $v_d = (dl_d)/(dt)$ and initial conditions ($t = 0 : \ l_d = 0$; $t = 0 : \ v_d = V^0_{d,\perp}$). The equation of the lateral migration length can be solved directly and has the solution

$$l_d(t) \ = \ \frac{ln(B\, V^0_{d,\perp} t \ + \ 1)}{B}; \qquad B = \frac{1}{8} C_{D,d} \left(\frac{6}{D_d}\right) \left(\frac{\rho_a}{\rho_d}\right). \tag{3.22}$$

By substituting the time in correlation 3.22 by the time of particle sedimentation, one can estimate the radius of the mixing zone as $R_{mz} = l_d(\tau_{sd})$.

When determining the heat transfer from the melt particles to coolant, especially for the case of high temperature melt when heat radiation dominates, it is very important to know the particle surface temperature. Since the particle surface temperature may vary a lot on the particle path through the mixing zone, it is essential to follow this transient. The height of the coolant pool is, therefore, divided into several equal sections and in each section the surface temperature of the melt particles generated at a specific section may be assumed to equal. Since the velocity of particles is known, it is easy to define the time of movement of a particle from the place of its generation to a specific section.

The change of the surface temperature of a melt particle depends on the heat conduction inside as well as on the heat transfer on the surface of it. In this aspect, oxidic melt particles are much different from the metallic ones and this could be an important factor, besides the melt superheat, which defines the amount of molten melt mass available in the mixing zone and ready to fuel the propagation of a potential steam explosion. In order to determine the surface temperature of melt particles on their path through the mixing zone, the transient 1D equation of heat conduction inside a spherical particle is solved up to the maximum time of particle stay in the mixing zone (τ_{sd}). The heat conduction in a spherical particle is governed by

$$\rho_d \frac{\partial(c_{p,d} T_d)}{\partial t} \ = \ \frac{1}{r^2} \frac{\partial}{\partial r} \left(r^2 k_d \frac{\partial T_d}{\partial r} \right). \tag{3.23}$$

This equation is solved with boundary conditions ($r = 0 : \ \partial T_d/\partial r = 0$ and $r = R_d : \ -k(\partial T_d/\partial r) \ = \ q_s \ = \ q_{fb} \ + \ q_{rad}$). The film boiling and radiation heat fluxes are given by

$$q_{fb} \ = \ h_{fb}(T_{d,s} \ - \ T_a), \tag{3.24}$$

$$q_{rad} = \varepsilon_d \sigma (T_{d,s}^4 - T_a^4). \tag{3.25}$$

where $T_{d,s}$ is the surface temperature of the particle.

Note that since the outside boundary condition is conjugated, Eqn.3.23 is solved in an iterative manner.

In order to account for the effects of phase change inside the particle, which may significantly reduce the speed of particle cool-down, the fixed-grid enthalpy method is applied. According to this method, Eqn.3.23 can be rewritten as

$$\rho_d \frac{\partial (C^0 T^*)}{\partial t} = \frac{1}{r^2} \frac{\partial}{\partial r} \left(r^2 k_d \frac{\partial T^*}{\partial r} \right) - \frac{\partial (S^0)}{\partial t}. \tag{3.26}$$

where $T^* = T_d - T_{d,mp}$ ($T_{d,mp}$ - melting temperature of the particle) and parameters C^0 and S^0 are given by

$$C^0(T^*) = \begin{cases} c_{sol} & (T^* < -\delta T) \\ \bar{c} + \frac{h_{fus}}{2\delta T} & (-\delta T \leq T^* \leq \delta T) \\ c_{liq} & (T^* > \delta T) \end{cases} \tag{3.27}$$

$$S^0(T^*) = \begin{cases} c_{sol}\delta T & (T^* < -\delta T) \\ c_m \delta T + \frac{h_{fus}}{2} & (-\delta T \leq T^* \leq \delta T) \\ c_{liq}\delta T & (T^* > \delta T) \end{cases} \tag{3.28}$$

Here, $\bar{c} = (c_{sol} + c_{liq})/2$.

Example calculations of particle cool-down and solidification were performed and the calculated particle surface temperature for different particle sizes is shown in Fig.3.9.

Knowing the particle surface temperature, or the time period during which the particle surface temperature stays higher than the melting point, one can estimate the amount of liquid melt mass accumulated in the mixing zone, which is an important factor to assess the power of a steam explosion resulting from melt-coolant premixing, if any.

In order to make exact the heat generation due to melt particles in the mixing zone, the particles are also divided into groups depending on the place of their generation along the melt jet. Each group, therefore, will have a different history of surface temperature variation on their path through the mixing zone, and the total heat generation by particles will consist of the sum from all particle groups.

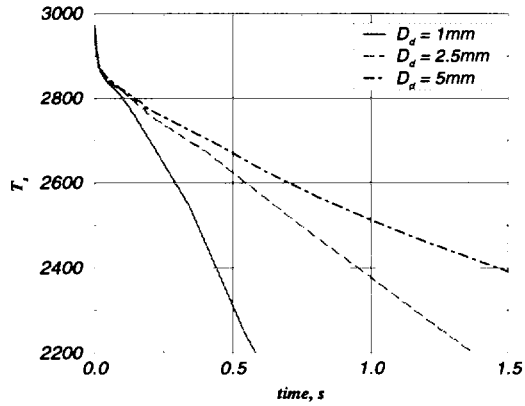

Figure 3.9: Variation of particle surface temperature in time ($h_{fb} = 200W/(m^2.K)$, $\varepsilon_d = 0.8$, $T_a = 293K$).

Treatment of the radiation heat

Since the mixing zone would contain a lot of steam with low heat radiation absorption capability and, for the radiation emitted by melt particle at temperature close to 3000K, water may becomes partly transparent to the radiation heat, not all heat radiated from the melt jet and particles could be absorbed in the mixing zone. In this work, this problem is resolved by means of a method proposed in [32]. The equivalent thickness of water available in the mixing zone is calculated and the absorption coefficient of radiative heat flux in this water thickness is determined. According to this, part of the radiative heat flux could escape from the mixing zone without participating in the heat-up and vaporization of coolant.

Heat generation due to metal oxidation

If the core melt contains metallic constituents, these metallic constituents may be oxidized when there is enough steam around them. For the ex-vessel melt-coolant mixing assessment, oxidation of Zirconium and stainless steel components contributes the most to the generation of non-condensible hydrogen and to the addition of heat in the mixing zone.

The oxidation reaction for Zirconium is

$$Zr + 2H_2O \rightarrow ZrO_2 + 2H_2 + Q_{Zr}, \tag{3.29}$$

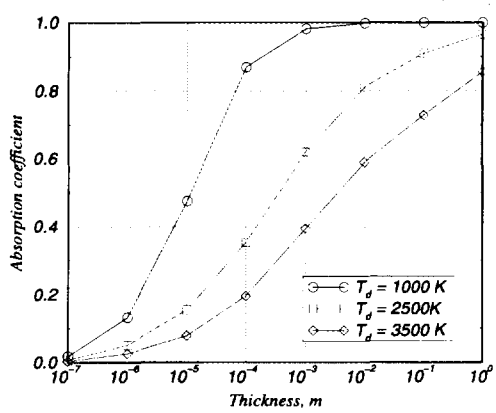

Figure 3.10: Absorption of radiative heat flux in water [32].

and the reactions for the constituents of stainless steel are

$$\begin{aligned} Fe + H_2O &\rightarrow FeO + H_2 + Q_1, \\ 2Cr + 3H_2O &\rightarrow Cr_2O_3 + 3H_2 + Q_2, \\ Ni + H_2O &\rightarrow NiO + H_2 + Q_3, \\ C + H_2O &\rightarrow CO + H_2 + Q_4, \end{aligned} \tag{3.30}$$

where $Q_{Zr} = 6.73$kJ/g Zirconium reacted and $(Q_1 + Q_2 + Q_3 + Q_4) = 0.645$kJ/g stainless steel reacted.

As can be seen, oxidation of Zirconium seems to be the most important contributor to heat generation in the mixing zone. Since the molar consumptions of steam for Zirconium and stainless steel oxidation is balanced by an equivalent molar generation of hydrogen, the containment pressurization is not affected by the oxidation of metallic constituents in the core melt.

In this work, only oxidation of Zirconium is considered. There are two major mechanisms limiting the oxidation reaction, namely steam availability and solid-state diffusion (oxide layer growth). The first mechanism is not accounted here, while the second mechanism is treated by a simple parametric approach, in which the law of parabolic oxidation rate is employed.

Coolant thermal hydraulics

At steady state, the water evaporated and escaping from the mixing zone is balanced by the water supply from outside water volume. The vaporization

rate can, therefore, be defined by

$$\dot{m}_v = \frac{[\sum Q - G_v c_{p,v}(T_s - T_w)]}{h_{fg}} \tag{3.31}$$

where G_v is the rate of vapor escaping from the mixing zone, $G_v = \alpha_v \rho_v U_v (\pi R_{mz}^2)$.

The vapor velocity in the mixing zone is estimated using the following expression

$$U_v \approx 1.4 \left[\frac{\sigma_w g(\rho_w - \rho_v)}{\rho_v^2}\right]^{1/4}. \tag{3.32}$$

Given the vapor velocity, average void fraction of the mixing zone can be determined as follows

$$\alpha_v = \frac{\dot{m}_v}{\rho_v U_v (\pi R_{mz}^2)}. \tag{3.33}$$

This average void fraction is used further to estimate the other characteristics of two-phase coolant, such as density (ρ_c) or velocity (u_c). The water is assumed to be at rest.

Solution procedure

The general scheme of solution procedure is presented in Fig.3.11.

In general, the solution procedure consists of a Monte-Carlo loop of 100.000 steps. As mentioned before, all the premixing parameters are calculated in an iterative loop until convergence. The parameters utilized to check for the convergence of the iterative procedure could be the mixing zone void fraction or the total melt mass present in the mixing zone at steady state.

Results of the assessment for ex-vessel premixing

Assessment of melt-coolant premixing is performed for Swedish LWRs, when the containment drywell is filled with water as a result of severe accident management activity. The range of uncertainties are specified and shown in Table 3.4.

Assessment is performed for two cases of jet composition. In one case, the discharged melt is mainly oxidic and, in the other case, it is metallic. The melt properties used in the assessment are presented in Table 3.4.

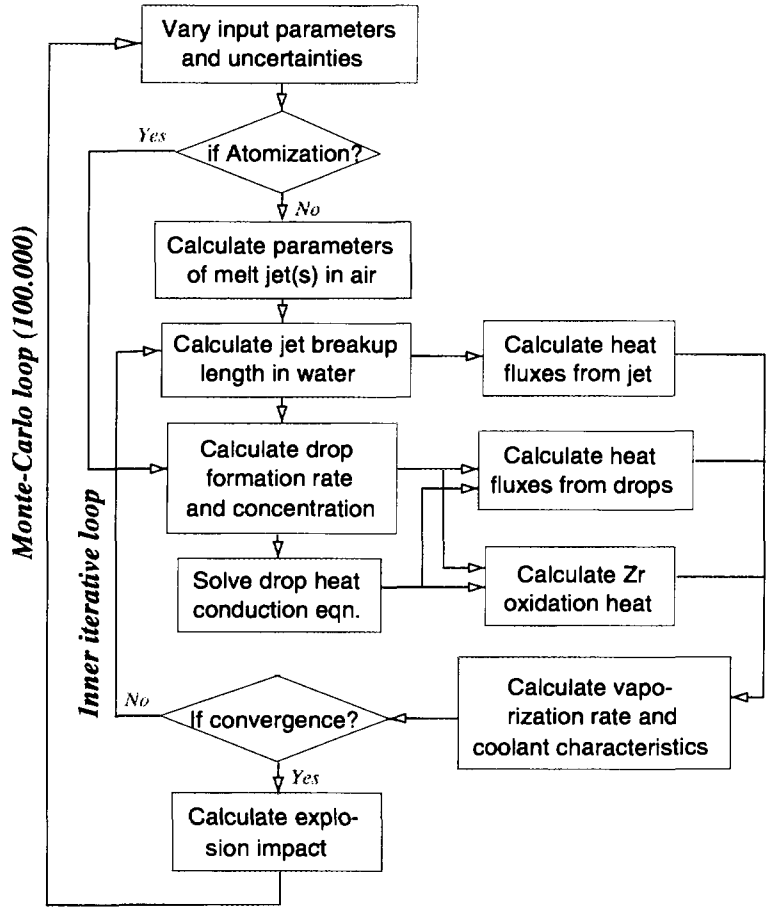

Figure 3.11: Solution procedure.

The results of assessment for the oxidic melt-water premixing are presented in Figs.3.12-3.19.

It can be seen from Figs.3.12-3.13 that the mixing zone is quite large, with diameter about 2 m. For high melt temperature, the steam production rate in the mixing zone is high, providing high local void fraction at low system pressure (60%-70%).

Figs.3.14-3.15 show energy release and steam generation rates which are in the same range of FARO experiments.

Figs.3.16-3.17 show debris mass and mass of fully-liquid debris in the mixing zone. Since the water pool is deep, the total particle mass is also large (100 to

400 kg). Mass of particles which are counted as fully liquid is however not large. It is because at high temperature, the radiative heat flux is significant, which causes solidification on the drop surface.

Figs.3.18-3.19 show the average surface temperature of corium droplets in the mixing zone. It varies from 1500K to 2400K. This result indicates that most of the particles are solidified while levitating and settling in the mixing zone. When reaching the bottom debris, the particles are essentially solid.

In case of metallic melt release, significantly higher melt superheat (up to 700K) was specified to simulate the overheat of metallic debris components while being in contact with decay-heated oxidic debris. The melt discharge rate 10 to 100 kg/s) was chosen as conservative bounding case, when large metal melt was accumulated in the lower plenum and discharged when a vessel penetration failed and the tube dropped away.

Results of the assessment for the metal melt-water premixing are presented in Figs.3.20-3.27.

As can be seen from the figures, higher melt superheat resulted in a much higher concentration of molten particle mass in the mixing zone and, therefore, higher impact of a potential steam explosion. Significant increase in the heat conduction in case of the liquid melt was found to affect the process of particle cooldown. Specifically, the decrease of particle surface temperature was found to be slower in comparison to the case of oxidic melt.

Table 3.4: Ranges of the scenario and phenomenological uncertainties used in the current assessment

Uncertainty	Symbol	Range	
		Oxidic	Metallic
- Water pool depth	H_w	(4..10)m	
- Water pool temperature	T_w	293K	
- Initial ex-vessel pressure	$P_{ex-vessel}$	1bar	
- Melt discharge rate	G_{dc}	(10..100)kg/s	
- Discharge diameter	D_{dc}	(5..15)cm	
- Melt superheat at discharge, K	$T_{m,dc} - T_m$	(0..150)	(0..700)
- Number of discharging melt jets	$N_{j,dc}$	1	
- Possibility of melt atomization in the air	$\mathcal{P}_{atom}$	0	
- Friction factor of core melt jet in coolant	$C_{D,j}$	0.44	
- Jet radiation emissivity	ε_j	0.8	0.2..0.4
- Melt particle average diameter	D_d	(1..4)mm	
- Melt particle friction factor	$C_{D,d}$	2	
- Initial lateral velocity of particles	$V^0_{d,\perp}$	(0.25..0.75)u_j	
- Drop radiation emissivity	ε_d	0.6	0.2..0.4
- Film boiling heat transfer coefficient	h_{fb}	200W/(m^2.K)	

Table 3.5: Melt properties

Property	Oxidic melt	Metallic melt
Density, kg/m^3	7960	7000
Viscosity, Pa.s	0.0053	0.002
Conductivity, W/(m.K)	2.88	30.
Specific heat, J/(kg.K)	565	500
Latent heat, J/kg	$3.62{\cdot}10^5$	$3{\cdot}10^5$
Melting temperature, K	2850	1700
Surface tension, N/m	0.5	0.5

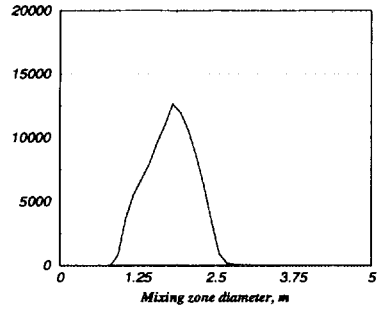

Figure 3.12: Mixing zone diameter.

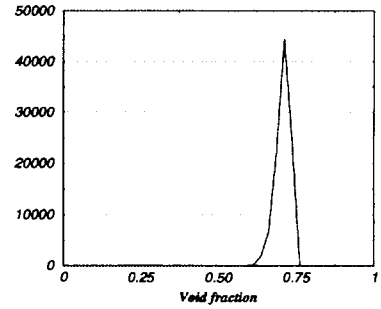

Figure 3.13: Average void fraction.

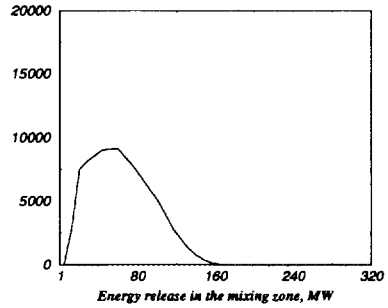

Figure 3.14: Total energy release.

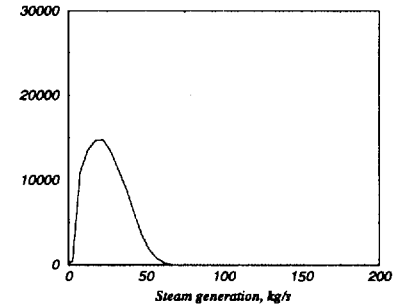

Figure 3.15: Steam generation rate.

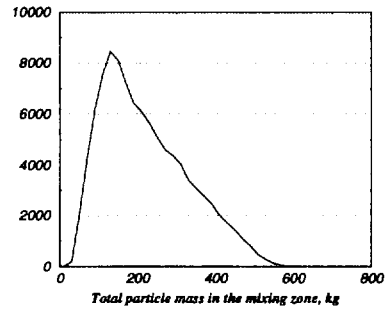

Figure 3.16: Total particle mass.

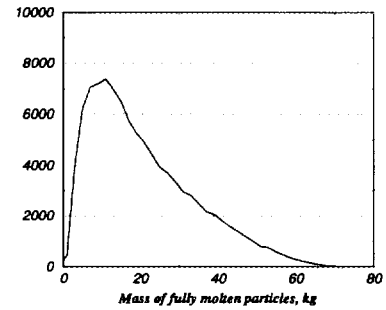

Figure 3.17: Molten particle mass.

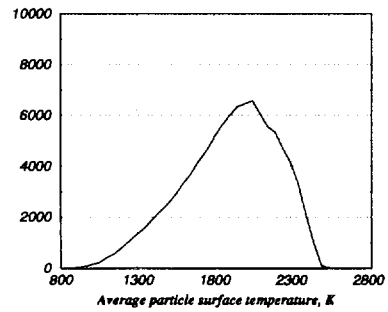

Figure 3.18: Average surface temperature of the particles.

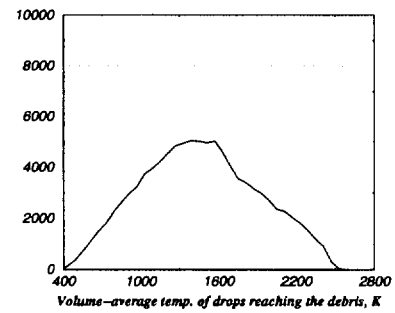

Figure 3.19: Volume-average temperature of the particles reaching the debris bed.

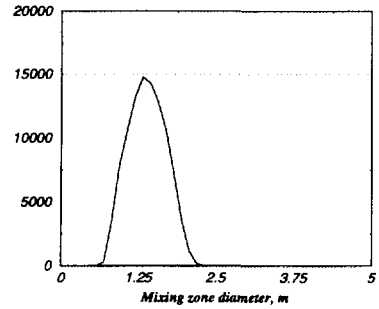

Figure 3.20: Mixing zone diameter.

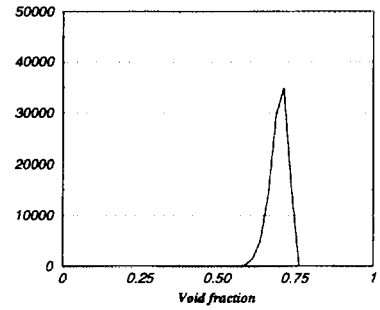

Figure 3.21: Average void fraction.

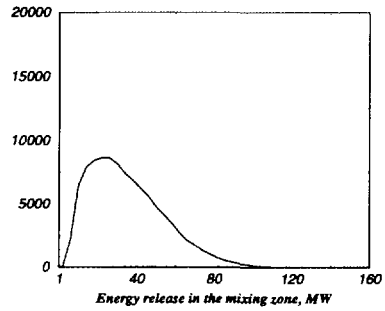

Figure 3.22: Total energy release.

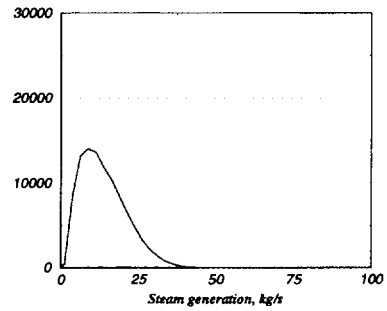

Figure 3.23: Steam generation rate.

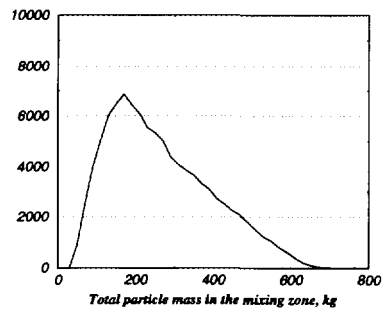

Figure 3.24: Total particle mass.

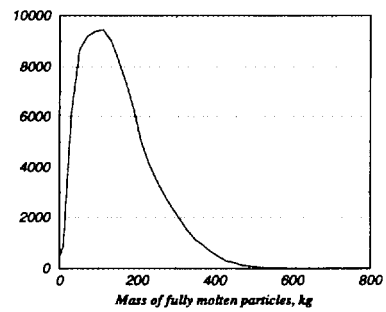

Figure 3.25: Molten particle mass.

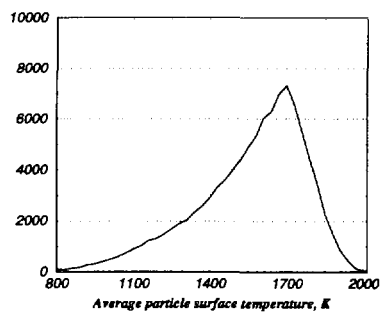

Figure 3.26: Average surface temperature of the particles.

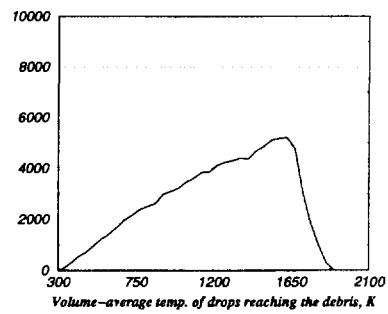

Figure 3.27: Volume-average temperature of the particles reaching the debris bed.

3.2.3 Mechanistic modeling of melt-coolant premixing

The process of ex-vessel melt-coolant premixing may also be modeled in a more mechanistic manner with application of detailed models of particle, water, and vapor transport. This part presents a mechanistic model of melt-coolant premixing, where the transient processes of melt discharge and melt-coolant mixing are accounted for and the particle and coolant fields are represented by pseudo-2D models.

Jet behavior

Behavior of the melt jet in the air and in water pool is treated in the same manner as in previous part. However, the positions of the jet leading edge and tail are calculated in time in order to follow the highly transient processes.

The jet fragmentation provides a mass influx to the fuel particle field, which is assumed to be linearly distributed along the jet body.The change of the jet temperature due to thermal exchange with the water field is assumed to be negligible. Nevertheless, heat flux from the jet surface is still a heat source to the coolant energy equation.

Particle transport

The particle mass, velocity, and temperature distributions are described by a 1D formulation. No sequential breakup of the melt particles is assumed and the particle size is a parameter to vary. The system of equations is

$$\frac{\partial m_d}{\partial t} + \frac{\partial m_d v_d}{\partial z} = \dot{m}_{frac}, \tag{3.34}$$

$$\frac{\partial (m_d v_d)}{\partial t} + \frac{\partial (m_d v_d^2)}{\partial z} = g\, m_d \left(1 - \frac{\rho_a}{\rho_d}\right) - \dot{m}_{frac}\, v_d - F_d(v_d - v_a), \tag{3.35}$$

$$\frac{\partial (m_d c_{p,d} T_d)}{\partial t} + \frac{\partial (m_d c_{p,d} v_d T_d)}{\partial z} = m_d \cdot \frac{6}{D_d} h_{d-a}(\bar{T} - T_d) + \dot{m}_{frac}\, T_j. \tag{3.36}$$

where D_d is the particle diameter and F_d is the friction coefficient for particle

$$F_d = \frac{1}{8} C_{D,d} m_d \cdot \frac{6}{D_d} \frac{\rho_a}{\rho_d} |v_d - v_a|. \tag{3.37}$$

It is worth noting that in this formulation, the temperature field inside a melt particle is assumed to be uniform. Therefore, only one average temperature could be applied for the particles located at a specific vertical plane.

In order to account for particle solidification, which may delay the decrease of the particle temperature, the fixed-grid temperature-based enthalpy approach to phase-change is applied.

In order to obtain a correct heat source for a 2D mixing zone, the particle mass concentration, defined from the system of 1D conservation equations, is then uniformly redistributed into a 2D mixing zone. The 2D spreading of the particles away from the jet can be defined for each vertical position by Eqn.3.21 presented in the previous part. The velocity of the melt particles at breakup from the jet is estimated using the shear velocity

$$V_{d,\perp}^{0} \propto \sqrt{C_f \frac{v_j^2}{2}} \tag{3.38}$$

Coolant behavior

The coolant field, consisted of water and steam, is described by a two-fluid, two-dimensional formulation. In order to simplify the modeling, only horizontal (center-ward) movement of water and vertical (upward) motion of steam are considered. Furthermore, the steam temperature is assumed to be constant and equal to T_{sat}. Behavior of the coolant field, therefore, can be described by 5 conservation equations

Steam mass conservation equation:

$$\frac{\partial(\alpha_v \rho_v)}{\partial t} + \frac{\partial(\alpha_v \rho_v v_v)}{\partial z} = \dot{m}_v - \dot{m}_c. \tag{3.39}$$

where $\dot{m}_v$ and $\dot{m}_c$ are the vaporization and condensation mass sources, respectively.

Water mass conservation equation:

$$\frac{\partial(\alpha_w \rho_w)}{\partial t} + \frac{1}{r}\frac{\partial(r\alpha_w \rho_w u_w)}{\partial r} = -\dot{m}_v + \dot{m}_c. \tag{3.40}$$

Momentum equation for steam upward movement

$$\frac{\partial(\alpha_v \rho_v v_v)}{\partial t} + \frac{\partial(\alpha_v \rho_v v_v^2)}{\partial z} = g\alpha_v(\rho_v - \rho_w) - F_v v_v - \dot{m}_v v_v, \tag{3.41}$$

where F_v is the friction coefficient.

Momentum equation for water horizontal movement

$$\frac{\partial(\alpha_w \rho_w u_w)}{\partial t} + \frac{1}{r}\frac{\partial(r\alpha_w \rho_w u_w^2)}{\partial r} = -\alpha_w \frac{\partial p}{\partial r} - F_w u_w - \dot{m}_c u_w, \qquad (3.42)$$

Note that in the water momentum equation, instead of defining the pressure term explicitly, the pressure gradient, $\partial p/\partial r$, is estimated from the difference in static hydraulic pressures between adjacent columns.

Energy conservation equation for water

$$\frac{\partial(\alpha_w \rho_w C_{p,w} T_w)}{\partial t} + \frac{1}{r}\frac{\partial(r\alpha_w \rho_w u_w C_{p,w} T_w)}{\partial r} = = Q_j + Q_d + Q_{db} + \dot{m}_c C_{p,w} T_{sat} \qquad (3.43)$$

where Q_j, Q_d, and Q_{db} are the heat fluxes from jet, particles, and debris bed, respectively.

Heat transfer between melt and coolant

Heat removal from melt to coolant is carried out by the convective and radiative heat transfers. In this work, all the heat flux from the melt is assumed to be consumed by water heating and vaporization. Therefore, vapor overheating is neglected.

For the film boiling convective heat transfer, the correlation developed by Liu and Theofanous [51] has been employed. The major concern is about the applicability of these correlations for film boiling at high pressure condition (which is relevant to the FARO experiments).

The radiative heat flux is treated in the same manner as in the probabilistic assessment part, i.e. the absorption coefficient is defined as a function of melt temperature and effective water thickness. As a result, the amount of radiative heat flux absorbed in the mixing zone can be estimated.

Solution procedure

The models are implemented into a code (SAPHIRA-FCI) written in the Java programming language to facilitate a better graphic presentation. The finite difference method with first-order time resolution is used to solve the system of conservation equations.

Prediction of the FARO test data

The code has been employed to predict the FARO test data. The FARO-series of experiments have been conducted at the JRC-Ispra to investigate melt/water mixing and quenching process. The experiments were performed inside a test vessel, which can withstand pressures up to 10MPa. Molten corium (up to 170 kg) with prototypical composition ($UO_2/ZrO_2/Zr$) was employed. The depth of the water pool is around 2m. So far, 8 mixing/quenching experiments have been performed. The first 7 experiments were realized in the TERMOS vessel and the last experiment in the new FAT vessel with significant larger free-board volume (3.7 m^3). Except for the last two experiments (L-24 and L-27) previous experiments were performed under relatively high initial vessel pressures (more than 2MPa).

In the FARO experiments the melt discharge time is relatively short ($\propto$ 1..1.2s) and the test section was closed during the experiment. As a result, intensive vaporization of water in contact with hot melt produced a large quantity of steam, which caused a large vessel pressurization. For such pressurization, the water and vapor properties change and they may strongly affect the process of melt-water mixing and thermal hydraulic interactions between melt and water. For the predictions here, variations of water and vapor properties in time are taken into account and the transient properties are calculated by interpolation of the tabulated data.

The FARO L-24 experiment is analyzed. This experiment was performed with a relatively low initial vessel pressure (5 bar), which corresponds approximately to the ex-vessel melt-coolant mixing conditions. The average particle size is chosen to be 2.5mm and no water swelling is considered in the numerical simulation.

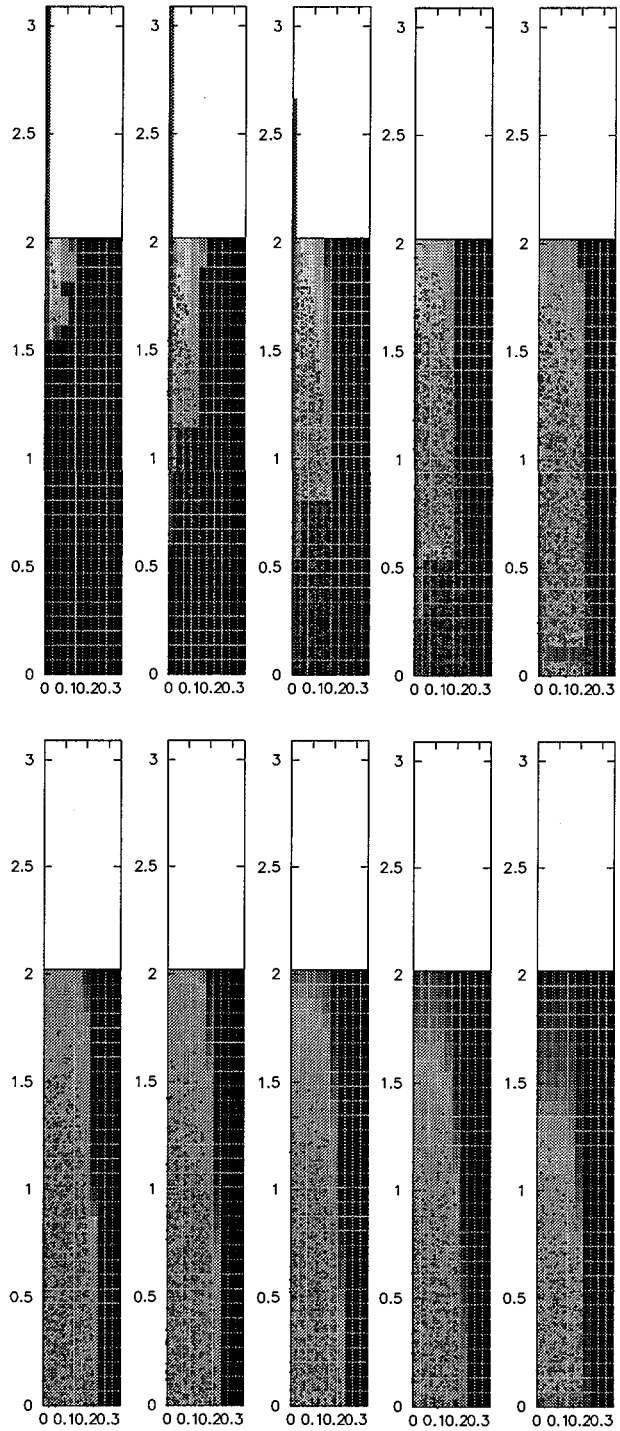

Figure 3.28: SAPHIRA-FCI simulation for FARO L24 experiments.

Fig.3.28 displays the predicted results for the jet location, particle distribution, and coolant voiding as a function of time. The time interval between the pictures is 0.12s. The first picture in the series is at 0.11s after the melt jet enters the water pool.

The calculated pressurization is compared to the measured data in Fig.3.29. Reasonably good prediction of the pressurization rate is indicated.

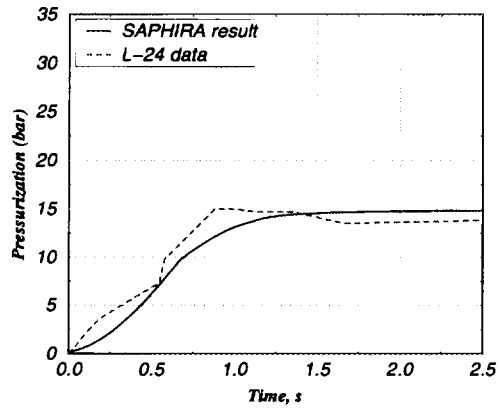

Figure 3.29: Calculated vessel pressurization in comparison with the FARO data for L24 test.

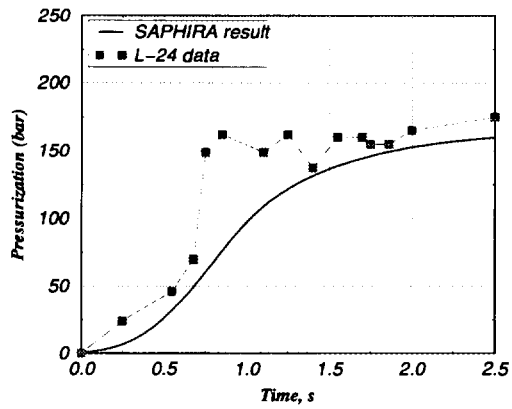

Figure 3.30: Calculated energy release in comparison with the FARO data for L-24 test.

The total amount of energy released to the coolant is also calculated and compared in Fig.3.30 with the L-24 experimental data.

Sensitivity analysis was also performed to investigate the effects of various factors on the melt-water interactions. Taking the L24 test as a standard case, the characteristics of the process were varied in order to clarify their effects.

Figure 3.31 shows the effects of the chosen particle diameter on the vessel pressurization. As can be seen from the figure, choice of a smaller particle diameter could result in a higher rate and final value of pressure increase.

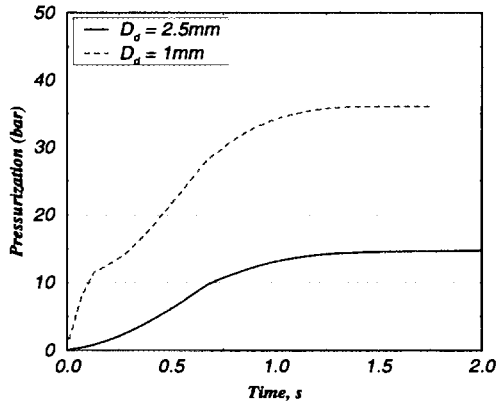

Figure 3.31: Effects of the particle diameter.

The water subcooling, even though not considered in the FARO experiments, may have significant impact on the melt-water premixing under prototypic severe accident conditions. Fig.3.32 shows the result of calculations, performed for the case of initial water subcooling equal to 40K. As expected, the water subcooling delays the beginning of pressurization and reduces the rate as well as the final value of the pressure increase.

3.2.4 Summary of the results

In this section, phenomenology of the melt-coolant premixing is considered from the point of view of both probabilistic assessment and mechanistic modeling. The probabilistic assessment was based on both mechanistic modeling and Monte-Carlo treatment of various scenario and phenomenological uncertainties. In the assessment a steady-state mixing condition was considered. The results of the assessment performed for the oxidic and metallic melt releases provide the probabilistic distributions of the factors important for the analysis of steam

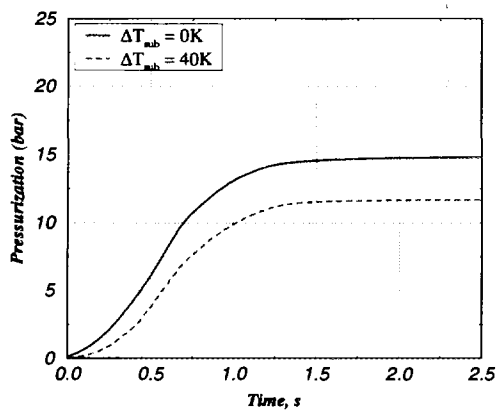

Figure 3.32: Effects of the water subcooling.

explosion energetics and long-term debris coolability. These are the melt surface temperature, the mixing zone void fraction, the masses of particles and of molten particles present in the mixing zone. The mechanistic modeling was based on a multi-field description of the mixing zone. In order to avoid numerical difficulties and accelerate the solution procedure, pseudo-2D treatments were introduced in the models of melt particle and coolant transport. Validation of the models and of the SAPHIRA-FCI code was performed by comparing the calculated results to the FARO experimental data. A reasonable agreement between the calculated results and experimental data for vessel pressurization and energy release was observed. Some sensitivity studies on the effects of particle size and water subcooling were also conducted.

3.3 Concluding remarks

The work presented in this chapter is focused on improving the understanding about the physics of the initial phase of the complicated process of melt-water interactions. The direct numerical simulation presented in the first part is concerned mainly with the phenomenology of hydrodynamic interfacial melt-water interactions. Specifically, the shear instabilities, which may lead to the deformation and fragmentation of melt jet or drops, are numerically investigated using 'first-principle' modeling. The modeling method is based on the direct simulation of the flow and interface motion, which is coupled with the level set front-capturing algorithm to eliminate the numerical diffusion. The simulation, performed to investigate the problems of Kelvin-Helmholtz instability develop-

ment as well as melt (jet, drop) fragmentation, showed a reasonably accurate picture of the interfacial behavior. The modeling approach developed was also applied to study the sensitivity of the melt-water mixing process on the field and the melt properties and the surface tension.

The phenomenological and mechanistic models of thermal hydrodynamic interactions, presented in the second part, were shown to be able to capture the most essential physical processes and feedbacks involved and to provide an integral picture of melt-water premixing. Comparison of the results of the simulation for a FARO experiment indicated good agreement between the calculated pressurization and the reported data. The models developed are a good tool to study the effects of many important factors, such as fragment size, subcooling, heat transfer mechanisms, etc., on the melt-water premixing process.

Chapter 4

Modeling of Melt-Concrete Interactions and Debris Coolability

Late phase of severe accident progression is associated with melt discharge from the RPV and its deposition on the containment floor to form a core debris bed. Geometry and structure of such a debris bed and its coolability are largely defined by the characteristics of the previous stages of melt-structure and melt-water interactions. Without early cooling and fragmentation, the core melt may form a high-temperature layer or a homogeneous debris cake on the containment basemat, which is difficult to cool. In contrast, a porous debris bed, formed as a result of melt fragmentation is much easier to cool. Under sustained decay heating, the debris temperature may increase and exceed the concrete decomposition temperature; concrete ablation begin and this process will only stop when the heat removal from the debris bed by heat transfer to its open surfaces and heat conduction to the concrete can balance the heat generation by decay heating. In addition, a melt pool could be generated through remelting of a non-coolable debris bed. Consequently, the configurations of core debris may include (i) a bed of hot particulate debris; (ii) a pool of molten core material; (iii) a debris cake; and (iv) various combinations and transformations (from one to another) of the basic configurations.

In order to obtain an insight into the complicated interrelationship of phenomena involved in the melt pool coolability issue, a synthesis of mechanistic models of physical processes occurring inside and outside a debris melt pool

interacting with water and concrete under severe nuclear reactor accident conditions has been developed. Numerical studies are then performed to investigate the sensitivity of the coolability of once formed melt pool to influencing parameters, e.g., the melt pool configuration, initial and boundary conditions, uncertainties in predicting physical mechanisms of corium-concrete interactions, debris-water heat transfer, variations of physical properties, etc.

4.1 Background and Problem formulation

When analyzing debris bed coolability, one has to deal with large uncertainties in initial and boundary conditions of the debris bed. Uncertainties accumulate from those of in-vessel melt progression, vessel lower head failure and ablation, melt-coolant interactions (fragmentation and steam explosion) and debris bed formation. Furthermore, the plant-specific design and accident management features and feedbacks from debris coolability-related phenomena diversify the boundary conditions of interest.

There is a wide spectrum of thermal-hydraulic and physico-chemical phenomena involved in the debris coolability issue. They include, for instance, the thermal hydraulics of particulate debris beds, the debris cake-concrete-water interaction, melt pool heat transfer and related processes. Studies of these phenomena are being simultaneously pursued to resolve various phenomenological uncertainties. Experimental studies have been performed to investigate the behavior of particulate beds and dryout phenomena occurring in the particulate debris beds for high decay heat generation [83] [86]. It appears that the current knowledge of particulate bed thermal hydraulics is not enough to estimate the dryout power in all the debris bed configurations that could happen under ex-vessel severe accident conditions. However, the present data base and models can be applied to assess the debris behavior in some limiting cases and to perform preliminary sensitivity analyses for the effects of phenomena affecting the real cases. The issue of debris cake-concrete-water interactions has initiated large experimental programs (BETA(KfK); MACE(EPRI,ANL); SURC(SNL); etc.) to investigate (i) concrete ablation, (ii) heat conduction in the concrete basemat, (iii) decomposition of concrete constituents, (iv) decomposition gas release, and (v) corresponding changes in concrete properties. Many computer codes, such as CORCON-Mod2-WU [58], WECHSL [65], MAAP-4/DECOMP [64], have been developed to address this issue. The melt coolability experimentation has not been extensive. Sandia National Laboratory (SNL) performed inductively heated experiments named SWISS[13]. A coolability test was also performed in the WETCOR facility at SNL using simulant high melting temper-

ature oxidic material with heated walls interacting with concrete at the bottom and cooled by water at the top. A series of large-scale experiments (MACE) have been performed at Argonne National Laboratory (ANL) investigating the coolability of molten corium by overlying water during melt interaction with concrete [70].

The objective of the this work is the coolability issue of a decay-heated core debris bed, located on the containment floor. Most important parameters of the issue from the safety view point are: (i) the time period required before a balance of the decay heat generation inside and heat removal from the debris bed could be achieved and the concrete ablation stops; (ii) the ablation rate of the basemat concrete; and (ii) the final ablation depth of the basemat concrete.

The melt pool configurations are concluded to be uncoolable (and calculations are terminated) if the concrete melting continues after its 1-m ablation (stabilized values of the pool-to-the-bottom-crust heat fluxes are larger than those can be conducted by the concrete). In cases of coolable debris beds, the parameter of interest is the final ablation depth.

4.2 The modeling approach

4.2.1 General features

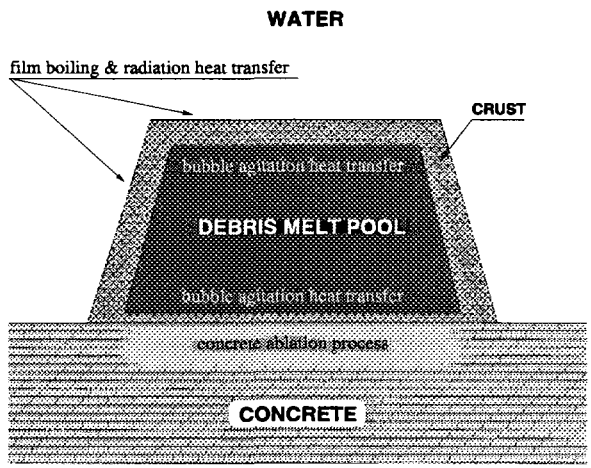

Figure 4.1: Conceptual picture of debris coolability and concrete ablation.

The modeling is based on the assumption that the core debris bed is com-

pletely formed and no further spreading will be expected. Initially, the debris bed may consist of a melt pool surrounded by the upper, side, and bottom crust layers (see Fig.4.1). The heat removal from such a debris bed is defined by the convection heat transfer from the bed top and sides, and the heat conduction to the concrete from the bed base.

It is clear that the coolability of the debris bed or the occurrence of concrete ablation, if any, depends on the initial configuration and characteristic of the bed, i.e. (i) the initial debris height, H_m; (ii) the decay heat generation rate q_v; (iii) composition of debris materials; (iv) the initial temperature of the debris bed.

Other related physical parameters are the initial temperature of concrete T^o_{conc}, concrete composition and properties, water temperature T_w, system pressure P_{cont}.

The modeling is based on the conservation laws applied to:

- energy balance of the debris melt pool;
- mass balance of the debris melt pool;
- energy and mass balances of top, side, and bottom crust layers;
- energy and balances of the molten slag layer beneath the bottom crust, if incomplete drain of molten slag through the porous bottom crust is assumed;
- energy balance (heat conduction and decomposition/melting) of concrete;
- mass conservation of interested melt pool metals participating in oxidation reactions with concrete decomposition products.

Melting of the concrete and formation of a molten concrete layer beneath the debris bed may render the conditions for core melt and molten concrete mixing. Due to the density difference, the products of concrete melting may drain through the bottom crust layer and mix with the core melt. The bottom crust layer, floating between two molten layers of difference densities, if thin, may also become unstable and crack, rendering a complete mixing between two melts and a possible sedimentation of the core melt, which is much denser than the concrete melt.

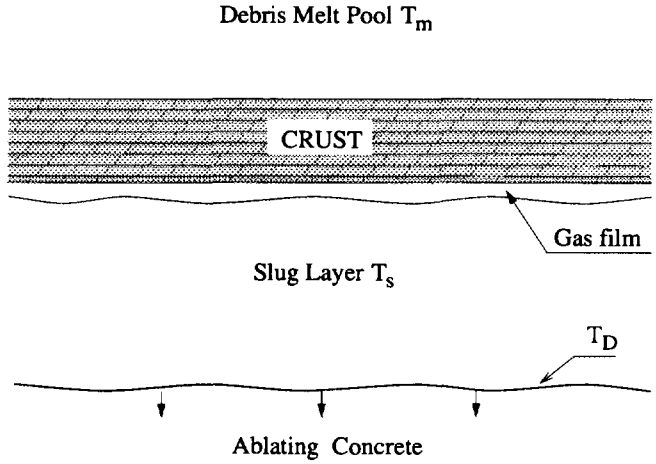

Figure 4.2: Concrete ablation and crust stability.

Behavior of a core debris bed and its coolability; the concrete ablation rate as well as the resulting ablation depth are governed by a set of physical as well as chemical interactions occurring inside the debris melt pool and on the debris-water/debris-concrete interfaces. These important interactions are included in this modeling through the closure correlations representing:

- the heat transfer from the debris bed to overlying water by film boiling and heat radiation;
- the heat transfer from the debris bed to concrete;
- heat transfer phenomena inside the melt pool affected by sparging gases and the variation of pool thermophysical properties due to the changes of its temperature and composition (mixing with concrete decomposition products);
- oxidation reactions of pool components with concrete decomposition products;
- concrete decomposition and melting.

The heat conduction phenomenon inside the concrete is described by one-dimensional heat conduction equation, whose solution can provide the temperature distribution in concrete and the conduction heat flux on the melt pool - concrete intersurface.

4.2.2 Heat balance of the debris melt pool

Assuming that some fraction of the formed decomposition slag drains through the porous bottom crust layer and continuously mixes with the core melt, and the lower boundary of the melt pool is moving together with the ablation front, we have the heat balance equation for the melt pool as follows:

$$
\begin{aligned}
(\rho_m c_{p,m} V_m \;+\; \rho_s c_{p,s} V_s)\frac{dT_m}{dt} \;=\; & Q_v V_m + \rho_m \frac{dV_m}{dt}[c_{p,m}(T_{m,sol} - T_m) - h_{fus,m}] + \\
+ \;& \rho_s \frac{dV_m}{dt}\frac{V_s}{V_m}[C_{ps}(T_{m.sol} - T_m) - h_{fus,s}] + \\
+ \;& \sum_i \sum_j V_{g,j}\rho_{g,j} f_{ij} M_{ij} h_{ij} - q_{top}A_{top} - q_{side}A_{side} - q_{bott}A_{bott} + \\
+ \;& \left(\frac{dV_s}{dt}\right)_{drained} \rho_s[f_{rs} m_m h_m - C_{ps}(T_m - T_s)] \qquad (4.1)
\end{aligned}
$$

where

M_{ij} is the reaction mass of metal i required for interaction with gas j;
h_{ij} is the heat release in the gas-metal reaction;
f_{ij} indicates the fraction of reacted gas;
f_{rs} is the fraction of reacted slag;
m_m is the mass of metal requirement in the slag-metal interaction;
T_s is the average drained slag temperature;
V_m is the volume of debris melt in the pool;
V_s is the volume of concrete slag in the pool.
V_g is the volume of the gas j passing the debris melt pool in a unit time.

The first term in the right hand side of Eqn.4.1 is the heat decay source. The second and third terms indicate the heat losses due to crust melting or freezing. The fourth term accounts for the heat source due to the gas-metal interactions when gas bubbles through melt pool. The fifth to seventh terms represent the heat loss to the top, side and bottom surfaces, respectively. The last term indicates the heat generated by the the slag-metals interactions and the heat loss to heating the concrete slag from the average slag temperature to that of the melt.

4.2.3 The mass balance of the debris melt pool

The debris melt pool can be considered to consist of two components named debris melt V_m and concrete slag V_s, whose volumes vary in time. The changes of the component volumes are governed by the following conservation equations

$$\frac{dV_m}{dt} = \left(\frac{dV}{dt} f_m\right)_{crust\ melting\ or\ freezing} \tag{4.2}$$

$$\frac{dV_s}{dt} = \left(\frac{dV}{dt} f_s\right)_{slag\ melting\ or\ freezing} + \left(\frac{dV_s}{dt}\right)_{drained}$$

$$= \left(\frac{dV}{dt} f_s\right)_{slag\ melting\ or\ freezing} + \left(\frac{q_D A_{bott}}{h_D \rho_{conc}}\right) f_s f_{dr} \tag{4.3}$$

where V is the volume of melting or freezing crust, f_m and f_s are the volume fractions of melt and slag, respectively, components in the debris melt pool, q_D is the fraction of bottom heat flux, taking part in concrete melting process, m_s is the weight fraction of concrete components coming into slag, and f_{dr} is the fraction of the formed slag draining through the bottom crust layer and mixing with melt pool materials.

4.2.4 Heat balance of the crust layers

The heat conduction inside the crust layer can be modeled by the one-dimensional heat conduction equation,

$$\frac{dT}{dt} = \alpha \frac{d^2T}{dx^2} + \frac{q_v}{\rho c_p} \tag{4.4}$$

The dynamics of the crust layer thickness is governed by the equation:

$$h_{fus} \rho \frac{d\delta}{dt} = -k \frac{dT}{dx}\Big|_{melt-crust\ intersurface} - q_{in} \tag{4.5}$$

where q_{in} is the heat flux at the melt-crust intersurface.

In order to simplify the heat conduction equation (4.4) we will assume that the characteristic time of heat conduction process τ_c is much less than that of freezing or melting process τ_m. In that case the transient term in (4.4) will be eliminated and, assuming that the temperature at debris melt-crust interface is equal to solidus temperature $T_{m,s}$, the heat conduction equation has

the following solution,

$$T = -\frac{q_v}{k}\frac{x^2}{2} + \frac{q_v\delta - q_{out}}{k}x + T_{m,s} \tag{4.6}$$

where q_{out} is the heat flux removed from the crust layer.

Finally, the equation of crust thickness becomes,

$$h_{fus}\rho\frac{d\delta}{dt} = q_{out} - q_v\delta - q_{in} \tag{4.7}$$

4.2.5 Heat and mass balances of the concrete slag layer

The bottom crust layer is bounded from one side by the debris melt pool and experiences the heat flux defined by above-mentioned equations. Because only a part of concrete slag can rise through the crust layer, the remaining part will form a slag layer beneath the crust, and therefore, the other side of the crust layer is in contact with slag layer separating the crust from the concrete melting front. For the slag layer we can write a heat balance equation, which is similar to that of the debris melt pool (Eqn.4.1)

$$\rho_s c_{p,s} V_{sl}\frac{dT_s}{dt} = -q_{up}A_{bott} - q_{down}A_{bott} - \frac{dV_{sl}}{dt}\rho_s[c_{p,s}(T_s - T_D) + h_D] \tag{4.8}$$

In the right hand side of equation (4.8) the first two terms present the heat fluxes on the boundaries and the last term presents the energy spent in the decomposition/melting of concrete and heating the formed slag from the melting temperature to $\overline{T_s}$.

The change of the slag layer volume V_{sl} is governed by following equation

$$\frac{dV_{sl}}{dt} = \left(\frac{q_D A_{bott}}{h_D\rho_{conc}}\right) f_s(1 - f_{dr}) \tag{4.9}$$

4.2.6 Concrete decomposition and melting

The heat flux coming from debris melt pool to concrete can be divided into two parts. One part goes to heat conduction in concrete, while the other goes to concrete melting process. In order to determine the heat conduction flux into

the concrete we solve one-dimensional transient heat conduction equation inside the concrete

$$\rho_{conc} c_{p,conc} \frac{dT}{dt} = k_c \frac{d^2T}{dx^2} \tag{4.10}$$

where x is coordinate associated with moving front of concrete melting.

From the solution of equation (4.10) we can define the conduction heat flux and therefore the concrete melting heat flux as follow

$$q_{cond} = -k \left(\frac{dT}{dx}\right)_{x=0} \tag{4.11}$$

$$q_D = q_{down} - q_{cond} \tag{4.12}$$

4.2.7 Closure correlations

Heat transfer on the boundaries of debris melt pool

Assuming that the temperature of the crust-pool interface equals the melt *solidus* temperature, the heat flux on the top, bottom, and side surfaces can be defined as follows,

$$q_{top} = h_{top} (T_m - T_{m,sol}) \tag{4.13}$$

$$q_{side} = h_{side} (T_m - T_{m,sol}) \tag{4.14}$$

$$q_{bott} = h_{bott} (T_m - T_{m,sol}) \tag{4.15}$$

where h_{top}, h_{side}, and h_{bott} are the heat transfer coefficients at the top, side, and bottom, respectively.

The heat transfer coefficients at the top, side, and bottom of the debris melt pool undergoing natural circulation can be determined by the following correlations,

$$Nu_{bott} = \frac{h_{bott} H_m}{k} = 0.345\, Ra^{0.233} \tag{4.16}$$

$$Nu_{side} = \frac{h_{side} H_m}{k} = 1.389\, Ra^{0.095} \tag{4.17}$$

$$Nu_{bott} = \frac{h_{bott} H_m}{k} = 0.850\, Ra^{0.19} \tag{4.18}$$

$$Ra = Gr \cdot Pr = \frac{g\beta q_v H_m^5}{\nu \alpha k}$$

where H_m is the debris melt pool height.

At the debris melt pool top and bottom surface the heat transfer is affected by bubble agitation. The heat transfer coefficient in this case can be expressed using Kutateladze's bubble agitation heat transfer coefficient [34]

$$h_{bott} = \begin{cases} 1.5 \times 10^{-3} \frac{k}{l} (Ku)^{2/3} & J_g < J_{tr} \\ 1.5 \times 10^{-3} \frac{k}{l} (Ku)^{2/3} \left(\frac{J_g}{J_{tr}}\right)^{-1/2} & J_g \geq J_{tr} \end{cases} \tag{4.19}$$

where

$$Ku = \frac{pJ_g}{g\mu} Pr,\ l = \left(\frac{\sigma_m}{g\rho_m}\right)^{1/2},\ J_{tr} = 4.3 \times 10^{-4} \frac{\sigma_m}{\mu_m} \tag{4.20}$$

and J_g is the superficial gas velocity.

Heat transfer from the crust to the surrounding water

Assuming that heat is taken out from the outside surface of the crust layer by surrounding water in two ways: film boiling and radiation, we have the following expression for the heat flux at the outside of crust layer:

$$q_{out} = q_{fb} + q_{rad} = h_{fb}(T_{cr} - T_w)\varphi + \sigma\varepsilon(T_{cr}^4 - T_w^4) \tag{4.21}$$

where T_{cr} is the crust temperature at the outside edge, h_{film} is the heat transfer coefficient of film boiling, φ is coefficient accounting for the augmentation of film boiling heat transfer due to bubbling, σ is Stephan-Boltzmann constant ($5.67 \cdot 10^{-8} W/m^2K$), and ϵ is the crust surface emissivity.

The film boiling heat transfer coefficient h_{fb} is evaluated using Berenson's correlation,

$$h_{fb} = 0.425 \left[\frac{k_v^3 \rho_v g(\rho_w - \rho_v)\Delta h_{wv}}{\mu_v (T_{cr} - T_{sat})\sqrt{\sigma_l / g(\rho_w - \rho_v)}}\right]^{1/4} \tag{4.22}$$

where subscripts w and v denote water and vapor, respectively; $\Delta h_{wv} = h_{wv} + 0.5 c_{p,v}(T_{cr} - T_{sat})$.

Oxidation of metallic components by the decomposition products

The oxidation reactions, that include the gas-metal and slag-metal interactions (see Table 4.1), depend on the melt composition. Due to the large oxidation potential of zirconium, it is preferentially oxidized before chromium and iron,

Table 4.1: Melt oxidation reactions in the debris melt pool

Reaction	Mass of needed metal (kg/kg)	Enthalpy release per kg of metal reacted (MJ/kg)
$Zr + 2H_2O \rightarrow ZrO_2 + 2H_2$	2.851	6.74
$Zr + 2CO_2 \rightarrow ZrO_2 + CO$	1.037	5.84
$Zr + SiO_2 \overset{<2000^\circ C}{\rightarrow} ZrO_2 + Si$	1.518	2.1
$Zr + SiO_2 \overset{>2000^\circ C}{\rightarrow} ZrO + SiO$		-7.2
$2Cr + 3H_2O \rightarrow Cr_2O_3 + 3H_2$		3.57
$2Cr + 3CO_2 \rightarrow Cr_2O_3 + 3CO$		2.75
$Fe + H_2O \rightarrow FeO + H_2$		0.078

should zirconium be locally present in the melt pool. If zirconium is absent as an initial condition or the zirconium inventory is exhausted due to oxidation, then chromium is oxidized. Finally, if zirconium and chromium are both locally absent from the melt pool, then iron is oxidized. In this work we assumed that there are only oxidation reactions of zirconium.

In order to track the content of free metallic zirconium remaining in the debris melt pool a mass balance equation for the fraction of free zirconium is written as below

$$\rho_m V_m \frac{df_{Zr}}{dt} = -\sum_i V_{g,i}\rho_{g,i} f_{Zr,i} M_{Zr,i} - \left(\frac{dV_s}{dt}\right)_{drained} \rho_s f_{rs} M_{Zr} \qquad (4.23)$$

where M_{Zr} is the mass of zirconium needed in oxidation reactions.

Note that in the case of basaltic concrete there are a two component gas, containing vapor H_2O and carbon-dioxide CO_2, and one reacted slag component - SiO_2. In this work we will neglect the oxidation of other metals in debris melt. The gas flow coming into the debris melt pool can be assumed equal to the gas

volume generated during the concrete decomposition. The gas flow at the top of debris melt pool is defined by subtracting the reacted gas from the coming gas flow. The oxidation fractions accounting for incomplete chemical reaction of the sparging gases as the gas bubbles rise through the debris melt pool f_{H_2O} and f_{CO_2} can be defined like in [34].

Based on the above described models, a computer program has been developed and serves as a tool in sensitivity studies and coolability analysis. A set of transient non-linear ordinary differential equations of heat and mass conservation is solved by means of the Runge-Kutta method. Closure laws are defined for each time step in an explicit manner.

In order to demonstrate the model validity, calculations were performed for conditions of SWISS-I and SWISS-II experiments, SURC-2 and SURC-4 experiments. It is however instructive to note that all mentioned tests had very limited time span, therefore other phenomena of long-term processes have not been represented in those experiments. Thus, the validation can not serve as a fair basis for still un-known effects of other phenomena in debris coolability issue.

4.3 Summary of prediction results

Below is the list of the experiments, whose results have been used to validate the debris coolability models, proposed in the previous parts of this work.

4.3.1 Validation against the SWISS experimental data

The SWISS tests were conducted by Sandia National Laboratories. Two tests were conducted, both with approximately 46 kg of superheated molten stainless steel deposited onto a 21.6-cm block of limestone-sand concrete that was contained in a cast MgO annulus. The stainless steel melt with a depth of approximately 18cm was induction heated at a power level of 1.3 to 1.7 watts/gram (9.1 - 11.9 MW/m^3), i.e. approximately four to five times the decay heaat. The initial superheat of stainless steel was 150 - 200 ^oC. In the SWISS-I test, water was added after 12 cm of concrete had eroded. In the SWISS-II test, a water pool was deposited on top of the melt approximately one minute after the melt contacted the concrete, i.e. before any significant erosion of concrete had occurred.

Table 4.2: List of tested experiments

Experiment	Type of melt	Type of concrete	Specific features
SWISS-I	stainless steel	limestone/ common sand	Water added after 12 cm erosion
SWISS-II			Water added after erosion beginning
SURC-4	stainless steel + Zr metal	basaltic	Oxidation of zirconium
SURC-2	consists mainly of UO_2 plus some other metals and oxides	basaltic	-"-
ACE-L2		siliceous	-"-
ACE-L6			-"-
ACE-L5		limestone/ common sand	No oxidation reaction
ACE-L7			Oxidation of zirconium

The calculations were performed for the above-mentioned conditions. The heat flux to the MgO wall was assumed equal to 0.1 MW/m^2, the concrete slag layer beneath the bottom crust was assumed not to be present (rising coefficient equal to unity), and the melt-concrete slag chemical interactions were neglected. The computational results of concrete erosion are presented in Fig.4.3 and Fig.4.4

The calculations were conducted for 40 min of physical time. At the end of process the heat flux into the water on the top stabilized at 0.79 MW/m^2 (the coefficient of augmentation of film boiling heat transfer due to gas bubbling is given as 3.) and a crust layer of several centimeters thickness was formed on the top and the side of the melt pool.

The above-mentioned calculations allow to estimate the validity of models

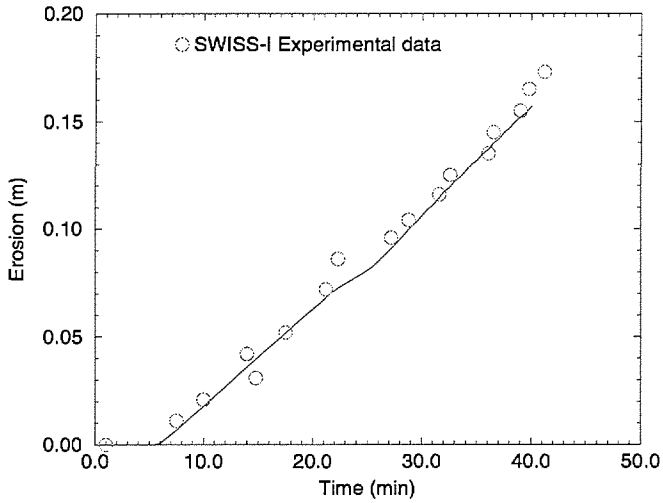

Figure 4.3: Prediction (line) of the SWISS-I erosion data (o)

and correlations of heat transfer inside and from the debris melt pool. They show that the Kutateladze's correlation of bubble agitation heat transfer, that takes place at the bottom and the top of melt pool, is very sensitive to the pool viscosity, which may change a lot in time as a function of the pool temperature and composition. The change of pool viscosity (as much as 500 times due to the large difference between melt and slag viscosities) can result in a 22-time change of heat transfer coefficient.

4.3.2 The effects of the metal oxidation - Prediction of the SURC-4 experimental data

The fourth test in the SURC series was designed to be a separate effects test using stainless steel which investigated the additional effects of zirconium metal oxidation on sustained core debris concrete interactions. In test SURC-4 Zr metal was added to molten stainless steel to create melt pools with up to 10% Zr interacting with basaltic basemat. The SURS-4 experiment was conducted in a 60 cm diameter interaction crucible constructed with a 40 cm diameter basaltic concrete cylinder in the base of a magnesium oxide (MgO) annulus. A 280 kW induction power supply and coil were used to heat and melt the 200 kg stainless charge within the test article and to sustain the interaction for the duration of the experiment. From the total power supply about 25.5% of it was

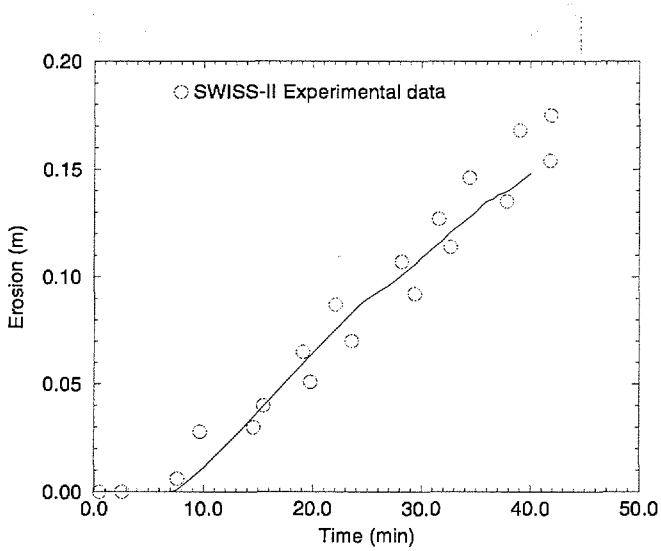

Figure 4.4: Prediction (line) of the SWISS-II erosion data (o)

transmitted to the stainless charge. 20 kg of zirconium metal was added to the melt pool after a constant rate of concrete erosion was established.

The calculations were performed using previous data set with some changes to the concrete properties (basaltic concrete instead of limestone/common sand). The ablation temperature was given as 1600 K like in experiment. The heat transfer model on top of crucible was changed. Heat conduction equation inside concrete was not solved and all heat flux coming from the melt pool was assumed to go to concrete ablation. The initial time for start of calculation was chosen as 102 min, when the beginning of ablation was registered in experiment. The initial temperature of melt at that time moment was chosen as 1800 K. The addition of 20 kg Zr metal was carried out at the time moment of 119 min. The temporary absence of volumetrical heat flux during the time from 124.1 min to 131.7 min due to power failure in experiment was also modeled. Note that in proposed code only the oxidation reactions of zirconium with SiO_2, H_2O, and CO_2 are considered.

The results of the calculated erosion depth are presented in Fig.4.5 and is quite reasonably coincided with experimental data. The addition of zirconium metal resulted in a dramatic change in ablation rate, i.e. increase from 21.6 cm/hr to 31.1 cm/hr, as reported in experiment. However the metallic zirconium was depleted very fast and the ablation rate decreased to the previous value.

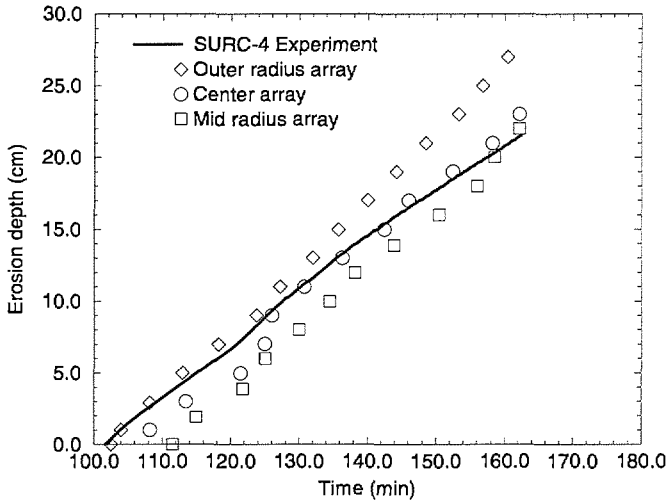

Figure 4.5: Prediction (line) of SURC-4 erosion data (o)

4.3.3 Prediction for the experiments using prototypic melt - the SURC-2 experimental data

The SURC-2 test in the SURC series was designed to be an integral test using a 203.9 kg molten mixture of 69 w/o UO_2, 22 w/o ZrO_2, and 9 w/o Zr over a 40 cm diameter basaltic concrete basemat. The SURC-2 experiment was conducted using the same geometry and instrumentation scheme as was used in SURC-4. The initial temperature of melt was 2700 K and the net power coming to the melt was at the level of 2.163 MW/m^3. During the course of the experiment, the power was increased to 2.884 MW/m^3 and was kept at that level through the end of experiment.

In this calculation the endothermic oxidation of metallic zirconium by silica, when the melt temperature is above 2273 K, was taken into account. That resulted in a sharp drop of the melt temperature to near solidus temperature. However the effect of endothermic reaction did not last very long, because the zirconium metal in the melt pool depleted fast. Therefore its influence on the long-term debris melt pool coolability can be neglected. The decreasing of solidus temperature due to the inclusion of concrete slag into the melt pool was also in effect. The calculated erosion depth is presented in Fig.4.6 and is in good agreement with the experimental data.

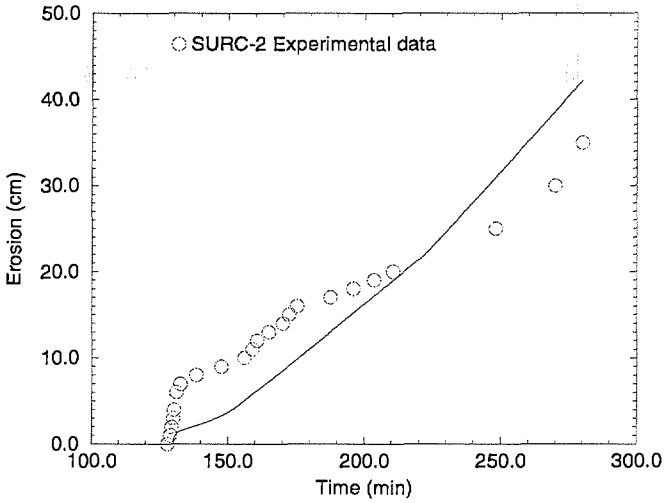

Figure 4.6: Prediction (line) of SURC-2 erosion data (o)

4.3.4 The effects of the pool boundary condition change - Prediction of ACE-series experimental data

Because of great difference between the liquidus and solidus temperatures of a multi-component debris melt pool, that can change in time following the change of pool composition (see Fig.4.7), the temperature boundary condition of the melt pool is an uncertain variable. In order to check the sensitivity of the prediction to the choice of the boundary condition, calculations were performed to predict the ACE-series experimental data, in which the boundary temperature varies and has some values lying between liquidus and solidus lines.

The ACE experiments were performed at Argonne National Laboratory in order to investigate various phenomena associated with MCCI. The tests were performed using different types of concrete and a range of melt composition (see Table 4.2). Each ACE MCCI test was performed with 300 kg of corium and a 200 kg concrete basemat having a surface area of 2500 cm^2. The corium was predominately fuel and core structure plus 8% by weight of the major concrete constituents. Presence of the concrete constituents represented erosion of the basemat during the jet impingement phase of the accident that would precede the early aggressive interaction and longer term erosion phases of the MCCI simulated in the ACE tests.

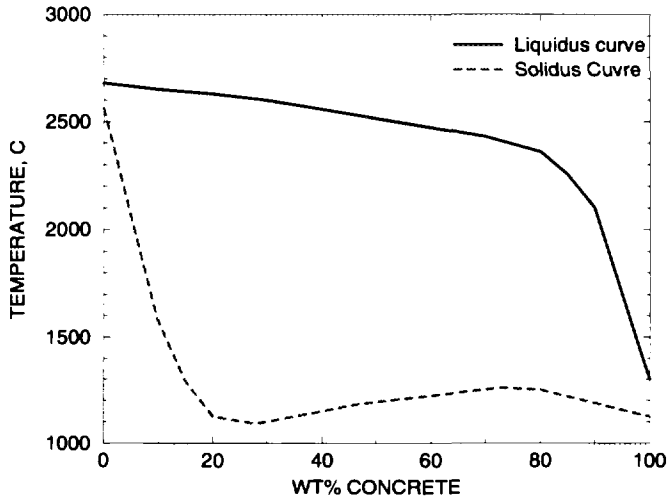

Figure 4.7: Phase diagram of Urania-Zirconia and Concrete Mixtures.

The computational results showed that the choice of interface temperature does not affect much the ablation rate in the long term context. Its effect is most pronounced at the beginning of ablation process, and the closer the interface temperature is to the liquidus value, the lower is the ablation rate. However variation of boundary temperature can give different melt pool temperature prediction. The best prediction of melt pool temperature was obtained for an interface temperature lying approximately at the middle of liquidus and solidus lines.

Note that in proposed model when the pool temperature exceeds a definite value (approximately 2375 K) the endothermic oxidation reaction of zirconium metal will take place instead of the exothermic one. Numerical analysis showed that this model option could also have a strong impact on the ablation rate at the beginning.

4.4 Concluding remarks

This section presents the models and the computer code, developed to predict the behavior and coolability of a core debris bed, which interacts with concrete from below and water from the other sides. The most essential physical processes, which may affect the short-term as well as long-term behavior of

the melt pool are considered and taken into account. These include the heat transfer from the melt pool to surrounding media, i.e. water and concrete, the formation of crust at the boundaries of the melt pool, the heat conduction inside the concrete, the change of the pool properties, i.e. density, viscosity, liquidus and solidus temperatures, etc., due to the mixing of concrete slag with pool materials and the change of pool temperature. The models and code were extensively tested against the available experimental data that were obtained for different types of concrete and melt, in different conditions (with and without water above).

The numerical experiments showed that the chosen correlation for bubble agitation heat transfer coefficient, which has a strong effect on the ablation rate, is very sensitive to the change of melt pool properties, especially the pool viscosity. Such changes are possible due to the dilution of the ablation products with pool materials.

Various important aspects of the debris-concrete interaction phenomenology, i.e. the interactions of the molten concrete slag with metallic components of the core melt and the variation of solidus and liquidus temperatures, which were investigated in the SURC- and ACE-series of experiments, were included and investigated in this work.

The predictions performed for the experiments using the prototypic core melt materials revealed strong sensitivity of the initial ablation rate to such parameters, as the choice of the boundary temperature and the inclusion of the endothermic oxidation reactions. Good agreement of calculated results with experimental data were achieved for the chosen value of boundary temperature lying between solidus and liquidus temperatures.

The satisfactory results received in this modeling work prove the ability of proposed model and code for predicting the core-concrete-water interactions. It is shown that the model developed is quite suitable for the purpose of sensitivity studies and quantification of debris coolability of scoping nature. The objective of following stage will be to test the proposed models and code in long-term conditions, when other phenomena, for example, the oxidation of iron and the crust formation, that affect the long-term coolability of the debris melt pool, may become essential.

Chapter 5

Conclusions

This thesis summarizes the results of research dedicated to the modeling of physico-chemical processes and phenomena involved in the melt-structure-water interactions during a light water reactor severe accident.

The melt-structure (reactor vessel) interactions occurring in the late phases of in-vessel melt progression have been investigated in Chapter 2. An effective modeling approach has been developed, which simulates the thermal transients occurring in an initially-quenched in-vessel debris bed located in the lower head of the reactor vessel. Debris melt pool formation, natural convection heat transfer in the molten debris pool and in a molten metallic layer, and vessel melting are included in the modeling. An innovative approach has been employed to describe the complex process of natural convection heat transfer inside a melt pool or fluid layer, which is based on an effective representation of the turbulent mixing in the vertical direction and the heat transfer through a developing boundary layer in the horizontal direction. The models developed were realized in a computer code named MVITA, which has been applied to study the thermal transients leading to vessel melt-through for the case without vessel external cooling and with external cooling to establish the margins for in-vessel melt retention. The debris bed configurations with and without a metallic layer on top were considered. It was found that for reactor design without vessel penetrations and without external cooling, vessel melt-through would happen at the pool upper corners, which leads to global vessel failure and deposition of large amount of melt mass to the containment. With vessel external cooling by water, the melt could be retained inside the vessel, provided there a thin metallic layer does not accumulate on top of the debris bed. When there is a thin metallic layer above the debris bed, the 'focusing' effect by the metallic

layer could significantly reduce the margin available for in-vessel melt retention, especially for the case of a high power reactor.

For reactor design with vessel penetrations in the lower plenum, these penetrations may fail as a result of the thermal attack from the core debris bed, causing melt discharge into the containment. The process of melt-structure interactions occurring during the discharge of molten melt through a local vessel failure is also considered in Chapter 2. The heat transfer inside a short hole has been investigated and a 2D model of hole ablation has been developed. The model has been implemented in the HAMISA code and employed to predict the experimental data obtained from the KTH hole-ablation experimental series. A simple model for melt discharge and hole ablation has also been developed and applied to perform a quantification study, in which distributions of important melt discharge parameters were obtained.

Chapter 3 is dedicated to the ex-vessel melt-coolant premixing and interactions, which are relevant for the Swedish BWRs as water would be available in the containment space below the RPV as a result of automatic flooding of the lower containment drywell in the event of uncovering of the core according to the Swedish accident management scheme. Aspects of interfacial phenomena associated with hydrodynamic behavior of high-density melt mass in flow field are studied in the first part of Chapter 3. An advanced modeling approach has been developed, based on 'first-principle' direct numerical simulation of multiphase-phase flows. The modeling approach employs a high-order Navier-Stokes solver, coupled with the Level Set front-capturing algorithm to mitigate numerical diffusion and other difficulties related to the property discontinuities at the interface. Development of Kelvin-Helmholtz instabilities, progression of a melt jet in water, and deformation/fragmentation of melt drops in flow field were simulated and investigated by means of the modeling approach developed. This has provided good insights into the hydrodynamic interfacial interactions.

Integral assessment of the melt-coolant premixing is provided in the second part of Chapter 3. Firstly, a steady-state melt-coolant mixing condition is considered and an integral model of melt-coolant interactions has been developed. The model includes a detailed description of heat conduction inside a melt particle and heat transfer between the melt particles and the surrounding. Heat radiation absorption in the two-phase mixing zone is treated with special care. The model developed has been employed to perform a probabilistic analysis, in which various scenario and phenomenological uncertainties were taken into account and, as a result, probabilistic distributions of important mixing zone parameters were calculated for some selected scenarios. This analysis could help to explain, for instance, the high explosivity of high-temperature metallic

melt during its mixing with water. Further, a mechanistic model of a transient two-dimensional mixing zone was developed. This model is based on simplified representation of the transport of the mixing zone constituents and has been validated against FARO experimental data. A sensitivity study has also been performed to investigate the effects of melt particle size and pool subcooling on the melt-coolant interactions.

Behavior of a core debris bed interacting with water above and concrete below has also received attention in this work and are studied in Chapter 4. A model has been developed and employed as a tool to perform sensitivity studies and coolability analysis. The most essential phenomena which could affect the short and long-term behavior of the debris bed have been considered and modeled. These include the heat transfer from the debris bed to surrounding media (water and concrete), the dynamics of crust at the boundaries of the melt pool, the heat conduction inside the concrete, the change of the melt properties on mixing with concrete slag. The model has been extensively validated against available experimental data and employed to perform quantification study of debris coolability for Swedish LWRs in the APRI framework. It was found that the top cooling may not be sufficient for the coolability of a deep debris layer.

In general, the modeling work performed in this work helps to advance the current understanding about the complex phenomenology of melt-structure-water interactions associated with the melt progression during a severe accident scenario in nuclear power plants. Insights into the processes of melt pool formation in a RPV, melt fragmentation in coolant, melt-coolant premixing, debris coolability, etc. have been gained by means of phenomenological and mechanistic modeling. Phenomenological modeling has been employed as an effective tool to perform probabilistic safety assessment, which helps to resolve different scenario and phenomenological uncertainties, whereas mechanistic modeling has been used to gain insight into a particular physics or phenomenon. Besides the improvement of the understanding about severe accident phenomenology gained from the current work, significant advances of the modeling methods applicable to analyze thermal hydrodynamics of multiphase flows have also been accomplished.

Bibliography

[1] Alsmeyer, H., Spencer, B., and Tromm, W., 1998, The COMET-Concept for Cooling of Ex-Vessel Corium Melts, *Proceedings of the International Conference on Nuclear Engineering ICONE-6*, San Diego, May 10-15, 1998.

[2] Amarasooriya, W.H., and Theofanous, T.G., 1991. Premixing of Steam Explosion: A Three-Fluid Model, *Nuclear Engineering and Design*, v.126, pp.115-157.

[3] Angelini, S., Yuen, W.W., Theofanous, T.G., 1995, Premixing-related Behavior of Steam Explosions, *Nuclear Engineering and Design*, v.155, pp.115-157.

[4] Annunziato, A., and Addabbo, C., 1994, COMETA (Core Melt Thermal-hydraulic Analysis) - A Computer Code for Melt Quenching Analysis, *Proceedings of the International Conference on New Trends in Nuclear System Thermohydraulics"*, Pisa, Itally.

[5] Asfia, F.J., and Dhir, V.K., 1994, Natural Convection Heat Transfer in Volumetrically Heated Spherical Pools, *Proceedings of the OECD/ CSNI/ NEA Workshop on Large Molten Pool Heat Transfer*, Grenoble, France, March 9-11, 1994.

[6] Babus'Haq, R.F., 1992, Forced-Convection Heat Transfer From a Pipe to Air Flowing Turbulently Inside It, *Experimental Heat Transfer*, v.5, pp.161-173.

[7] Babus'Haq, R.F., 1993, Forced-Convection Heat Transfer in the Entrance Region of a Pipe, *Int. J. Heat Mass Transfer*, v.36, No.13, pp.3343-3349.

[8] Berg, E.V., Burger, M., Cho, S.H., and Schatz, A., 1994, Modeling of the Breakup of Melt Jets in Liquids for LWR Safety Analysis, *Nuclear Engineering and Design*, v.149, pp.419-429.

[9] Berthoud, G., and Valette, M., 1993, Calculations of the Premixing Phase of an FCI with the TRIO MC Code, *Proceedings of the CSNI Specialists Meeting on Fuel-Coolant Interactions"*, Santa Barbara, California, USA.

[10] Berthoud, G., and Valette, M., 1994, Development of a Multidimensional Model for the Premixing Phase of a Fuel-Coolant Interaction, *Nuclear Engineering and Design*, v.149, pp.409-418.

[11] Berthoud, G., 1995, 1996, Progress Made in the Area of Molten Fuel Coolant Interaction, *Proceeding of the FISA 95 Symposium on EU Research on Severe Accidents*, pp.119-139, 20-22 November 1995, Luxembourg; also "Molten Fuel-Coolant Interactions" in EUR-17126 EN, Luxembourg, 1996.

[12] Berthoud, G., Oulmann, T., and Valette, M., 1996, Corium-Water Interaction Studies in France, *Proc. FISA-95*, Luxembourg.

[13] Blose, R.E., et al., 1987, Sustained Heated Metallic Melt/Concrete Interactions with Overlying Water Pools. *NUREG/CR-4747, SAND85-1546 R3, R4, R7.*

[14] Bonnet, J.M., Rouge, S., and Seiler, J.M., 1994, Large Scale Experiments for Core Melt Retention, *Proceedings of the OECD/CSNI/NEA Workshop on Large Molten Pool Heat Transfer*, Grenoble, France, March 9-11, 1994.

[15] Bui, V.A., and Dinh, T.N., 1995, An Approximation of Turbulent Prandtl Number in Thermally Developing Flows, *Proceedings of the Second CFD Colloquium on Process Simulation*, Helsinki University of Technology, Espoo, Finland, pp.149-163.

[16] Bui, V.A. and Dinh ,T.N., 1996, Modeling of Heat Transfer in Heat-Generating Liquid Pools by an Effective Diffusivity-Convectivity Approach, *Proceedings of the 2nd European Thermal-Sciences Conference*, Rome, Italy, May 1996.

[17] Bui, V.A., Dinh, T.N., and Sehgal, B.R., 1996, In-Vessel Core Melt Pool Formation during Severe Accidents, *ANS Proceedings of 1996 National Heat Transfer Conference*, HTC-Vol.9, Texas.

[18] Bui, V.A., Dinh, T.N., and Sehgal, B.R., 1997, Numerical Simulation of Surface Instability Phenomena Associated with Fuel-Coolant Interaction, *Proceedings of the Eighth International Topical Meeting on "Nuclear Reactor Thermal Hydraulics (NuReTH-8)"*, Kyoto, Japan.

[19] Bui, V.A., Dinh, T.N., and Sehgal, B.R., 1998, Advances in MVITA Modeling of Thermal Processes in the Reactor Pressure Vessel Lower Plenum with a Core Melt Pool, *Proccedings of the International Conference on Nuclear Engineering, ICONE-6*, San Diego, CA, USA, May, 1998.

[20] Burger, M., Cho, S.H., Berg, E.v., and Schatz, A., 1995, Breakup of Melt Jets as Pre-Condition for Premixing: Modeling and Experimental Verification, *Nuclear Engineering and Design*, v.155, pp.215-251.

[21] Cao, Y., and Faghri, A., 1990, A Numerical Analysis of Phase-Change Problems Including Natural Convection, *J. Heat Transfer*, v.112, pp.812-816.

[22] Chawla, T.C., and Chan, S.H., 1982, Heat Transfer From Vertical/Inclined Boundaries of Heat-Generating Boiling Pools, *J. Heat Transfer*, v.104, pp.465-473.

[23] Cheung, F.B., Shiah, S.W., Cho, D.H., and Tan, M.J., 1992, Modeling of Heat Transfer in a Horizontal Heat-Generating Layer by an Effective Diffusivity Approach, *J. Heat Transfer*, v.192.

[24] Chu, C.C., and Corradini, M.L., 1989, One-Dimensional Transient Fluid Model for Fuel/Coolant Interaction Analysis, *Nuclear Engineering and Design*, v.101, pp.48-71.

[25] Ciccarelli, G., and Frost, D.L., 1994, Fragmentation Mechanisms Based on Single Drop Steam Explosion Experiments Using Flash X-ray Radiography, *Nuclear Engineering and Design*, v.146.

[26] Copus, E.R., et al., Core-Concrete Interactions Using Molten Steel with Zirconium on a Basaltic Basemat: The SURC-4 Experiment, *NUREG/CR-4994, SAND87-2008.*

[27] Davis, F.J., and Young, M.F., 1994, Integrated Fuel-Coolant Interaction (IFCI 6.0) Code User's Manual, *NUREG/CR-6211, SAND94-0406*, April 1994, Sandia National Laboratories, Albuquerque, NM87185.

[28] Dinh, T.N., Bui, V.A., Nourgaliev, R.R., Okkonen, T., and Sehgal, B.R., 1995, Modeling of Heat and Mass Transfer Processes During Core Melt Discharge From A Reactor Pressure Vessel, *Proceedings of the Seventh International Topical Meeting on "Nuclear Reactor Thermal Hydraulics, NURETH-7"*, Albany, N.Y., USA, NUREG/CP-0142, Vol.3, pp.1809-1829.

[29] Dinh, T.N., Bui, V.A., Nourgaliev, R.R., Okkonen, T., and Sehgal, B.R., 1996, Modeling of Heat and Mass Transfer Processes During Core Melt Discharge From A Reactor Pressure Vessel, *Nuclear Engineering and Design*, v.163, pp.191-206.

[30] Dinh T.N. and Nourgaliev, R.R., 1997, Turbulence Modeling for Large Volumetrically Heated Liquid Pools, *Nuclear Engineering and Design*, v.169, pp.131-150.

[31] Dinh, T.N., Bui, V.A., Nourgaliev, R.R., and Sehgal, B.R., 1997, Modeling of Heat Transfer Processes in Reactor Vessel Lower Plenum During Late Phase of In-Vessel Core Melt Progression, *Proceedings of the International Topical Meeting on Nuclear Reactor Thermal-Hydraulics, NURETH-8*, v.1, pp.157-164, Kyoto, Japan.

[32] Dinh, A.T., Dinh, T.N., Nourgaliev, R.R., and Sehgal, B.R., 1998, Simulation of Melt Coolant Micro Interactions in a Steam Explosion, *CD-ROM Proceedings of the Third International Conference on Multiphase Flow, ICMF'98"*, Lyon, France, June 8-12, 1998.

[33] Dinh, T.N., Dinh, A.T., Green, J.A., and Sehgal, B.R., 1998, An Assessment of Steam Explosion Potential in Molten Fuel-Coolant Interaction Experiments, *Proceedings of the 6th International Conference on Nuclear Engineering - ICONE-6*, May 10-15, 1998.

[34] Farmer, M.T., Siencki, J.J., Chu, C.C., and Spencer, B.W., 1993, The MELTSPREAD-1 Computer Code for the Analysis of Transient Spreading and Cooling of High-Temperature Melts, *Code Manual*, ANL, Argonne, IL, October 1993.

[35] Fletcher, D.F., and Denham, M.K., 1995, Validation of the CHYMES Mixing Model, *Nuclear Engineering and Design*, v.155, pp.85-96.

[36] Wiktor Frid, 1987, Behavior of A Corium Jet in High Pressure Melt Ejection From a Reactor Pressure Vessel, *Ph.D. Dissertation*, Royal Institute of Technology, Stockholm.

[37] Chester Gingrich, "IFCI info: FCI Code Comparison".

[38] Huhtiniemi, H., Magallon, D., and Hohmann, H., 1997, Results of Recent KROTOS FCI Tests: Alumina vs. Corium Melts, *OECD/CSNI Specialist Meeting on Fuel-Coolant Interactions*, Tokai, Japan.

[39] Jacobs, H., Berg, E.v., Berthoud et al., G., 1996, Studies of Principal Processes during Melt-Water Premixing, *FISA-95 - EU Research on Severe Accidents* - EUR 16896EN, ed. G. Van Goethem, W. Balz and E.D. Loggia, Luxembourg, pp. 165-183.

[40] Jahn, M., and Reineke, H.H., 1974, Free Convection Heat Transfer with Internal Heat Sources: Calculations and Measurements, *Proceedings of the 5th Int. Heat Transfer Conference*, Tokyo, Japan, Vol.3, paper NC-2.8.

[41] Kaiser, A., Shütz, W., and Will, H., 1997, PREMIX 12: Description and First Results, *FZK internal report* IRS4-Notiz Nr. 1376/97.

[42] Kayser, G., 1994, The SCARABEE BF1 Experiment with a Molten UO_2 Pool and Its Interaction, *Proceedings of the OECD/ CSNI/ NEA Workshop on Large Molten Pool Heat Transfer*, Grenoble, France, March 9-11, 1994.

[43] Kmetyk, L.N., 1994, MELCOR 1.8.2 Calculations of Selected Sequences for the ABWR, *SANDIA Report, SAND94-0938, UC-610*, July 1994.

[44] Kolev, N.I., 1993, The Code IVA3 for Modeling of Transient Three-Phase Flows in Complicated 3-D Geometry, *Kerntechnok* 58, 147-15.

[45] Kolev, N.I., 1996, Three Fluid Modeling with Dynamic Fragmentation and Coalescence: Fiction od Daily Practice?, *OECD/CSNI Workshop on Transient Thermal-Hydraulic and Neutronic Codes Requirements*, Annapolis, Md, USA, 5-8 November 1996.

[46] Kulacki, F.A., and Goldstein, R.J., 1972, Thermal Convection in a Horizontal Fluid Layer with Uniform Volumetric Energy Sources, *J. Fluid Mechanics*, v.55, part 2, 271-287.

[47] Kulacki, F.A., and Nagle, M.E., 1975, Natural Convection in a Horizontal Fluid Layer With Volumetric Energy Sources, *J. Heat Transfer*, v.97, pp.204-211.

[48] Kulacki, F.A., and Emara, A.A., 1977, Steady and Transient Thermal Convection in a Fluid Layer with Uniform Volumetric Energy Sources, *J. Fluid Mechanics*, v.83, part 2, pp.375-395.

[49] Kymäläinen, O., Hongisto, O., Antman, J., Tuomisto, H., and Theofanous, T.G., 1992, COPO: Experiments for Heat Flux Distribution from a Volumetrically Heated Corium Pool, *Proceedings of the 20-th Water Reactor Safety Information Meeting*, Bethesda, Maryland, October 21-23, 1992.

[50] Kymäläinen, O., Tuomisto, H., Hongisto, O., and Theofanous, T.G., 1994, Heat Flux Distribution From A Volumetrically Heated Pool With High Rayleigh Number, *Proceedings of the OECD/CSNI/NEA Workshop on Large Molten Pool Heat Transfer*, pp.199-205, Grenoble, France.

[51] Liu, C., and Theofanous, T.G., 1995, Film Boiling in Single- and Two-phase Flows. Part I: Experimental Studies. Part II: A Theoretical Study, *Proceedings of the ANS National Heat Transfer Conference*, Portland, Oregon, August 5-9, 1995.

[52] MAAP-4 User Manual.

[53] Magallon, D., and Hohmann, H., 1995, High Pressure Corium Melt Quenching Tests in FARO, *Nuclear Engineering and Design*, v.155, p.253.

[54] Magallon, D., Huhtiniemi, H., and Hohmann, H., 1996, An Overview of FARO and KROTES Test Results, *Proceedings of PSA'96*, Utah, USA.

[55] Magallon, D., Will, H., Turland, B.D., Annunziato, A., Dobson, G.P., Horváth, G.L., Lummer, M., Väth, L., Valette, M., and Valisi, M., 1995, High Temperature Melt/Water Mixing: Results and Calculations of FARO, PREMIX and MIXA Experiments, *Proceeding of the FISA 95 Symposium on EU Research on Severe Accidents*, pp.140-164, 20-22 November 1995, Luxembourg.

[56] Merilo, M., Farmer, M.T., and Spencer, B.W., 1997, Status Report on the MACE M3B Experiment, *Proceedings of CSARP Meeting*, Bethesda, Maryland, May 5-8, 1997.

[57] Meyer, L., 1996, The Interaction of a Falling Mass of Hot Spheres with Water, *ANS Proceedings of 1996 National Heat Transfer Conference*, August 3-6 1996, pp.105-114.

[58] Norkus, J.K., and Corradini, M.L., 1994, Modeling of Molten Core Concrete Interactions and Fission Product Release, *EPRI TR-104052*.

[59] Okkonen, T., Dinh, T.N., Bui, V.A., and Sehgal, B.R., 1995, Quantification of the Ex-vessel Severe Accident Risks for the Swedish Boiling Water Reactors - A Scoping Study Performed for the ARPI Project. *SKI Report 95:76*, July 1995.

[60] Okkonen, T., N. Dinh, A. Bui and R. Sehgal, 1996, Quantification of the Ex-Vessel Severe Accident Risks for the Swedish Boiling Water Reactors, *SKI Research Report Series*, No.95:76, Swedish Nuclear Power Inspectorate (SKI), 195p.

[61] Osher, S., and Sethian, J.A., 1988, Fronts Propagating with Curvature-Dependent Speed: Algorithms Based on Hamilton-Jacobi Formulations, *J. Computational Physics*, v.79, pp.12-49.

[62] Pilch, M.M., and Erdman, C.A., 1987, Use of Breakup Time Data and Velocity History Data to Predict the Maximum Size of Stable Fragments for Acceleration-Induced Breakup of a Liquid Drop, *Int. J. Multiphase Flow*, v.13, No.6, pp.741-757.

[63] Pilch, M.M., 1996, Continued Enlargement of the Initial Failure Site in the Reactor Pressure Vessel, *Nuclear Engineering and Design*, v.164, pp.137-146.

[64] Plys, M., and Wang, Z., 1991, Concrete Erosion Calculations, Appendix J, *Assessment of Ex-Vessel Debris Coolability*, by S. Levy et al.

[65] Reimann, M., and Stiefel, S., The WECHSL-Mod2 Code: A Computer Program for the Interaction of A Core Melt with Concrete Including the Long-Term Behavior, Model Description and User's Manual, *KfK Report KfK-4477.*

[66] Rempe, J.L., et al., 1993, Light Water Reactor Lower Head Failure Analysis, *Technical Report*, NUREG/CR-5642 EGG-2618, October 1993.

[67] MELCOR Version 1.8.0, COR Package Reference Manual, Sandia National Laboratories. Feb 17, 1989.

[68] Saito, M., Sato, K., and Imahori, S., 1988, Experimental Study on Penetration Behaviors of Water Jet into FREON-11 and Liquid Nitrogen, *Proceedings of 1988 National Heat Transfer Conference*, Houston, TX, pp.173-183.

[69] Sehgal, B.R., and Spencer, B.W., 1992, Spreading of Melt in Reactor Containment (SMELTR), *Proceedings of the second OECD(NEA)CSNI Specialist Meeting on Molten Core Debris-Concrete Interactions*, Karlsruhe, Germany, April 1-3, 1992. KfK 5108. NEA/CSNI/R(92)10.

[70] Sehgal, B.R., and Spencer, B.W., 1992, ACE Program Phase D: Melt Attack and Coolability Experiments (MACE) Program, *Proceedings of 2nd OECD(NEA) CSNI Specialist Meeting on Molten Core Debris-Concrete Interactions*, Karlsruhe, Germany.

[71] Sehgal, B.R., Andersson, J., Bui, V.A., Dinh, T.N., and Okkonen, T., 1996, Experiments on Vessel Hole Ablation During Severe Accidents, *Proceeding of the International Seminar on "Heat and Mass Transfer in Severe Reactor Accidents"*, Izmir, Turkey, 1995; Begel House Publ. Inc., 1996.

[72] Sehgal, B.R., Bui, V.A., Dinh T.N., and Nourgaliev, R.R., 1998, Heat Transfer Processes in Reactor Vessel Lower Plenum during Late Phase of In-Vessel Core Melt Progression, J. Advances in Nuclear Science and Technology, Plenum Publ. Corp, Vol.26 (to appear).

[73] Sehgal, B.R., Green, J.A., and Dinh, T.N., 1997, Experimental and Analytical Investigations of Vessel-Hole Ablation during Severe Accidents, *Proceedings of the Fifth International Topical Meeting on Nuclear Thermal Hydraulics, Operations, and Safety (NuTHOS-5)*, Beijing, China, April 1997.

[74] Shah, R.K., and London, A.L., 1978, Laminar Flow Forced Convection in Ducts, *Academic Press*, New York.

[75] Steinberner, U., and Reineke, H.H., 1978, Turbulent Buoyancy Convection Heat Transfer with Internal Heat Sources. *Proceedings of the 6th Int. Heat Transfer Conference*, Toronto, Canada, v.2, pp.305-310.

[76] Strizhov, V., 1994, OECD RASPLAV Project, *Proceedings of the OECD/CSNI/NEA Workshop on Large Molten Pool Heat Transfer*, Grenoble, France, March 9-11, 1994, pp.445-468.

[77] Sussman, M., Smereka, P., and Osher, S., 1994, A Level Set Approach for Computating Solutions to Incompressible Two-Phase Flow, *J. Computational Physics*, v.114, 146-159.

[78] Tan, M.J., Cho, D.H., and Cheung, F.B., 1994, Thermal Analysis of Heat Generating Pool Bounded From Below by Curved Surfaces. *J. Heat Transfer*, v.116.

[79] Theofanous, T.G., 1989, Some Considerations on Severe Accidents in Loviisa, Theofanous & Co., Inc. January 1989, IVO Proprietary Report.

[80] Theofanous, T.G., Amarasooriya, W.H., Yan, H., and Ratnam, U., 1991, The Probability of Liner Failure in a Mark-I Containment, *NUREG/CR-5423*.

[81] Theofanous, T.G., et.al., 1996, Lower Head Integrity under In-Vessel Steam Explosions Loads, *DOE/ID-10541*, June 1996.

[82] Theofanous, T.G., Liu, C., Additon, S., Angelini, S., Kymäläinen, O., Salmassi, T., 1996, In-Vessel Coolability and Retention of a Core Melt, DOE Report DOE/ID-10460, v.1&2.

[83] Tsai, F.P., Catton, I., and Squarer, D., 1983, On Dryout Heat Flux of an Inductively Heated Heterogeneous Bed. *Proceedings of International Meeting on LWR Severe Accident Evaluation*, Cambridge, Massachusetts.

[84] Turland, B.D., 1994, In-Vessel Phenomena Relevant to the Achievement of Debris Coolability by Ex-Vessel Flooding of a PWR, *Proceedings of the OECD/ CSNI/ NEA Workshop on Large Molten Pool Heat Transfer*, Grenoble, France, March 9-11, 1994.

[85] Turland, B.D., and Dobson, G.P., 1996, Molten Fuel Coolant Interactions: A State of the Art Report, EUR 16874 EN, Luxembourg.

[86] Wang, C.H., and Schrock, V.E., 1989, Modelling of Debris Bed Cooling, UCB-NE-4144. University of California at Berkeley.

[87] Yabe, T., Ishikawa, T., Kadota, Y., and Ikeda, F., 1990, A Multidimensional Cubic-Interpolated Pseudoparticle (CIP) Method without Time Splitting Technique for Hyperbolic Equations, *J. Phys. Soc. Jpn*, v.59, pp.2301-2304.

[88] Yabe, T. and Wang, P.Y., 1991, Unified Numerical Procedure for Compressible and Incompressible Fluid, *J. Phys. Soc. Jpn*, v.60, pp.2105-2108.